

**INTEGRATION OF EIT, SOIL STRUCTURE AND PLANT PHYSIOLOGY
MODELS FOR 3D IMAGING OF CROP ROOT FUNCTION PHENOTYPE**

**A thesis submitted to The University of Manchester for the degree of
Master of Philosophy
in the Faculty of Engineering and Physical Sciences**

2014

ROBERT RICHARD HAYES

SCHOOL OF ELECTRICAL AND ELECTRONIC ENGINEERING

Contents

1	Introduction	14
1.1	Context	14
1.2	Electrical Impedance Tomography (EIT)	16
1.3	Tools and Techniques	18
1.3.1	COMSOL Multiphysics and MATLAB	19
1.3.2	Kalman Filter (KF)	20
1.4	Aims and Objectives Summarised	21
1.5	Thesis Organisation	22
1.6	Novelty	22
2	Literature Review	24
2.1	Background	24
2.2	Soil Properties	25
2.2.1	Soil Texture	25
2.2.2	Soil Structure	26
2.2.3	Porosity	27
2.2.4	Hydraulic Conductivity	27
2.2.5	Soil Water Content	27
2.2.6	Field Capacity	28
2.2.7	Wilting Point	28
2.2.8	Available Water	28
2.2.9	The Unsaturated zone	28
2.3	Measurement Techniques	28
2.3.1	The Thermogravimetric Method	29
2.3.2	Electrical Methods	29
2.4	Discrete and Coupled Models	33
2.4.1	Discrete Modelling	34
2.4.2	Coupled Models	41
2.5	Parameter Estimation Problems	43
2.6	Discussion and Conclusions	45
2.7	Summary	48
3	Forward Problem	50
3.1	Fluid Flow	51
3.1.1	Qualitative Analysis	52
3.1.2	Soil Texture	55
3.1.3	Saturated Hydraulic Conductivity	57
3.1.4	Soil Water Retention Characteristics	65
3.2	Electrostatics	71

3.2.1	Parallel Plate Arrangement	71
3.2.2	Varied Heights of Water	72
3.2.3	Comparison with EIDORS	74
3.2.4	Complex Impedance Implementation using COMSOL	76
3.3	Coupling Mechanisms.....	78
3.3.1	Archie's Law	79
3.3.2	Topp Model.....	79
3.3.3	Complex Refractive Index Model (CRIM).....	80
3.3.4	Experimental Validation and Comparison	80
3.3.5	Investigating the source of error	84
3.4	Multiphysics.....	86
3.5	Summary	88
3.5.1	Fluid Flow.....	88
3.5.2	Soil Parameterisation	89
3.5.3	Electrostatics and Coupling Mechanisms.....	89
3.5.4	Multiphysics.....	90
4	Inverse Problem	91
4.1	Basic Image Reconstruction	91
4.2	Image Reconstruction of Simulated Soil Moisture Distribution	95
4.3	Image Reconstruction of Experimental Soil Moisture Distributions.....	95
4.4	The Kalman Filter	99
4.4.1	Basic Mode of operation	99
4.4.2	State Vector	100
4.4.3	Dynamic & Observation Models	100
4.4.4	The Discrete Kalman Filter Algorithm	101
4.5	Extended Kalman Filter (EKF)	104
4.5.1	State Vector	104
4.5.2	Dynamic & Observation Models	104
4.5.3	Linearisation	105
4.5.4	Extended Kalman Filter Algorithm.....	106
4.5.5	Limitations of the Extended Kalman Filter.....	107
4.6	Ensemble Kalman Filter (EnKF)	108
4.6.1	State Vector	108
4.6.2	Ensemble Kalman Filter Algorithm	109
4.7	Kalman Filter Based Inverse Solver.....	111
4.7.1	Hybrid Reconstruction.....	111
4.7.2	Kalman Filter Only	113
4.8	Summary	115

5	Conclusions and Future Work	116
5.1	Literature Review & Decisions Made	116
5.2	Difficulties Faced	117
5.3	Forward Problem	118
5.3.1	Fluid Flow	118
5.3.2	Soil Parameterisation	118
5.3.3	Electrostatics and Coupling Mechanisms	119
5.3.4	Multiphysics.....	120
5.4	Inverse Problem	120
5.4.1	Hybrid Reconstruction	120
5.4.2	Kalman Filter Only	120
5.5	Future Work	121
5.5.1	Implementation of Proposed Algorithms	121
5.5.2	Validation of Proposed Algorithms	122
5.5.3	Complex Impedance Measurement	123
5.5.4	Plant Soil Interactions	123
5.6	Final Words	124
6	References.....	125
7	Appendix	134

List of Tables

Table 1. Repeatability Testing Data	63
Table 2. Vessel geometry details	74

List of Figures

Figure 1. Soil Texture Triangle [37].....	26
Figure 2. Integration of soil transport, root growth and electrostatics models. .	47
Figure 3. 3D Simulated soil water distribution at a time, t , for a point injection.	51
Figure 4. A comparison between experimental and simulated wetting fronts incident on a rectangular soil core from a point injection under atmospheric pressure.	54
Figure 5. Particle layering following sedimentation	56
Figure 6. Diagram of the variables involved in the determination of the hydraulic gradient.	58
Figure 7. Experimental setup.....	60
Figure 8. A plot of Flux against Hydraulic conductivity for both compacted and non-compacted soil cores.	61
Figure 9. A plot of Flux against Hydraulic conductivity for both increasing and decreasing hydraulic gradients.	62
Figure 10. A comparison between experimental and simulated wetting fronts incident on a cylindrical soil core.	64
Figure 11. Experimental Setup.	67
Figure 12. Poor repeatability of soil water retention curve for a single soil core.	68
Figure 13. Soil water retention curves for a single soil core.	69
Figure 14. Verification that spatial variation of hydraulic conductivity is negligible	69
Figure 15. Temperature with respect to soil water content.	70
Figure 16. Schematic diagram of the rectangular vessel. Left: Front view, Right: Top view.....	71
Figure 17. Left: Vessel wall showing electrode Right: Constructed measurement vessel	72
Figure 18. Plot of capacitance vs. fill level for measured and simulated capacitance data.....	73
Figure 19. Simulated electric fields for a half filled rectangular vessel.....	73
Figure 20. COMSOL Model/Mesh	74
Figure 21. EIDORS/NETGEN Mesh with Electrodes Highlighted in Red	75
Figure 22. Simulated boundary voltage comparison between EIDORS and COMSOL Multiphysics.	75
Figure 23. Simulated, Analytical and Measured complex spectroscopic impedance data.	77

Figure 24. Measured and simulated capacitance measurements vs. soil saturation level.	82
Figure 25. Measured and simulated capacitance measurements vs. level of soil saturation using rapeseed oil.....	83
Figure 26. Measured and simulated capacitance measurements vs. level of sand saturation using distilled water	84
Figure 27. Variation of the dielectric constant of water with respect to temperature.....	85
Figure 28. Error in predicted capacitance vs. temperature induced drift in dielectric constant of water for determining the extent to which the temperature dependence of the dielectric constant of water contributes to measurement error.	86
Figure 29. Simulated effective saturation using the Richards equation and subsequent conversion to conductivity distribution using Archie's law for a series of time steps.....	87
Figure 30. Predicted boundary voltages for a time dependant fluid flow scenario.	88
Figure 31. Simulated potential distribution for a single excitation pattern in COMSOL Multiphysics	92
Figure 32. Reconstructed conductivity distributions for a number of basic inclusions.	94
Figure 33. Reconstructed conductivity distributions for a number of time steps using LBP	95
Figure 34. Photograph of Experimental Setup.....	96
Figure 35. Two Plane ERT Vessel Geometry.....	96
Figure 36. Reconstructed resistivity (Ω/m) distributions using NLGN, 5 iterations, for upper and lower electrode planes for a section of time steps throughout a drying cycle. Blue indicates low resistivity, red indicates high resistivity	97
Figure 37. Plot of average resistivity vs Time Step (Each Step being 5 minutes)	98
Figure 38. Shrinkage caused the soil to pull away from the wall electrodes	98
Figure 39. Operation of the discrete Kalman Filter [153].....	100
Figure 40 . Schematic diagram of the operation of the Kalman filter [153]	103
Figure 41. Schematic diagram of the operation of the EKF [153]	107
Figure 42. Schematic diagram of the operation of the Ensemble Kalman Filter	110
Figure 43. Hybrid Reconstruction	112
Figure 44. Kalman Filter Only	114

Abstract

Climate change necessitates breeding programmes for the development of plant varieties that are tolerant to drought and other environmental stresses. Rapid identification of new plant varieties that will thrive in future climates is increasingly important. Presently, above soil features are monitored in industrial greenhouses and field trials. Indicators of preferential genetic traits are often based on loosely related features (phenotypes) such as an extra ear of corn on a maize plant. The root system is critical to plant water uptake, however this cannot easily be assessed without destroying the crop or disturbing the plant/soil matrix through extractive sampling.

A new visualisation tool is being developed for seed breeders, providing on-line data for each individual plant in a screening programme. It will be used to indicate how efficiently each plant utilises the water and nutrients available in the surrounding soil. This will facilitate early detection of desirable genetic traits with the aim of increased efficiency in identification and delivery of tomorrow's drought tolerant food crops.

Visualisation takes the form of Electrical Impedance Tomography (EIT), a non-destructive and non-intrusive imaging technique. Measurements are to be obtained for individual plants thus allowing water absorption levels for each specimen to be inferred.

This document will discuss progress made in the design and implementation of a new model-based 3D reconstruction method for the interpretation of data acquired using the University of Manchester LCT2 ERT data acquisition instrument. There were two main aspects of the project:

(1) A multiphysics based forward solver was implemented in COMSOL Multiphysics. This forward model is comprised of a fluid flow model (Richards' equation), coupled to an electrostatic model (Poisson's equation) via a mixture model (Archie's Law). Each individual element was validated experimentally in isolation and the results are presented, finally the integrated model is demonstrated.

(2) Two inversion schemes are proposed, these schemes utilise the multiphysics forward solver described above in combination with both traditional inversion techniques implemented in the EIDORS reconstruction suite and Kalman Filter techniques to form a hybrid reconstruction scheme and also a solver based solely on the Kalman Filter to provide an inversion free, iterative parameter estimation scheme. The advantages and disadvantages of each method are discussed and suggestions regarding their implementation are given.

Declaration

No portion of the work referred to in the thesis has been submitted in support of an application for another degree or qualification of this or any other university or other institute of learning.

Copyright Statement

- i. The author of this thesis (including any appendices and/or schedules to this thesis) owns certain copyright or related rights in it (the "Copyright") and s/he has given The University of Manchester certain rights to use such Copyright, including for administrative purposes.
- ii. Copies of this thesis, either in full or in extracts and whether in hard or electronic copy, may be made only in accordance with the Copyright, Designs and Patents Act 1988 (as amended) and regulations issued under it or, where appropriate, in accordance with licensing agreements which the University has from time to time. This page must form part of any such copies made.
- iii. The ownership of certain Copyright, patents, designs, trade marks and other intellectual property (the "Intellectual Property") and any reproductions of copyright works in the thesis, for example graphs and tables ("Reproductions"), which may be described in this thesis, may not be owned by the author and may be owned by third parties. Such Intellectual Property and Reproductions cannot and must not be made available for use without the prior written permission of the owner(s) of the relevant Intellectual Property and/or Reproductions.
- iv. Further information on the conditions under which disclosure, publication and commercialisation of this thesis, the Copyright and any Intellectual Property and/or Reproductions described in it may take place is available in the University IP Policy (see <http://documents.manchester.ac.uk/DocuInfo.aspx?DocID=487>), in any relevant Thesis restriction declarations deposited in the University Library, The University Library's regulations (see <http://www.manchester.ac.uk/library/aboutus/regulations>) and in The University's policy on Presentation of Theses

Acknowledgements

I would like to express my gratitude to my supervisors Dr Bruce Grieve and Dr Oliver Dorn for their guidance, expertise and for the opportunity to undertake the research project detailed in this thesis.

I would also like to thank my advisor Professor Trevor York for his advice and suggestions throughout the period of my studies, Dr Frank Podd for his advice and assistance in the early stages of my research and Dr Simon Hammersley for many helpful discussions and technical assistance.

I am grateful to the staff in the mechanical engineering workshop for the fabrication of various pieces of experimental apparatus that have been essential for the completion of this work.

I would like to thank the Engineering and Physical Sciences Research Council for providing funding for the duration of my research project and also Syngenta for sponsoring the University Innovation Centre.

Finally I would like to thank my loving parents for their care, support and encouragement throughout my studies.

Dedication

I would like to dedicate this work to my late Grandmother, Mrs Lorna Harker, who sadly passed away in October 2014, during the final stages of the preparation of this thesis.

Publications

R R Hayes et al 2010 An investigation into the use of a mixture model for simulating the electrical properties of soil with varying effective saturation levels for sub-soil imaging using ECT J. Phys.: Conf. Ser. 255 012002

R. Hayes et al 2012 Capacitively-Coupled Impedance Measurements for ERT, 6th International Symposium on Process Tomography, Cape Town, South Africa, 26-28 March 2012

1 Introduction

1.1 Context

A review of 15 climate models [1] suggests that in the 21st century one of the greatest threats to the planet Earth is climate change. There is an increasingly convincing trend in evidence supporting the notion that observed warming over the most recent decades is attributable to human activity and in particular the increase in greenhouse gases. As the concentration of greenhouse gases present in the atmosphere continues to rise, temperatures are expected to continue to rise well beyond the 21st century. Through coupling mechanisms between the Earth's energy and water cycles, this induced warming is bound to alter hydrological conditions [2]. These changes may have more pronounced effects on human wellbeing than the warming phenomena itself. Amongst such hydrological changes, soil moisture changes, which are a reflection of agricultural water availability, are of great concern due to their direct relation to global food production and supply of life essentials [3].

Climate change has been and continues to be the greatest influence on global food production in the arid and semi-arid tropical countries of the developing world, i.e. Asia, Africa, the Americas and areas of Europe [4]. Large areas of Africa and South America expect major water scarcity by 2025 [5]. These arid and semi-arid regions account for approximately 30% of the world's total area and are host to approximately 20% of the total world population [4]. Crops are one of the world's major water consumers and as climate change leads to water scarcity there is an increase in competition for water. This severely limits irrigation and constrains food production [6] thus the ability to rapidly identify new plant varieties that will be tolerant to drought, and other stresses, is going to be key to breeding the food crops of tomorrow. Furthermore more efficient utilisation of available water is desired in order to ensure that soil health is maintained through decreasing the rate of excessive irrigation, thus reducing nitrogen loss and loss of other nutrients to the water table.

Currently, above soil crop features (phenotypes) are monitored in industrial scale greenhouses and field trials during seed breeding programmes so as to provide an indication of which plants have the most likely preferential genetics to thrive in the future global environments. These indicators of plant vigour are often based on loosely related features which may be straightforward to examine, such as an additional ear of corn on a maize plant, but which are labour intensive and often lacking in direct linkage to the required crop features.

As a response to these concerns, there has been a great deal of interest in understanding features that have a direct influence on crop survivability, such as root-soil interactions [7]. In particular, to develop a greater knowledge of the interactions between root systems and the surrounding soil structure by employing scientific methods with an emphasis on monitoring or predicting root growth and root water uptake.

Observing plant-soil interactions calls for the ability to observe the dynamic interplay between plant root growth, soil structure and soil moisture profiles in a natural environment. Given that the efficiency of roots in extracting moisture from the surrounding soil is critical to surviving in arid regions it is thus desirable to observe sub-surface moisture profiles. Imaging of the moisture distribution in the sub-surface environment carries a number of technical challenges. For breeding programmes and field scale monitoring any instrumentation must be portable, relatively low cost, internally powered and weather resistant. High resolution imaging modalities such as magnetic resonance imaging (MRI) and X-ray computed tomography (CT), whilst offering superior image quality, cannot be used in this capacity as the technology is costly (>£30k), equipment large (>0.5m³) and power requirements are very high (>500W). Furthermore these methods typically require that the plant specimen to be studied is taken to the equipment, the implication being that these techniques require that the plant is either grown in an environment that is not akin to natural growth conditions (eg. confined within an X-Ray tube) and/or must be disturbed and moved to the instrument for a discrete time measurement. Therefore a compromise must be made to reduce size, power consumption and cost at the expense of image quality. For these reasons, electrical impedance based imaging modalities are a promising candidate technology that facilitate the ability to acquire dynamic measurement data in a natural setting for a large screen of plants by virtue of its scalability, compatibility with such environments and its relatively low cost. Initial investigations using the University of Manchester/Syngenta Low Cost Tomography 2 (LCT2) instrument [8] suggest that root water uptake may be monitored using electrical impedance imaging [9]. This is further supported by the work of Garré [10].

The aim of this research programme is to contribute to the delivery of a new tool for seed breeders utilising electrical impedance tomography (EIT) technology. This tool will indicate how efficiently a plant specimen utilises the water and nutrients available in the surrounding soil. It will be designed for use in greenhouses and/or field trials during seed breeding programmes as an on-

line, in-situ tool for monitoring root water uptake for the purpose of sub-surface phenotyping and early detection of desirable genetic traits. This will facilitate the identification and delivery of drought tolerant food crops and securing the food supply of tomorrow. Further implications of the research programme include increased control in maintaining soil health by ensuring excessive water is not used in agricultural food production. The particular aspect of this new tool that this thesis will address is:

“Improving the fidelity of images and/or quantitative data acquired utilising the existing LCT2 EIT data acquisition instrument.”

As such the focus is on techniques which may be utilised for interpreting the data obtained using an established hardware platform. In particular the thesis will consider methods by which prior knowledge of the region being imaged may be utilised to constrain or inform data interpretation.

The following sections will briefly introduce the candidate technology and some of the key tools and techniques employed throughout this thesis. For a more in depth discussion on the chosen technologies, tools and techniques the reader is advised to refer to chapter 2, the literature review.

1.2 Electrical Impedance Tomography (EIT)

EIT is a non-intrusive, non-destructive and in some cases non-invasive imaging technique that is relatively low cost, relatively easy to implement and is able to offer high frame rates. Despite the relatively poor image resolution, which the techniques proposed in this thesis will in part attempt to reconcile, it is an excellent choice for observing dynamic processes, such as root water uptake or irrigation infiltration.

The basic premise of EIT is to obtain an image of the distribution of electrical properties, such as the electrical conductivity or electrical permittivity within a region of interest from a series of measurements made at the boundary. A typical EIT arrangement would be that of a ring of metallic electrodes placed around the periphery of a region of interest. A low frequency (typically <1MHz) current is injected between electrode pairs and the resulting boundary voltages between each of the remaining electrode pairs is measured in turn. Once all available measurements have been obtained for a given excitation location, the excitation electrode location is updated by injecting current between a different electrode pair and another series of boundary voltages is measured. This process is repeated until all possible electrode combinations have been utilised. The resulting boundary voltages are directly influenced by the electrical

properties within the measurement space and can thus be “inverted” to provide the user with a conductivity or permittivity map of the region of interest. Within the confines of the application, this thesis is concerned with the soil moisture distribution, as inferred from the conductivity and permittivity distributions, reconstructed using several well established and much studied coupling mechanisms. It is proposed that, root water uptake may thus be inferred from the recovered conductivity and/or permittivity distributions by monitoring the time evolution of the moisture distribution.

It is anticipated that a number of parameters to be evaluated quantitatively and reported to seed breeders, for example volumetric water content, with relatively high temporal and spatial resolution thus allowing for the inference of approximate spatial root densities. It should be noted that individual roots will be not resolved in the visualisation process. However, absolute position of roots is not of primary importance, the priority is in providing a sub-surface phenotyping tool for monitoring, dynamically, the ability of the root bundle to interact with its surrounding environment and draw on the available water, i.e. the research project is concerned with understanding the influence the root bundle has on the surrounding soil water content, not resolving individual roots.

In this application it is important to note that in a field based breeding programme, the technique cannot be considered as non-invasive as electrodes must be inserted into the soil surrounding the plant. However, the technique should not interfere excessively with root growth, irrigation infiltration and/or root water uptake i.e. the processes that are being observed, nor should it harm the specimen or soil sample under investigation, therefore the method can still be considered as non-intrusive and non-destructive.

Despite the many advantages of EIT imaging modality, the technique poses its own significant technical challenges, especially in light of the intricacy of the medium being interrogated, i.e. soil. Electrical impedance imaging is a “soft field” reconstruction problem. That is to say that all regions of interaction are altered by the sample under investigation [11]. Furthermore it is an under-determined problem i.e. the number of measurement data available is much fewer than the number of parameters being estimated. This is due to the number of unique measurements being severely constrained by the number of electrodes placed on the boundary, where the number of measurements is given by $N(N-3)$ where N is the number of electrodes (assuming the use of an adjacent measurement strategy - see Chapter 2 for details) and the number of unique measurements (i.e. excluding reciprocal data) is given by $N(N-3)/2$. For

illustrative purposes, consider a single plane of 16 electrodes placed on the periphery of a cylindrical measurement vessel, as typical for process monitoring applications; there are 208 possible boundary measurements, of which only 104 are unique due to reciprocity. From these 104 unique measurements, the number of parameters being estimated may be in the order of several thousand, or in some cases, tens of thousands. In the case of other measurement strategies, the number of unique measurements may be less given the same number of electrodes. This technique also suffers from being an ill-posed problem [12] in the sense that measurement noise may contribute significantly to the error in the estimated distribution, therefore there is always some level of uncertainty associated with the inverted image and any metrics inferred from the result of the inversion routine. Furthermore the medium, soil, exhibits both conductive, wet, dominating phases and dielectric, dry, dominating phases, the reader is directed to the Literature Review chapter, sections 2.2.5 through 2.2.9 for details on soil water content and associated terms and phases. The implication of this is the formation or breaking of conducting paths between measurement electrodes and a transition between the dominance of the real and imaginary impedance components. As a result of water loss, soil is prone to shrinking and cracking which further complicates the measurement process due to the quality of the connection at the boundary points between the medium and the electrodes. In addition to this, the presence of root tissue will influence the measurement process and will complicate the inversion process.

1.3 Tools and Techniques

The prediction of boundary measurements, referred to as the forward solution in the EIT and inverse problems communities is an essential step in analysing experimentally obtained boundary voltage data. In this case the prediction of electrical measurements for detecting water movement in soil measured via EIT requires the consideration of several theoretical backgrounds including, fluid dynamics in a non-saturated porous media, in addition to the traditional electrical field prediction step. Multiphysics simulation allows the relationships between these different physics backgrounds to be coupled hence providing a means by which the modelling of numerous physical processes can be combined in one software package. It is anticipated that introducing the consideration of fluid dynamics, via modelling the time evolution soil moisture distribution profile, into the reconstruction process, will enable soil water content and other soil parameters to be directly estimated from the time varying conductivity distributions using either:

- Constrained traditional inversing algorithms
- Statistical methods (such as the Ensemble Kalman Filter, EnKF)
- A hybrid method integrating both traditional and statistical methods

Furthermore, multiphysics simulation is advantageous in that it does not require routines for interfacing two or more independent software packages hence potentially reducing computation time.

Simulation carries a number of additional benefits including:

- (1) Facilitating the optimisation of sensor design though enabling a number of sensor geometries to be evaluated without the need to manufacture numerous different sensors.
- (2) Controlling error introduced by measurement instrumentation and/or the experimental setup by allowing the signal-to-noise ratio to be set precisely and also allowing different noise power density functions (PDFs) to be tested.
- (3) Allowing image reconstruction algorithms to be compared and optimised since simulation allows precise definition of the 'unknown' permittivity distribution that is to be reconstructed.

This thesis will propose the use of several reconstruction methods as implemented in the popular MATLAB programming language and will utilise the commercial software 'COMSOL Multiphysics' during the prediction step/forward solution to solve both the Richards' equation and Poisson's equation as coupled using Archie's Law, the complex refractive index model (CRIM) and/or the Topp model.

1.3.1 COMSOL Multiphysics and MATLAB

COMSOL Multiphysics (previously known as FEMLAB) is a fully featured finite element method (FEM) modelling package facilitating the solution of many physical problems as implemented in the form of partial differential equations (PDE's). COMSOL Multiphysics offers a complete modelling and simulation solution, from defining the geometry, meshing, specifying the physics mode and computing the solution. Furthermore, COMSOL offers sophisticated post processing options for visualising and analysing the computed solution.

In addition to being a stand-alone product, COMSOL Multiphysics' LiveLink™ for MATLAB module offers robust functions for interfacing with MATLAB. MATLAB is a high level mathematical programming

language/environment developed by Mathworks, it is particularly suited to matrix manipulation and the solution of a large number of mathematical and engineering problems. The functions within the LiveLink™ for MATLAB module allow the user to utilise the vast functionality of MATLAB to create and/or manipulate a COMSOL Multiphysics model, solve a physics problem and post process the model solution from the MATLAB command line interface. This may be useful in order to customise and parameterise the geometry, physics mode or solution scheme, for example to optimise a number of parameters. This is advantageous as it allows the user to define and update parameters within a COMSOL model from within a MATLAB script, facilitating the ability to automate or batch process simulations. This is particularly useful for the implementation of statistical methods such as the ensemble Kalman filter (EnKF) allowing batch simulations in order to produce an ensemble of predictions. Furthermore it facilitates the assimilation of predictions with respect to an incoming stream of measurement data and updating of model parameters in order to obtain an optimal parameterisation.

1.3.2 Kalman Filter (KF)

Statistical methods and/or iterative parameter estimation techniques such as the KF offer distinct advantages over traditional inverting techniques, particularly for the study of dynamic processes. The KF can be considered as an optimal estimator i.e. it is used to infer parameters of interest from indirect, noisy, inaccurate or uncertain observations, such as boundary voltage measurements in the context of soft field tomography, such as in EIT. As such the KF can be utilised to completely avoid the inversion step and the associated disadvantages of traditional inverting schemes.

The KF has a sequential structure that is particularly convenient for processing remote measurement data from dynamic systems in real-time. In addition it provides information on the accuracy of the predictions at each time step and it is able to account for a large range of potential model errors [13]. The KF moves sequentially from one time step to the next and naturally divides into several distinct steps, most notably a prediction step and an update step. The KF workflow can be summarised as follows [13]:

1. Initialisation - The KF is initialised according to prior knowledge at of the state at the initial time step. An ensemble is generated around a mean.
2. Forecast - The ensemble is propagated forward in time utilising the prescribed non-linear model.

3. Comparison - As measurement data becomes available, each ensemble member is updated according to the error covariance between the prediction and the measurement.

As the error between measurement data and predicted data converges, the parameters desired may be extracted from the now optimally modelled scenario.

One major disadvantage of the KF method is that it may require many runs of the 'forward solver' or model to generate an ensemble size that produces a stable solution, this may be time consuming and computationally expensive. For the purposes of this research work, these disadvantages are not of concern.

1.4 Aims and Objectives Summarised

This research work aims to contribute to the delivery of a new tool for seed breeders that will indicate how efficiently a plant specimen utilises the water and nutrients available in the surrounding soil. The particular aspect this body of work contributes to this overall objective by suggesting methods by which the fidelity of the images and/or the quantitative data derived from the data acquired utilising the University of Manchester/Syngenta LCT2 EIT measurement instrument is increased. As such the focus is on data assimilation techniques for interpreting the data obtained using an established hardware platform.

Whilst the overarching goal is to provide a root water uptake monitoring tool, this work focuses on improving the detection of a dynamic water distribution in a soil core, without the presence of a plant specimen. The reason for this approach is that during the early stages of the research project, it became increasingly clear that soil as a medium is extremely complex, even when strict test procedures are adhered to, the inherent properties of the soil meant that experimental difficulties were experienced. As such it was considered that adding a plant specimen at this stage would complicate matters beyond the scope and time constraints of the project.

It should be noted that a major portion of this work consists of the identification, experimental validation and implementation of physical models and coupling mechanisms suitable for predicting soil water distributions and the resulting electrical measurement data at the boundary such that the forward problem, which is critical to both traditional inverting techniques and the prediction step of statistical techniques, may be implemented. Furthermore, substantial effort was placed in characterising 5 common agricultural soils as found in the United Kingdom such that the model's chosen could be calibrated.

1.5 Thesis Organisation

This thesis is structured as follows:

- Chapter 2 reviews the current literature, touching on advances in the field of sensing and imaging techniques for use in monitoring the subsurface environment and various modelling techniques whilst offering a thorough justification for the methods adopted in this thesis.
- Chapter 3 introduces the forward problem and will consist of a brief discussion of each of the individual elements of the forward solver followed by an experimental validation of each of the individual elements of the forward solver in isolation, concluding with a discussion on the integration of each element and presenting a multiphysics based forward solver.
- Chapter 4 provides some basic image reconstructions using EIDORS for simulated and experimental data, followed by an introduction to the Kalman Filter and concluding with two proposed reconstruction schemes, based on the forward solver described above, in combination with both traditional and statistical inversion techniques.
- Chapter 5 provides concluding statements on the work carried out as part of this research program, stating what has been achieved, difficulties experienced and concluding with suggestions for future work.

1.6 Novelty

Primary sources of novelty in the research include the presentation of a multiphysics model that predicts fluid flow in a non-saturated porous medium and subsequently predicts the resultant electric fields when coupled via one of several identified and verified coupling mechanisms.

Further to the novelty of the creation of said model, is the novelty associated with its use in the context of EIT reconstruction, in particular as the prediction step in a parameter estimation method such as the KF.

Further indications of novelty include the ability to demonstrate the potential use of capacitance measurements to infer soil moisture distributions tomographically. At the time of preparing this thesis, there has been no literature identified describing the use of ECT systems for imaging soil moisture distribution. This lack of literature may be attributable to the difficulty inherent in making capacitance measurement in wet soils due to the conductive paths formed between electrodes. However with higher measurement frequencies in the region of ~ 14 MHz, soil moisture content may be inferred from capacitance measurements, as has been demonstrated using single point capacitance based soil moisture probes. Further to this, the analytical model developed by Dr Frank

Podd [15] suggests that the capacitive element of a complex impedance measurement may be extracted using spectroscopic measurements and will not require measurement frequencies as high as 14 MHz.

This work would also contribute to the existing base of knowledge surrounding the use of ERT for soil moisture tracking. There are a number of ERT measurement systems presented in the literature. However these are typically employed on larger scales than those of the aim of this project. One research group is known to have used an ERT system on a similar scale, i.e. lysimeter scale. This group has used an ERT system for imaging the distribution of a tracer in an irrigated soil core of diameter 116 cm [16][17], imaging preferential flows[18] and for imaging root water uptake[19]. The instrument used is a lab based instrument with a large number of electrodes (212) and high acquisition times (6.5 to 8.5 hours).

Only one complex impedance instrument for soil moisture tracking has been described in the literature, however to date this has not been tested on soils, only on phantoms suspended in water. The developed model/techniques when combined with Dr Frank Podd's analytical model [15] should facilitate the consideration of complex impedance data.

At the time of writing, the research undertaken for the requirements of this thesis has led to the publication of 2 conference articles. The papers accepted are now published in the Journal of Physics Conference Series [20] and the conference proceedings of the 6th International Symposium on Process Tomography [21].

2 Literature Review

2.1 Background

A review of 15 climate models [1] suggests that in the 21st century one of the greatest threats to the planet Earth is climate change. There is an increasingly convincing trend in evidence supporting the notion that observed warming over the most recent decades is attributable to human activity and in particular the increase in greenhouse gases. As the concentration of greenhouse gases present in the atmosphere continues to rise, temperature is expected to continue to rise well beyond the 21st century. Through coupling mechanisms between the Earth's energy and water cycles, this induced warming is bound to alter hydrological conditions [2]. These changes may have more pronounced effects on human wellbeing than the warming phenomena itself. Amongst such hydrological changes, soil moisture changes, which are a reflection of agricultural water availability, are of great concern due to their direct relation to global food production and supply of life essentials [3].

Climate change has been and continues to be the greatest influence on global food production in the arid and semi-arid tropical countries of the developing world, i.e. Asia, Africa, the Americas and areas of Europe [4]. These arid and semi-arid regions account for approximately 30% of the world's total area and are host to approximately 20% of the total world population [4].

Some studies [4][25][26] suggest this warming phenomenon may result in positive agricultural changes in mid and high latitudes due to the introduction of new crop species and varieties, increased crop yields and the expansion of suitable areas for crop cultivation. However climatic variability and change will seriously endanger sustained agricultural production in tropics such as those of Asia and southern Europe in coming decades.

In response to these predictions and the limitations of current methods, there has been a great deal of attention to better understand plant-soil interactions over recent times [7]. In particular, to develop a greater knowledge of the interactions between root systems and the surrounding soil structure by employing scientific methods with increased emphasis on monitoring or predicting root water uptake.

Currently desirable genetic traits are identified by methods including the examination of above soil features commonly referred to as phenotypes in industrial greenhouses and field trials during seed breeding programmes. These methods aim to provide an indication of which plants have the desired genetic traits to thrive in the future global environments. These indicators are often

based on loosely related features which may be straightforward to examine but are labour intensive and often lacking a direct linkage to the required crop features. The root system is critical to plant water uptake, however at present this can not easily be assessed without destroying the crop or disturbing the plant/soil matrix through extractive sampling. As a result, it is desirable to be able to monitor the sub-soil environment around the root zone using non-destructive and where possible non-intrusive methods.

Some studies into plant water uptake, for instance [28][29], focus on measurement technologies and applications, i.e. the acquisition and interpretation of physical measurement data for one or more plants or soil samples, while others [30]-[33], focus entirely on simulation based studies. Other methods focus on correlating measurement techniques with simulation or modelling techniques to better interpret physical measurements, for example, in the simplest of cases, the use of mathematical mixture models to interpret single dielectric permittivity measurement in terms of a point measurement of soil moisture content [35][36].

The following sections will briefly introduce some relevant properties of soils and explore the current measurement methods used for determining both point and spatial moisture distributions. Further to this, a number of simulation based studies will be discussed and potential methods for combining techniques will be identified.

2.2 Soil Properties

As this research project is concerned with agricultural land use this section will introduce some key properties of soil which are critical to crop yield, in particular properties related to the availability of water.

2.2.1 Soil Texture

Soil is comprised of four basic components, with the texture being defined by the ratios between these components. The four components are sand, silt, clay and organic matter. However, traditionally organic matter is neglected in determining soil texture. The ratios of soil mineral particles are obtained by observing the particle size distribution (PSD) of a soil sample by sieving the soil to separate the subsequent components. Considering Figure 1, a traditional soil-texture triangle, it can be seen that there are eleven major textural classes, based upon the British Standards system of particle size grading, established by the Soil Survey of England and Wales, 1974 [37]. The texture of the soil is a critical consideration as it can affect drainage, water storage, working properties and crop suitability and can not easily be altered.

Soils with larger pores, such as a sandy loam will drain easily and quickly after an irrigation event, are easily worked and warm up quickly in the spring. However they exhibit a lower moisture-holding capacity than clay soils and therefore require more frequent irrigation. Also in cases where vegetative cover is lacking, they are subject to accelerated erosion. Although clay based soils hold more water, the pore space is much smaller and the work required to extract the water from the pores is much greater.

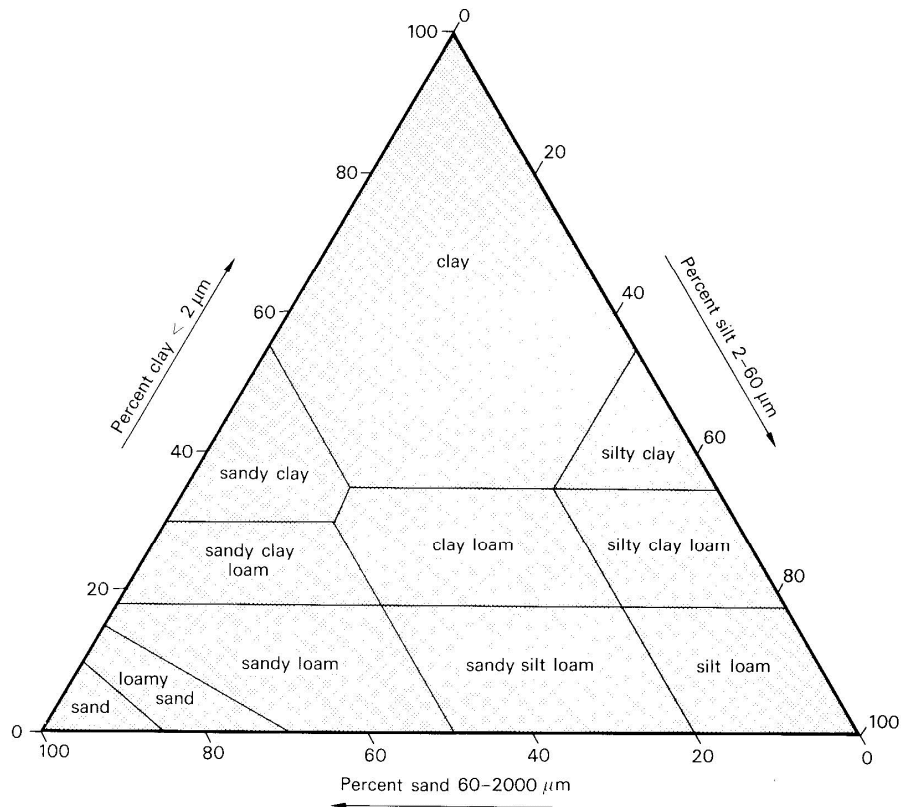


Figure 1. Soil Texture Triangle [37]

2.2.2 Soil Structure

The physical architecture or structure of soil should not to be confused with soil texture. Whilst texture is defined by the particle size distribution of the subsequent mineral particles, structure is defined by the way in which these particles are arranged. Subsequently, it is possible to influence soil structure much more practically than soil texture. The structure of soil is easily altered through external actions. Soil structure “regulates soil aeration and gaseous exchange rates, the movement and storage of water, soil temperature, root penetration and development, nutrient cycling and resistance to structural degradation and erosion. It also “promotes seed germination and emergence, crop yields and grain quality” [38].

2.2.3 Porosity

Pores within the soil are essential for the transmission of air, water and nutrients. They are also highly influential on root penetration. Porosity is defined by the ratio:

$$\text{Pore Space Ratio (PSR)} = \frac{\text{Volume of Pores}}{\text{Total Soil Volume}} \quad (2.1)$$

Since the porosity of a soil varies with water content, the soil moisture content must also be known when determining porosity. Generally pores >60 µm are referred to as macropores whilst pores <60 µm are referred to as micropores.

2.2.4 Hydraulic Conductivity

Hydraulic Conductivity describes the readiness with which a particular soil transmits fluids through its structure. Soils with low hydraulic conductivity are not easily irrigated. Furthermore hydraulic conductivity is non-homogenous and varies with water content. Hydraulic conductivity is highly influenced by both soil texture and soil structure as it depends greatly on both pore size and pore continuity.

2.2.5 Soil Water Content

Soil Water Content is generally defined as the amount of water which can be lost through the heating of soil for at least 24 hours at a temperature of 105°C and is expressed as a percentage, which is determined either on a weight or volume basis, as expressed in the following two relationships:

$$\text{Soil Water Content (\%)} = \frac{\text{weight of water}}{\text{weight of oven dry soil}} * 100 \quad (2.2)$$

$$\theta = \frac{\text{volume of water}}{\text{volume of dry soil}} \quad (2.3)$$

Structural Water is the remainder of water within the soil after oven drying at 105°C has occurred, to extract this water the soil must be heated to 700°C, this would cause detriment to the soil. For this reason, structural water is neglected in the definition of soil water content.

2.2.6 Field Capacity

Field capacity is the maximum level of moisture that may be held via capillary forces within the soil pores, any additional water will drain away freely. A soil sample is said to be at field capacity when it has been saturated fully, i.e. the pore space is completely filled with water and then allowed to drain until the free drainage of water ceases. This occurs when the matric potential equals that of gravitational forces.

2.2.7 Wilting Point

At the wilting point (WP), the degree of tension that the soil exerts on the water within its smaller pores is greater than that which a plant can exert thus the plant is unable to extract the moisture from the soil and will begin to wilt. Thus the wilting point is the minimal level of moisture the plant requires not to wilt. The wilting point is critical to crop health as once the plant begins to wilt it will lose turgor and will not recover even when water is again delivered to the roots. The wilting point is dependent on several factors, such as soil texture, soil structure, the transpiration rate of the plant and the temperature.

2.2.8 Available Water

Available water (AW) is the water content that the plant is able extract from the soil pores and lies in between the field capacity and wilting point. The AW is higher for clay soils, and lower for sandy soils.

2.2.9 The Unsaturated zone

As water infiltrates the soil as a result of rainfall or an irrigation event, air within the pores is displaced. Once all the soil pores are filled with water the soil is deemed to be saturated. Following this infiltration of water gravity draws any water beyond the field capacity down through the soil toward the water table thus the region immediately below the surface is inherently non-saturated and is therefore referred to as the unsaturated zone or the 'vadose zone'. It is in this region that agricultural soil resides and thus this research project focusses on tracking water movement within a non-saturated soil sample.

2.3 Measurement Techniques

A survey of the current literature has shown that there is a need to address and expand upon current approaches to soil moisture and plant water uptake monitoring in order to better understand plant-soil interactions and their subsequent effects on soil moisture content. Various methods exist for soil water measurement and inferring the root water uptake of plants. The two most commonly used are the thermogravimetric method and electrical techniques

[40], such as time domain reflectometry (TDR) and the capacitance method. This chapter will discuss the aforementioned measurement techniques and their applications. In addition some recent measurement based studies will be discussed.

2.3.1 The Thermogravimetric Method

The thermogravimetric method involves extracting soil cores from the field. The sample is then weighed both before and after oven drying. The oven drying process typically takes between 24 and 48 hours at 105°C. Multiplication of the gravimetric water contents and the bulk density yields the soil water content. This method provides a simple and direct measure of soil water content however it is extremely time consuming and is destructive to the site since taking core samples affects the water infiltration rates at, and near to, the sampling points. Despite the disadvantages of this method it remains a standard calibration method due to the high accuracy of the measurement [40]-[42].

2.3.2 Electrical Methods

Non-destructive, electrical techniques such as TDR and capacitance probes are very similar in a number of ways, most notably, the principle of inferring soil moisture content from electrical measurements. Both cases rely on the strong dependence of electrical signals on dielectric permittivity [43]. The dielectric permittivity can be related to soil water content using a calibration curve [44]. These probes can accommodate applications ranging from single point measurements, to larger scale applications where they are deployed en masse in order to determine spatial soil moisture distributions [45]. The way in which the dielectric constant is measured, however, varies between the TDR and capacitance methods.

2.3.2a Time Domain Reflectometry (TDR)

TDR instruments measure the propagation time of a step shaped electromagnetic pulse along a wave guide typically consisting of two or more metal rods [46]. The apparent i.e. composite, bulk dielectric permittivity of the soil can be calculated directly from the propagation time and the length of the rods, assuming that the magnetic permeability of the soil is unity. This is a reasonable assumption since soils rarely contain significant amounts of ferromagnetic components [47]. One major advantage of the TDR method is the need for only one universal calibration equation, such as that developed by Topp et al [36]. Extensive testing has shown this equation to be reasonably accurate for many soils [48]. However its validity has not been demonstrated over a full

range of possible water contents and porosities [47]. One further advantage is the ability to obtain soil water content and electrical conductivity using a single probe [48]. In most applications TDR is simple if the material to be measured can be treated as a low-loss or loss-free dielectric material, however complications occur when TDR is applied to highly conductive or very wet soils, where soil water content exceeds approximately 60% of the soil saturation/field capacity, for example during an extreme weather event, where the dielectric loss factor cannot be neglected [40]. These complications and the relatively high price of TDR probes has led to the development of alternative soil moisture sensors that also exploit the strong relationship between apparent dielectric permittivity and soil moisture content [43]. From a review of the current literature capacitive based probes are the most prevalent example of these alternative sensors.

2.3.2b Capacitance Measurements

Capacitance probes measure the capacitance between two or more metal rods or annular electrodes which are inserted into the ground such that the soil acts as the dielectric layer between the electrodes. The bulk dielectric permittivity can be calculated from the measured capacitance.

Capacitance probes have a number of interesting properties for the instrumentation of automatic soil moisture measurements, most notably the ability to be inserted to the required depth from the surface without disturbing the soil and a simple calibration process. The calibration process consists of establishing the relationship between the signal provided by the probe and the soil moisture content by using a reference method. This relation is actually a combination of two phenomenon. Firstly the relationship between the probes output signal and the soil dielectric permittivity, which may be determined experimentally. Secondly the relation between soil dielectric permittivity and soil water content. This may be determined using theoretical models or empirically [49]. This calibration is non-linear and a marked reduction in sensitivity to dielectric permittivity is found under dry conditions as some of the water is bound to clay particles [50].

Disadvantages of the commercial capacitance probes include a limited sphere of influence. This is limited to the region between the electrodes. The sphere of influence is typically small, maybe only a few cm [50] whereas the sphere for TDR probes has been reported to be up to 8-10cm [51], however, this depends on electrode geometry. In addition, heterogeneity in this sphere of influence may dramatically affect the relationship between the signal provided by the probe and the soil volumetric water content [52].

At lower measurement frequencies the effects of soil type and soil conductivity are prevalent. The result is a requirement for higher excitation frequencies (10-150MHz). This may be a technical challenge, in terms of circuit design and instrumentation, however in use, this serves as an advantage as the probes exhibit some, albeit limited, immunity to soil type and soil conductivity [40]. The result is a simplification of the calibration process. In many cases a single calibration curve may be used for numerous soil types [53]. Using suitable calibration curves soil moisture contents may be determined reliably for greater than 60% soil saturation [54]. Capacitance probes can provide reliable results over the typical range of saturation levels i.e. between 0 and 60% saturation [40].

Temperature sensitivity of the capacitance measurement is not negated by higher measurement frequencies, but may be corrected through data processing. Still, the need for temperature correction may be reduced in many applications due to temperature dampening effect of soil [53]. This is in part attributed to the evaporation of moisture from the soil surface reducing the extent to which soil is warmed. Some warming due to sunlight and elevated ambient temperatures is inevitable.

TDR probes typically cost in excess of £500 and hence do not lend themselves well to larger scale monitoring. Capacitance probes are a more suitable measurement device for large scale monitoring, providing comparable results to TDR probes over typical soil saturation ranges and cost around £200.

2.3.2c Measurement based studies

Initial investigations using the University of Manchester/Syngenta LCT2 instrument [8] suggest that root water uptake may be monitored using electrical impedance imaging [9]. This work compares data for a control pot containing only soil and a seeded pot, both subject to a 12 hour day/night cycle in a controlled growth room with artificial lighting. The data shows a regular, significant and repeatable change in soil impedance at an identical point in the tomographic image reconstructions for both the control and seeded pots. The data for the seeded pot shows a sharp increase in conductivity after a short feed event, followed by a period of stability until the lights come on. At this point there is an apparent draw on the water and nutrients as shown by decreasing conductivity. This continues into the night cycle at a reduced rate due to the inertial nature of the plants transpiration. The control pot feed event results in a sharp decrease in bulk conductivity, this is assumed to be due to run off from the saturated soils. This is followed by a gradual increase and then decrease in the conductivity due to the nutrients in the soil gradually heating and then losing

this heat energy under the glare of the artificial lights. The assumptions made by the research team have been supported through generated electrical resistance tomography (ERT) movies showing the dynamic effects of the root bundles on soil water and nutrient distribution for cross sectional profiles of the experimental soil cores.

Work at the Jülich institute by Koestel et al uses ERT to track the transport of a two different tracers, a chloride solution and the food dye, brilliant blue, through a large soil core [16][17]. The soil column is a sandy loam soil. 212 electrodes are used in a dipole-dipole configuration. The acquisition time is 6 hours and measurements are taken 3 times per day. The images produced clearly demonstrate the distribution of the tracers. A related paper covers the quantitative interpretation of the ERT data, aiming to determine the transport characteristics of four tracer experiments using the same experimental setup [59]. Garré et al, also of Jülich institute, have described the imaging of preferential flows using the same ERT measurement system [18] and more recently to monitor root zone water dynamics [19].

Zimmermann et al [62] presented a laboratory based spectral electrical impedance tomography (EIT) instrument with a general focus on monitoring flow and transport processes in soils and sediments on a laboratory scale. The measurement system operates in the range 1 mHz to 45 kHz and is based on a current injection swapping technique whereby additional measurements are taken with the injection currents reversed. This removes the effects of parasitic current i.e. errors introduced by leakage or excitation currents which flow through impedances between the sample and ground. This eliminates the dependence of measured impedance on the injection currents and the error due to parasitic current flow. Separate current and voltage electrodes are used to avoid phase errors associated with charge-up effects at the electrodes, for a discussion on this phenomena please refer to a short paper by Dahlin [63]. 32 channels are used for current injection and 96 channels for voltage measurement. Current is sequentially injected using different electrode pairs. Unused electrodes are switched off to minimise the load at the current electrodes. The relays are mounted near the electrodes using connectors with integrated relays. The instrument was tested with metallic and biological objects such as raw peeled potato and shown to have high phase accuracy of 1 mrad in the range 1 Hz to 1 kHz; however no results for soils were presented.

A common trend amongst these groups with the exception of Grieve et al. and Garré et al. is a focus on soil moisture content and not directly root water uptake. It is however, possible to infer root water uptake and growth from soil

moisture content measurements but this often requires substantial understanding of the processes involved in the root zone. Ideally, if such effort must be made to understand these processes it may be beneficial to focus on monitoring the root system directly.

Ozier-Lafontaine and Bajazet used a spectral impedance measurement system, in this case to analyse the root growth of a tomato plant [64]. This study describes a method by which root mass is estimated using a simple two electrode system, one placed on the plant stem, and one in the soil amongst the root bundle. The study demonstrated a relationship between root capacitance and root weight, however it also demonstrated some considerable variance based on soil electrode placement. One further concern is that the height of the stem electrode has a considerable effect on the measured impedance; this suggests that great care must be taken when inserting the plant electrode. In addition, the method is semi-invasive and five out of twenty plant specimens were damaged by the stem electrode resulting in unreliable measurement data. An alternative electrode design must be specified for reliable application.

Other higher resolution imaging modalities such as x-ray computed tomography (CT) [65] and magnetic resonance imaging (MRI) [28] have been used in laboratory environments to observe root growth and root water uptake, allowing the visualisation of fine root structures and soil water profiles. However, while offering superior image resolution, they cannot be used in the required capacity (i.e. mass deployment in a field or industrial greenhouse) as the technology is costly ($>£30k$), equipment is large ($>0.5m^3$) and power requirements are very high ($>500W$). The requirement is for a remote instrument that can be deployed en masse; therefore a compromise must be made to reduce size, power consumption and component cost at the expense of image quality. For this reason, electrical impedance imaging techniques are a more appropriate candidate technology.

2.4 Discrete and Coupled Models

In order to infer root water uptake from soil moisture distributions it must be understood how water moves through the soil on the most basic level i.e. in the absence of a root system such that root water uptake can be distinguished from normal transport characteristics. In the unsaturated zone, soil moisture profiles are dynamic and non-homogenous; therefore it is not possible to arbitrarily assume that the difference between two soil moisture profiles is the result of root water uptake. In addition to understanding unsaturated zone flow in isolation, it is essential that the dynamic relationship between root growth, root water and nutrient uptake and the soil moisture profile is understood. This

will facilitate a greater ability to infer the influence that the root bundle has on the soil moisture content, especially in the case where root water uptake measurement is sought from a resistivity or permittivity map, as imaged using electrical tomographic techniques where the fine root structure cannot be visualised. The following sections will include a description of the progress made in the modelling of soil water transport in the unsaturated zone and the developments made in the field of root growth and root water and nutrient uptake and discuss the current state of the art modelling techniques and software packages.

Further to the simulation of soil hydrological processes, as electrical methods are proposed for use in the sensing of the soil moisture distribution, some popular modelling approaches will briefly be discussed for the prediction of electrical fields as influenced by the soil moisture profile.

A number of separate hydrological and electric field simulation techniques will be identified and it is essential that these be coupled in order to carry out a multiphysics simulation. The requirement of the multiphysics simulation is to predict a soil moisture distribution using a hydrological model, and then subsequently the electrical measurements, for example capacitance measured at the surface electrodes, according to the electric field model. These measurements can then be used to reconstruct a permittivity distribution from which the spatial moisture content can be inferred. A complementary discussion on a select number of well established coupling mechanisms between electric field simulation and hydrological simulation will be presented in the latter part of this section. As there is a strong dependence of soil resistivity and dielectric permittivity vs. soil moisture content, as discussed previously, this relationship will be the focus of these discussions.

2.4.1 Discrete Modelling

2.4.1a Soil Transport Modelling

The water unsaturated zone in the earth's crust has been the focus of much scientific study. The movement of water and solutes in this region, also often referred to as the Vadose zone, has been of importance in traditional applications of ground water hydrology, soil physics and agronomy for some time [66]. The search for analytical solutions to model water flow and solute transport continues to be of scientific interest as the nature of soil hydraulic properties renders the governing flow equations non-linear, making it a challenging problem.

Richards' equation is universally considered as the most appropriate mathematical model for unsaturated zone flow. Process based models for the flow of water in the unsaturated zone on the local scale are typically based on Richards' equation [67][68]. The is given by

$$(C + S_e S) \frac{\partial H_p}{\partial t} + \nabla \cdot (-K \nabla (H_p + D)) = Q_s \quad (2.4)$$

where C is specific moisture capacity (m^{-1}), S_e is the effective saturation of the soil, S is a storage coefficient (m^{-1}), H_p is the pressure head (m), D is the vertical elevation (m), t is time (d), K is the hydraulic conductivity (m/d) and Q_s is a fluid source defined by volumetric flow rate per unit volume of soil (d^{-1}).

As the Richards equation is dependent on soil hydraulic conductivity which varies both spatially and with soil moisture contents constitutive relations are required to describe the interdependence of saturation and hydraulic conductivity such as the Brooks and Corey or van Genuchten-Mualem functions [69]. The relationship describing hydraulic conductivity with respect to water content is known as a soil retention curve. This curve must be obtained experimentally via controlled drying, logging both soil tension and moisture contents either using a moisture content probe or gravimetrically throughout the drying period [70].

For many years the Richards equation was applied almost exclusively to homogeneous soils, however, real soil is indeed heterogeneous. An implicit assumption that models of homogeneous soils could provide sufficiently accurate solutions for a heterogeneous soil is often made on the basis that heterogeneity is simply a perturbation that may provide noise but will not alter the basic structure of the solution. However, this has not gone unchallenged and field studies have indicated that soil hydraulic properties are highly spatially variable and a number of modelling studies have shown that the use of average hydraulic properties does not usually reproduce even the average behaviour of a heterogeneous soil [71]. It has been suggested that a dual-porosity flow model results when the Richards equation is combined with a double hump style composite equation for the soil hydraulic properties, for example Othmer et al [72] and Durner et al [73] divided the porous medium into two or more overlapping regions and suggested using a van Genuchten-Mualem type function to describe the soil hydraulic properties for each region.

A number of commercial software suites exist for solving Richards' equation. The HYDRUS 3D software developed by Šimůnek et al [34] is a commercial Microsoft Windows™ based modelling environment for the analysis of water flow and solute transport in variably saturated media. The software package includes FEM models for simulating both two and three-dimensional movement of water and solutes in variably saturated media using Richards' equation. The model includes parameter optimisation algorithms for inverse estimation of soil hydraulic properties and a graphic interface for data pre-processing, generation of finite element meshes and graphic display of results. Another such software suite is COMSOL Multiphysics [74], this software provides a complete modelling environment including definition of geometry, meshing, specifying the physics problem to be solved, solving and visualising the result. COMSOL Multiphysics also includes the ability to interface with MATLAB [75] allowing the import and export of model data and pre/post-processing data. COMSOL Multiphysics features a large number of physics modules which can be coupled, including the Earth Science module for the simulation of water flow and solute transport in variably saturated media including the application of Richards' equation to a user defined geometry [76] and the AC/DC module for the simulation of electric fields and currents.

2.4.1b Root System Modelling (Root Architecture and Uptake)

Simulation of plant growth and root water and nutrient uptake has been an area of high activity for a considerable period of time and some great advances have been made. Modelling of root uptake started in the 1960s with the simulation of mass flow and diffusion of nutrients into a single root represented by a cylinder with a constant radius by solving a simple form of the convection-dispersion equation for a circular geometry [77][78]. This study included only root water uptake, however Nye and Marriot extended the approach in 1969 to include nutrient uptake using a Michaelis-Menten type boundary condition at the soil-root interface [79]. For a more recent extension of this work please refer to the model of Roose et al [80]. In their study they explored the sensitivity of the solution to changes in the equation parameters i.e. the diffusion co-efficient, root absorbing power, soil buffer capacity and nutrient flux at the root surface. Barley further extended the modelling approach to include multiple roots [81] and as a next step Baldwin et al included root competition as a series of linear sinks, considering only diffusion and not mass flow [82]. Alm et al developed and validated a finite element model of the radial and axial conductivities of individual roots for two desert succulents [83].

Advances have also been made in root growth modelling. The earliest simulations of root architecture considered branching patterns of roots axes in two dimensions, according to simple growth rules, such as the analytical model of Hackett and Rose [84][85] and the numerical simulations of Lungley [86]. The first model to explicitly consider three-dimensional root architecture was the ROOTMAP simulation by Diggle [87], which generated age, position and orientation information of root segments over time as a function of root elongation rate and branching intensity, which were implemented as temperature dependant variables. Later models include the works of Pagès et al and Shibusawa [88][89]. Pagès et al's model was an architectural model of maize roots that included geometric and kinetic rules for branching, based on empirical observations. This model permitted the visualisation of a three-dimensional wire view of the root system or alternatively, the visualisation of cross sections as would be seen in a trench excavation [88]. SimRoot developed by Lynch et al [32] was developed to include root radius in addition to the wire-frame views of earlier models. This model is able to model the relationship between root form and its functional properties such as resource acquisition or efficiency.

Coupling of such efforts have enabled the modelling of various root-soil dynamics. Clausnitzer and Hopmans [90] presented a three-dimensional root growth model including the interaction between root growth and soil-water movement while emphasising the effect of soil strength on root architecture. Somma et al [78] expanded this work to include solute transport, nutrient uptake and the interactions between plant growth and nutrient concentration thus providing a tool for studying the dynamic relationship between root architecture and soil. The model simulates the growth and activity of a root system as a function of local soil water and nutrient conditions. The convection-dispersion equation is used to describe solute transport in the soil domain whilst root water uptake is considered as a function of matric and osmotic potential. Nutrient uptake is calculated using Michaelis-Menton uptake mechanisms, which states that nutrient influx, i.e. the amount of nutrients taken up per unit length of root and time, depends on the nutrient concentration at the root surface [91]. Uptake can vary along the root axis and between roots as a function of root age. Doussan [92] presented a new model for the hydraulic architecture of root systems in which a root network is considered as a series of nodes and interconnecting segments. The model is used to calculate the water potential at each of the root nodes from a system of equations expressed in terms of the length of the interconnecting segments, the Xylem conductivity, the water

potential of the surrounding soil, the radial conductivity and the surface area of the interconnecting segments. In this study the root architecture was generated using the root architecture model of Pagès et al [88].

In more recent years a number of realistic root models including meshing functions have been developed and implemented in MATLAB [30][31][93] and FORTRAN 90 [33], respectively. In addition to this, several commercial products such as HYDRUS 3D [34] and COMSOL Multiphysics allow the simulation of soil water transport and in the case of HYDRUS 3D, root uptake in three dimensions.

A realistic root growth model is the basis upon which a realistic root water uptake simulation relies. A number of root growth models have been developed. Leitner and Schnepf [30] describe a Lindenmeyer system (L-system) algorithm which makes it easy to generate 3D geometries of growing root structures.

The root growth algorithm is implemented in MATLAB allowing the generated root structures to be easily coupled with existing MATLAB and COMSOL Multiphysics models. Parameters from literature or experiments can easily be used to define the root system growth criteria such as degree of geotropism i.e. the tendency of roots to grow or bend in the direction of gravitational pull, the branching order, spacing between branches etc. This allows realistic maize root systems to be generated using typical maize parameters that are defined for each order of the root system.

This algorithm, part of a toolbox known as RootBox, also includes meshing functions utilising the MATLAB algorithm Distmesh [94] to mesh the soil around the root system. This allows the root system geometries to be coupled with arbitrary root water and solute uptake models in COMSOL Multiphysics. The software is open source, freely available and intuitive to use.

A related paper by Schnepf and Leitner [31] presents a numerical approach for plant and soil interaction models based on the 3D root geometries generated using RootBox. The paper describes the method by which the soil around the 3D root system is meshed using the MATLAB Distmesh algorithm. Nutrient uptake is modelled at the root surface according to Michaelis-Menten kinetics. Furthermore nutrients are assumed to move within the soil liquid phase due to diffusion only. The model is thus based on the diffusion equation with non-linear flux boundary conditions at the root surfaces and zero Neumann boundary conditions i.e. no fluid enters or leaves at the bounding box. Initial soil conditions are homogenous in the current results; however irrigation events could easily be added. The model is further capable of describing the release of organic compounds into the soil. The solution is computed using the finite

element solver COMSOL Multiphysics for solving the diffusion equation with both linear and non-linear flux boundary conditions at the root surface.

The R-SWMS code, by Javaux et al [33], implemented in FORTRAN 90 and MATLAB simulates water flow in heterogeneous non-saturated soils with plants in three-dimensions using integrated root water uptake and soil water transport models. The R-SWMS code is a numerical model for the prediction of three-dimensional coupled soil-root water fluxes based on the water potential gradient between soil and root nodes with an uptake stress function, which couples the models of Somma et al [78] and Doussan [92]. Water flow is described by the Richards equation with a three dimensional sink term [68]. Water flow within the root xylem and between the soil-root interface and root xylem is solved by discretising the root network as a system of connected root nodes, in accordance with the Doussan model [92]. The model of Somma et al [78] is adapted to solve the soil and root network flow equations for the water potential. These equations are linked by the soil-root radial fluxes. Radial fluxes located in a soil voxel are summarised to provide a local sink term. The root system is generated using the model of Somma et al [78].

The commercial software package HYDRUS 3D discussed previously allows the inclusion of root water uptake models with user definable parameters in the solution of Richards' equation.

COMSOL Multiphysics whilst not including root water uptake as a standard feature has the flexibility to allow the inclusion of root water uptake through user definable physics models as has been shown by Schnepf and Leitner [31]. The ability to: import root structures from a MATLAB based root model, to solve both Richards' equation, and to predict root water uptake using arbitrary root uptake models, makes COMSOL Multiphysics a very flexible and powerful tool.

2.4.1c Electrostatics

The forward problem in electrical tomography is to calculate the potential distribution for a known conductivity or permittivity distribution and then to determine the corresponding voltages measured at the surface electrodes. Electrical properties such as electrical conductivity and permittivity determine the behaviour of materials under the influence of external electric fields. For example conductive materials have a high electrical conductivity and allow both direct and alternating currents to flow, whereas dielectric materials have high permittivities and only allow the passage of alternating currents to flow. The time harmonic electric and magnetic fields satisfy Maxwell's equations. This

model is the most popular electric field model for use in forward problem of electrical tomographic imaging predicting electric fields as a function of frequency [95]. However assuming no free charge conditions i.e. a static electric field, the electric scalar potential, V , between two electrodes mounted on a vessel satisfy Poisson's equation [96]

$$-\nabla \cdot (\epsilon_0 \epsilon_r \nabla V) = \rho \quad (2.5)$$

where ϵ_0 and ϵ_r are the permittivity of free space and the dielectric constant respectively, ρ is the space charge density. The electric field (E) and displacement field (D) can be obtained from the potential gradient

$$E = -\nabla V \quad (2.6)$$

$$D = \epsilon_0 \epsilon_r E \quad (2.7)$$

For the plastic surfaces of the vessel, the conditions of zero surface charge are applied at the boundary as there is zero flow in this domain, thus

$$n \cdot D = 0 \quad (2.8)$$

In practice, the current at the boundary is not known, only the current along some wires attached to the electrodes can be known. Thus, the electrodes must also be modelled [95]. The Gap Model [97] approximates the current density by assuming it is constant at the surface of each electrode and is zero in the gaps between electrodes. This model is simple; however it is not accurate, it provides an overestimate because it ignores the shorting or shunting effect of the electrodes i.e. it ignores that the electrodes themselves provide a low-resistance path for current [97]. A more accurate model is the complete electrode model which takes into account contact impedance which may be caused by electro-chemical effects, which give rise to a thin highly resistive layer at the boundary surface [98].

Commercial products such as ANSYS Maxwell [99] provide the capabilities to simulate electrical fields. However like HYDRUS 3D, assuming the data can be exported, which may not be the case for many commercial products, it must be interfaced with secondary software to couple both electric field simulations with soil hydrological simulations. This may prove difficult and time consuming, both in terms of development time and computation time. COMSOL Multiphysics,

includes solvers for Poisson's equation, Richards equation and additional equations may be implemented by the user. This is advantageous as both electric fields and hydrological scenarios can be implemented in the same environment and interfaced via MATLAB. EIDORS [100] is free software written in MATLAB and available under the GNU license, this software can predict boundary voltages given a conductivity and/or dielectric distribution in addition to offering a number of inversion routines for reconstructing images from experimental or simulated boundary measurement data [101][102]. This software also includes an implementation of the complete electrode model thus taking into account contact impedances at the electrode-medium interface. However this may pose difficulties in taking into account fluid flow. Despite such difficulties, the software may be used as a reference or in conjunction with COMSOL Multiphysics as part of a hybrid reconstruction scheme.

2.4.2 Coupled Models

As previously mentioned in section 2.3.2, the dielectric permittivity of a partially saturated soil matrix varies as a function of water content. The implication of being able to describe this relationship mathematically is the ability to infer the water content in a soil sample via electrical measurement.

Fluid flow and electrostatics models can be coupled via the dielectric permittivity. A dielectric permittivity vs. soil saturation curve must be known; this may be obtained experimentally or predicted using theoretical methods.

A number of methods have been proposed to predict the dielectric constant of water saturated soils. Two of the more popular methods are the Topp model and the Complex Refractive Index Method (CRIM).

The popular empirical model known as the Topp model was developed by Topp et al by compiling data for many soils under varying moisture conditions [103]. This model is given by

$$\varepsilon = 3.03 + 9.3\theta + 146\theta^2 - 76.7\theta^3 \quad (2.9)$$

where ε denotes the effective dielectric constant of the soil mixture and θ denotes the soil water content. Advantages of the Topp model include its applicability to many soils [48]. No soil parameterisation is required [47]. Only soil water content must be known. However it was developed for use with TDR probes and hence is most applicable at >50MHz and its validity has not been demonstrated over a full range of possible water contents and porosities [47].

The complex refractive index method (CRIM) involves using simple mixing laws to calculate the dielectric constant of a material (ϵ_T) given the dielectric constant ϵ_i and the volume fraction (V_i) as given by

$$\sqrt{\epsilon_r} = \sum_i V_i \sqrt{\epsilon_i} \quad (2.10)$$

This can be expanded for the case of a soil sample at a given level of water saturation (θ), where θ is the volume fraction of the pore space that is filled with water, the remainder being filled with air [35]. The system is composed of soil (ϵ_s), water (ϵ_w) and air (ϵ_a). Porosity is given by Φ and the dielectric constant for a given soil saturation level is expressed as

$$\sqrt{\epsilon_T} = (1 - \Phi)\sqrt{\epsilon_s} + \theta\Phi\sqrt{\epsilon_w} + (1 - \theta)\Phi\sqrt{\epsilon_a} \quad (2.11)$$

Assuming that the soil and air components have negligible conductivity, the dielectric constants of both soil and air can be assumed to be entirely real [35][104].

An obvious limitation of both models is they assume localised homogeneity and complete mixing. They also do not take into account electro-chemical interactions amongst the constituent components [35].

The third identified coupling mechanism is relevant for the resistive or wet phase of soil saturation and relates bulk conductivity to soil saturation. The most prevalent method found in the literature is Archie's law [105].

Since most soils are formed by non-conducting materials, Archie's law assumes that the electric currents are mainly caused by ionic content in the pore space rather than through the soil particulate. Originally, Archie's law was valid only for the effective conductivity of a fully-saturated rock or soil, but it can be extended to variably saturated porous media.

Archie's law relates the effective or bulk conductivity to the fluid conductivity σ_L , fluid saturation S_L and porosity ϵ_p :

$$\sigma = S_L^n \epsilon_p^m \sigma_L \quad (2.12)$$

Where, m is the "cementation" exponent, which describes pore connectivity. $m = 1$ represents a volume average of the conductivities of a fully saturated,

insulating porous matrix and a conductive fluid. The saturation coefficient n is normally close to 2. The ratio:

$$F = \frac{\sigma_L}{\sigma} \quad (2.13)$$

is referred to as the formation factor.

As Archie's Law does not take into account the relative permittivities of either the wetting fluid or the solid. The relative permittivity of the porous medium is typically considered to be that of air, 1.

2.5 Parameter Estimation Problems

Parameter estimation problems or inverse problems such as those in the proposed application are often solved using partial differential equation (PDE) models of the system under investigation. Due to the nature of such problems, there is often a lack of data to constrain a unique solution, this is due to the problem being an ill posed and under determined problem. Typically, many parameters are to be estimated from a relatively low number of measurements obtained at the boundary of the region of interest. For example given 16 small electrodes placed around the periphery of a circular vessel, using a dipole-dipole excitation-measurement strategy, there would be 208 possible measurements, taking into account reciprocity, only 104 unique measurements. From these 104 unique measurements an attempt to estimate several thousand parameters may be in order.

Cardiff and Kitanidis propose a framework for the solution of such problems using COMSOL Multiphysics that is applicable to a broad range of physical systems governed by PDE's [106]. Their work utilises a general adjoint state formulation which reduces the computation time of sensitivity matrices in a number of common problems. The work is demonstrated using an example inverse problem concerning the characterisation of aquifers; in particular aquifer transmissivity, their solution is based on pump test data. Given the previously discussed benefits of COMSOL Multiphysics, the ability to solve the inverse problem utilising COMSOL Multiphysics directly and time efficiently is an attractive prospect. However, there is a cost associated with this method, to implement the method of Cardiff and Kitanidis, the "optimisation" toolbox is required. In addition, this method will still suffer from the disadvantages of associated with the inversion step typical of inverse problem solvers. Subsequently, a non-dynamic inversion will be unlikely to provide the required image/parameter estimation fidelity due to the data at each time step being an

inextricable combination of both structural and dynamic information. Time lapse data is more closely linked to the distribution of hydraulic properties thus a time-lapse inversion scheme is desirable.

An alternative approach for utilising the modelling potential of COMSOL Multiphysics in solving the inverse problem, whilst avoiding the typical disadvantages of the inversion step would be to employ statistical methods such as the Kalman filter. In particular, methods such as the ensemble Kalman filter (EnKF). Such methods would avoid the inversion step and associated disadvantages. The EnKF has a sequential structure that is particularly convenient for processing remote measurement data from dynamic systems in real-time. In addition it provides information on the accuracy of the predictions at each time step and it is able to account for a large range of potential model errors [13]. The EnKF moves sequentially from one time step to the next and naturally divides into several distinct steps, most notably a prediction step and an update step. The EnKF workflow can be summarised as follows [13]:

1. Initialisation - The EnKF is initialised according to prior knowledge at of the state at the initial time step. An ensemble is generated around a mean.
2. Forecast - The ensemble is propagated forward in time utilising the prescribed non-linear model.
3. Comparison - As measurement data becomes available, each ensemble member is updated according to the error covariance between the prediction and the measurement.

As the error between measurement data and predicted data converges, the parameters desired may be extracted from the model. One major disadvantage of the EnKF method is that it may require many runs of the 'forward solver' or model to generate an ensemble size that produces a stable solution.

The EnKF method is particularly interesting in applications such as monitoring hydrological conditions and has been demonstrated by Reichle et al [13]. Further to this work, Camporese et al [14] have presented a method combining time-lapse cross-hole ERT data inversion techniques with the EnKF method. In this instance the EnKF is used to relate the dynamic observations of the time-lapse ERT data inversion to local hydraulic properties. Whilst this method allows the spatial soil hydraulic properties to be estimated, typical ERT inversion techniques are relied on for determining the soil moisture content and thus the method is still subject to the limitations surrounding typical inversion

techniques and subsequently local hydraulic property estimations are ultimately limited by the fidelity of the ERT inversion in determining soil moisture content.

Other works such as that of Irving and Singha [109] and Pollock and Cirpka [110] address the uncertainty of traditional inversing methods by introducing fluid flow properties to constrain the reconstruction. Irving and Singha [109] utilise a Bayesian Markov-chain-Monte-Carlo (MCMC) whilst Pollock and Cirpka [110] utilise predictive moment-generating equations with corresponding adjoint formulations for generating sensitivity data and a quasi-linear geostatistical inversion approach.

2.6 Discussion and Conclusions

Based upon the result of the literature search a number of decisions have been made. It has been decided that the Richards equation is the most appropriate soil transport model to use. This model has been extensively tested over the previous 30 years and stands as the most widely used soil transport model to date. There are several options for the implementation and solving of this partial differential equation including bespoke software which may be time consuming to implement or a number of commercial products which may be costly to purchase.

R-SWMS is free software written in FORTRAN 90 and runs in the Linux environment. This software enables the simulation of plant root growth and root water uptake however it does not afford the ability to predict boundary voltage measurements. As a result R-SWMS would need to be used alongside additional software for the simulation of the resulting electrical fields and subsequent boundary measurements. Furthermore, due to the native programming language and operating system on which this code runs, there would be a requirement for familiarisation with the Linux environment and most challengingly familiarisation with the FORTRAN programming language which may be time consuming. In addition, the very large body of code contained in the R-SWMS code, without supporting documentation presents a steep learning curve. The commercially available HYDRUS software however is well documented and runs in the familiar Microsoft Windows environment. However it also lacks the ability to simulate electrical measurements thus suffers many of the same disadvantages as the R-SWMS code, i.e. it would require the use of an additional software package to predict the electrical boundary voltages based on the HYDRUS solution. In addition it is not clear if the meshes or generated data can be exported in a format suitable for use in electrical simulation or to be post-processed as required. If the data can be exported, there is still the need for intermediate software to couple the hydrological simulation to an electric field simulation.

Furthermore the cost associated with HYDRUS 3D ranges from approximately £1200 (2012) for HYDRUS 3D Lite to £1930 (2012) for HYDRUS 3D Professional, in all cases, the cost is given for a single licence. This is relatively costly since additional electric field simulation software must also be sourced. Software by ANSYS was considered for electric field simulation however the same limitations as with HYDRUS apply regarding importing/exporting of data and the potential for relatively complicated methods being required for physics coupling. COMSOL Multiphysics costs approximately £3580 (2012) including both the AC-DC module and the Earth Sciences module allowing the simulation of both electric fields and soil hydrology respectively, whilst allowing the user to import and export pre/post-processing data without the need for additional software. In addition COMSOL Multiphysics interfaces with MATLAB via the included LiveLink™ for MATLAB module allowing post-processing of generated data, editing and visualisation within the popular MATLAB environment. MATLAB is already available on the current workstation and is widely used in both research and academic institutions thus the developed techniques may propagate efficiently within the scientific community where appropriate. The COMSOL Multiphysics earth science module allows the solution of Richards' equation for user defined geometries and this module can be coupled easily with the AC-DC module for the solution of Poisson's equation with no requirement for any interfacing software to be written. This enables the simulation of electrical fields with respect to predicted soil moisture distributions in a computationally efficient way and with relative ease of implementation.

Subsequently it has been decided that despite a substantial setup cost, COMSOL Multiphysics is the most advantageous software suite to use for the modelling of soil moisture distributions as interrogated by electromagnetic techniques such as EIT. There are five distinct advantages of this software:

- 1) COMSOL Multiphysics includes both a FEM Richards Equation and Poisson's equation solver; hence there is no need to implement the solvers for the chosen models.
- 2) Multiphysics coupling between soil transport models and electrostatics models is possible within one software package using the Topp, CRIM or Archie's equations, hence eliminating the need for any software development to couple two independent software packages. This reduces both development time and also potentially computation time.
- 3) In the future, RootBox may be used to generate realistic root growth structures; this software includes meshing functions to mesh the soil

domain surrounding the root structure. This mesh can then be directly imported into COMSOL Multiphysics where soil transport models and root water uptake models can be solved for the mesh.

- 4) Both COMSOL Multiphysics and RootBox can be called from the MATLAB interface allowing interaction between RootBox and COMSOL Multiphysics. Subsequently, simulated data may be processed and interpreted in the MATLAB environment. This enables the use of data processing algorithms implemented in MATLAB such as those included in the EIDORS software to be applied to the simulated data. Figure 2 shows the way in which the individual elements of the system may be integrated.
- 5) The COMSOL Multiphysics software is flexible and allows the user to script many equations that are not available by default in the purchased toolboxes and also to automate processes such as electrical excitation and measurement patterns.

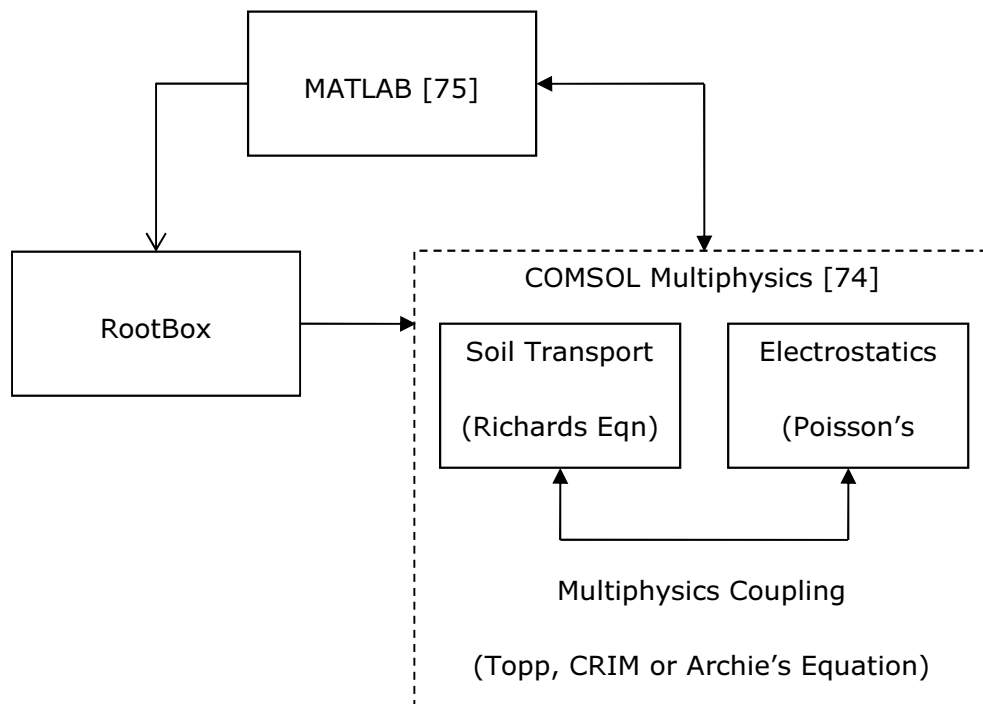


Figure 2. Integration of soil transport, root growth and electrostatics models.

The coupling mechanisms will be investigated experimentally, where appropriate and the most accurate model used for coupling the soil transport models and electrostatics models will be implemented.

The EnKF will be investigated in some depth with the aim to implement a model based, statistical parameter estimation scheme that will utilise knowledge of the soil medium via modelling within COMSOL Multiphysics to improve the fidelity of “reconstructed” images and data. This method will not provide traditional “reconstructions”, the model will itself converge to represent the observed fluid distribution.

2.7 Summary

As a result of the current literature it is clear that tomographic techniques are most appropriate for inferring the 3D spatial moisture distribution on the lysimeter scale, i.e. around the root zone of a maize plant as contained in a cylindrical vessel of 3-6 litres in volume. In particular electrical tomographic methods may excel in the field of in-situ monitoring of crops due to relatively low power requirements, instrument size and component costs hence allowing mass deployment in the field or industrial greenhouse environment.

The relative strengths of the capacitance probe, i.e. low cost, simple calibration and the ability to make accurate measurements over a typical range of soil moisture contents, suggest that it may be a beneficial addition and/or alternative to typical geophysical tomographic techniques such as ERT. Most notably it may be beneficial to implement an ECT system typical of two-phase flow monitoring applications [111], as opposed to a typical geophysics ERT system. This may avoid issues associated with loss of contact between the electrodes and the medium due to soil shrinking and negate the effect of a poor conductive path between electrodes in dry soils while still providing measurements up to and possibly exceeding 60% soil saturation. The disadvantage of a small sphere of influence associated with typical capacitance probes will not occur with a typical ECT sensor array.

A preferable approach would be to measure both resistance and capacitance to implement an EIT instrument. This would enable the measurement of complex impedance and hence allow for correction of conductivity effects, potentially negating the need for higher measurement frequencies, although this will increase component costs over measuring only one component of impedance. Primarily the research will focus on the utilisation of the LCT2 instrument as described previously; however the developed techniques will take into consideration the potential benefits of ECT and in particular complex impedance EIT imaging.

Richards’ equation is universally accepted as the governing equation for soil water movement in the unsaturated zone and a number of software suites for the solution of this problem have been identified, these software suites

include R-SWMS, HYDRUS 3D and COMSOL Multiphysics. It has been noted that COMSOL Multiphysics has a more extensible architecture allowing the user to import/extract model data and post-processing data, there is no certainty that HYDRUS will allow this and R-SWMS lacks documentation and support.

Recent developments in coupled root water uptake and root growth modelling include the models R-SWMS as mentioned above and the L-system based root growth model RootBox. R-SWMS solves the Doussan model and includes root water uptake in the solution of Richards' equation by including a volumetric sink term. R-SWMS is written in FORTRAN with little documentation or support and hence exhibits a steep learning curve. On the other hand RootBox is implemented in the popular programming language MATLAB and includes meshing functions for meshing the soil domain around the generated root structure. The generated mesh can be imported into COMSOL Multiphysics and coupled with arbitrary root water uptake and soil transport models.

For the prediction of EIT measurement data, two potential models have been identified, these include the full Maxwell equations and the Poisson equation. The full Maxwell equations allow measurement frequency to be taken into account; this is advantageous as dielectric permittivity is frequency dependant. However Poisson's equation is a simpler model and is valid for electrostatic measurements. Both solvers for electrostatics and quasi-statics are included in the COMSOL Multiphysics AC-DC module. This offers the advantage of allowing electric field simulation using the same software as used for the soil hydrology simulation.

Three well documented coupling mechanisms have been identified, i.e. the Topp model, CRIM equation and Archie's law. These equations will be tested in order to determine the best match to experimental data; however the initial impression is that the CRIM equation is more suitable for describing dielectric permittivity since it allows the parameterisation of the soil to be included in the prediction of dielectric constant vs. soil saturation curve. Archie's law will be used to describe the link between bulk conductivity and water content.

Statistical methods and/or iterative parameter estimation techniques such as the EnKF offer distinct advantages over traditional inversing techniques, particularly for the study of dynamic processes. As such statistical methods in particular the EnKF will be utilised to negate the need for traditional inverse techniques. The disadvantage of this method however is the potentially large number of ensembles that may be required to produce a stable solution.

3 Forward Problem

The forward problem refers to the prediction or simulation of boundary voltage measurements and is an essential step in inverting experimentally obtained boundary voltage data. In this case the prediction of electrical measurements on the boundary requires the consideration of fluid dynamics in a non-saturated porous media in addition to the traditional electrical field prediction step. Multiphysics simulation allows the relationships between these different physics backgrounds to be coupled hence providing a means by which the modelling of numerous physical processes can be combined. It is anticipated that introducing the consideration of fluid dynamics, via modelling the time evolution soil moisture distribution profile, into the reconstruction process, will enable soil water content and other soil parameters to be directly estimated from the time varying conductivity distributions using either:

- Constrained traditional inverting algorithms
- Statistical methods (such as the Kalman Filter)
- A hybrid method integrating both traditional and statistical methods

This chapter will present and discuss the validity of the individual elements required in the formulation of the forward solution. Various models will be presented and simulated data is compared with both experimental and analytical data.

Furthermore, 3 coupling mechanisms are evaluated. In doing so, simulated electrical conductivity data based on a bulk conductivity value predicted using Archie's law and simulated capacitance data, based on the dielectric permittivity predicted by the Topp and CRIM models are compared with experimental data.

Finally, a multiphysics based forward solver will be presented with a basic demonstration.

3.1 Fluid Flow

The Richards equation governs the saturated-unsaturated flow of water in non-swelling soils [117] and is given by

$$(C + S_e S) \frac{\partial H_p}{\partial t} + \nabla \cdot (-K \nabla (H_p + D)) = Q_s \quad (3.1)$$

where C is specific moisture capacity (m^{-1}), S_e is the effective saturation of the soil, S is a storage coefficient (m^{-1}), H_p is the pressure head (m), D is the vertical elevation (m), t is time (d), K is the hydraulic conductivity (m/d) and Q_s is a fluid source defined by volumetric flow rate per unit volume of soil (d^{-1}).

Richards' equation allows the soil water distribution at a given time to be predicted. Figure 3 is an example soil water distribution obtained from the solution of the Richards equation for a rectangular soil geometry of dimensions 130mmx120mmx15mm with a centrally located point fluid source as simulated using the COMSOL Multiphysics Earth Science module. The soil retention characteristics and saturated hydraulic conductivity in this example were chosen arbitrarily.

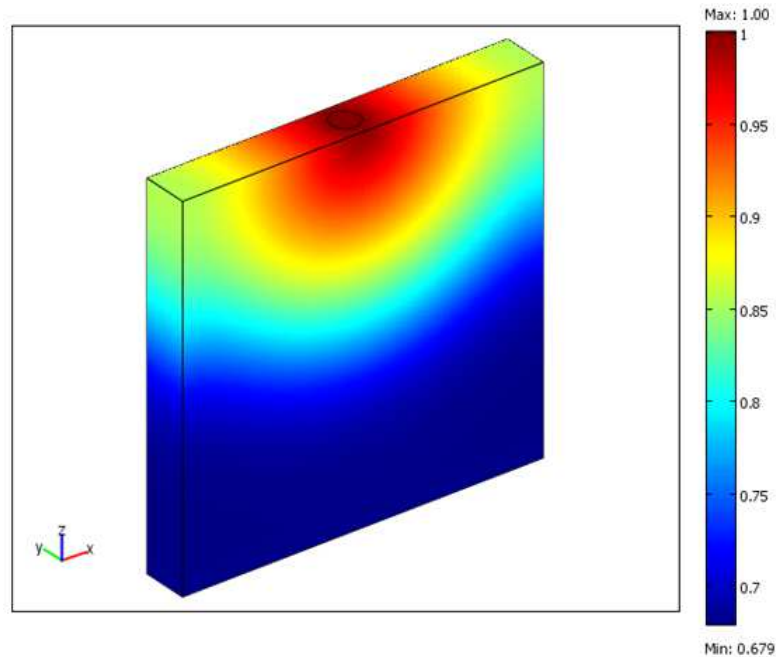


Figure 3. 3D Simulated soil water distribution at a time, t , for a point injection.

Root water uptake can be included in the Richards equation via a sink term. If a root network is considered as a series of nodes and interconnecting segments, the Doussan model can be used to calculate the water potential at each of the root nodes from a system of equations expressed in terms of the

length of the interconnecting segments, the Xylem conductivity, the water potential of the surrounding soil, the radial conductivity and the surface area of the interconnecting segments [118].

3.1.1 Qualitative Analysis

Initial soil transport simulations were carried out for a rectangular soil core with a point water source located in the centre of the top surface. The rectangular geometry was selected as it allows the spread of water to be recorded visually in the experimental case. The simulated moisture distributions were then compared to digital video of a wetting front incident on an experimental soil core of the same dimensions. In the case of the simulation the boundary conditions on the soil surface were chosen such that no evaporation effects would be modelled as given the time scale of the experimental case evaporation effects would be negligible. Similarly the bottom surface was set such that no drainage effects would be simulated since the experiment would be stopped when the wetting front reached the bottom of the vessel. The purpose was to qualitatively evaluate the solution to the Richards equation solution using COMSOL Multiphysics Earth Science Module. The shape of the incident wetting front and the ratio of wet to dry soil was evaluated visually. Absolute saturation values were not considered as these were not able to be evaluated visually for the experimental case.

The soil parameters entered in the model were estimated using typical parameters for the given soil texture. For the experimental case, the soil was packed in such a way as to best achieve a uniform packing density. This was carried out by sieving the soil to create a very fine texture, the soil was then loosely poured into the vessel in stages, filling the vessel in approximately 5cm increments, tapping the vessel onto a hard surface 10-15 times for each 5cm layer of soil.

The results of the experiment showed that the solution to the Richards equation was, visually, in good agreement to the observed wetting front and the progression of the wetting fronts were well time matched. It was noted that the experimental wetting front exhibited a very well defined transition from dry to wet soil. A comparison between experimental data and the simulated wetting front is shown in Figure 4. For the time steps in Figure 4 the area of wetted soil volume for both the simulated and observed wetting fronts was estimated by eye. The data was normalised to take into account the different aspect ratios of the two images for each time step and the average error between simulated and observed data was calculated to be less than 10%. The error observed increased as the wetting front progressed further through the soil core, this is likely due to

an unavoidably greater level of soil compaction at the bottom of the vessel. Any discrepancies between the shape and rate of progress of the simulated and observed wetting fronts are attributed to the varying spatial compaction in the experimental case, as despite all efforts to create a uniformly packed soil, it is unlikely that a homogenous packing density was indeed achieved. Furthermore the error in the estimated soil parameterisation would have contributed to this error. The extent of this error may be reduced by prior parameterisation of a sub-sample of the soil sample being observed.

This experiment shows that the solution to the Richards equation can be used to accurately simulate a wetting front incident on a soil sample given relevant soil parameters. In the worst case scenario i.e. where no soil parameterisation is available the parameters may be estimated using iterative parameter estimation techniques based on an observed wetting front as evaluated visually. The following sections will document the parameterisation of a soil sample experimentally in order to obtain accurate soil hydraulic properties which can then be entered into the simulation in order to provide a more accurate prediction of fluid flow. The following will be discussed, soil texture, saturated hydraulic conductivity and soil water retention characteristics and subsequently, the Van Genuchten parameterisation, as derived from the soil water retention curves.

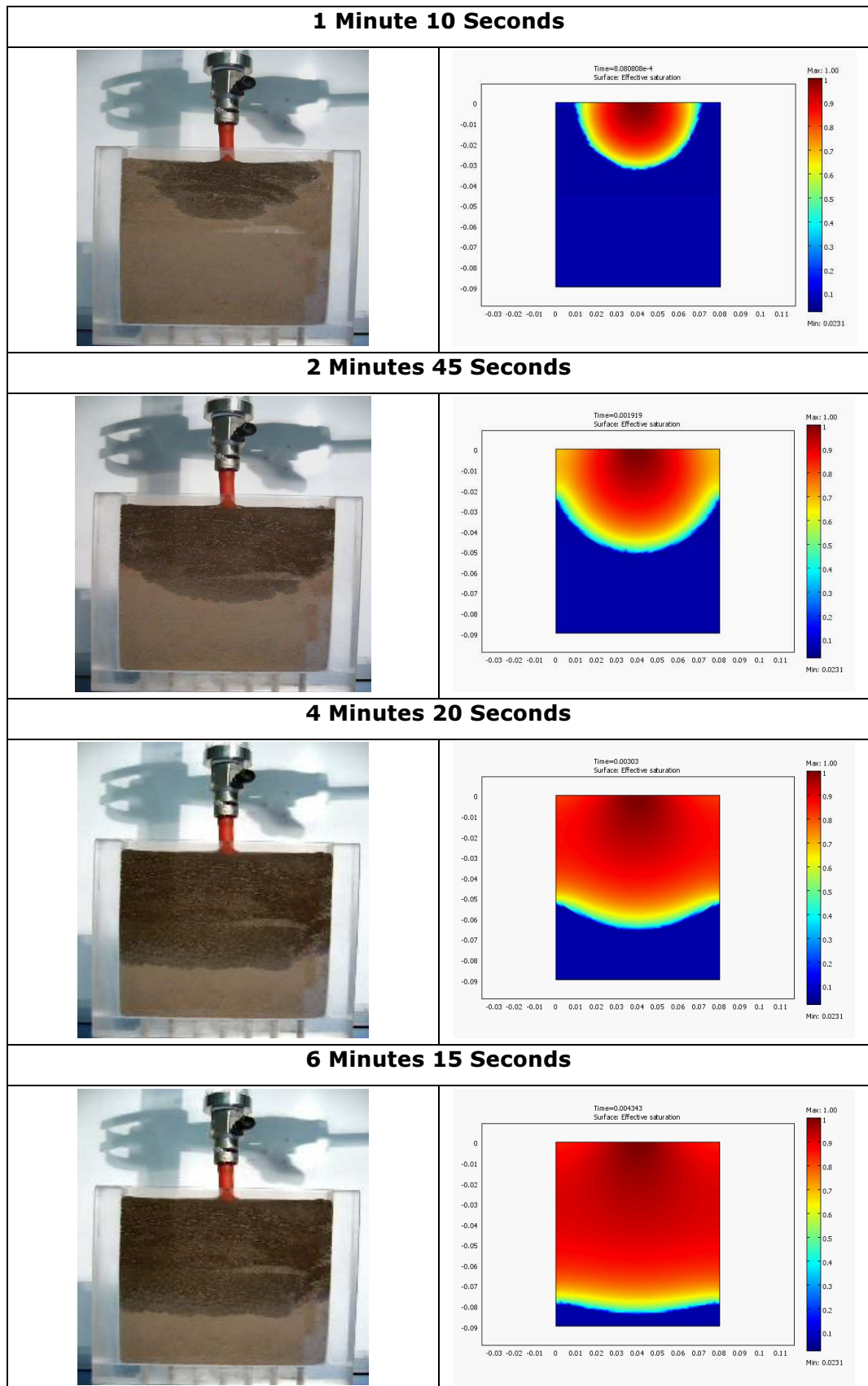


Figure 4. A comparison between experimental and simulated wetting fronts incident on a rectangular soil core from a point injection under atmospheric pressure.

3.1.2 Soil Texture

The soil-texture triangle shown in Figure 1 demonstrates a method by which soils are classified based on the ratio of the constituent components sand, silt and clay. It can be seen that there are eleven major textural classes, based upon the British Standards system of particle size grading, established by the Soil Survey of England and Wales, 1974 [119]. The texture of the soil is its most important property. A soil sample may be classified by using increasingly fine sieves to sift through soil and separate the constituent components thus allowing the ratio of each to be obtained. The soil-texture triangle can then be employed to determine which of the 11 soil classes the particular sample belongs to.

Each type of soil has very different qualities and can vastly affect the growing conditions for crops. Soil texture can affect drainage, water storage, working properties and suitability for the growth of crops. For example, soils with larger pores, such as a sandy loam, will hold less water than a clay soil but plant roots will more easily be able to extract the available water than for a clay soil, a sandy loam will also drain more quickly. Conversely a clay soil can hold more water but the suction required to extract this water is much greater. As stone and other large particle content increases within a soil sample it can hold less water, making crops more susceptible to drought.

Approximation of Soil Texture through Sedimentation in a Glass Jar

An alternative method by which soil texture may be approximated is by observing the sedimentation process within a glass jar. This involves mixing a sample of sieved soil and water in a jar and then allowing the medium to settle. It is anticipated that the sedimentation process will cause the heavier/denser particles, i.e. sand to settle at the bottom, with the lighter soil particles sitting above the sand. A measurement taken of the depth of sediment layers would provide an approximation of the ratio of sand, silt and clay within the soil.

400g of sieved soil and 800 ml water were added to a 1000ml beaker. The contents were stirred for 5 minutes, to try to create a homogeneous mixture within the beaker. The contents were then left to settle for 18 hours. In order to approximate the soil texture, the sediment layers, as shown in Figure 5, were measured with a ruler and the ratio between sand, silt and clay particles was calculated.

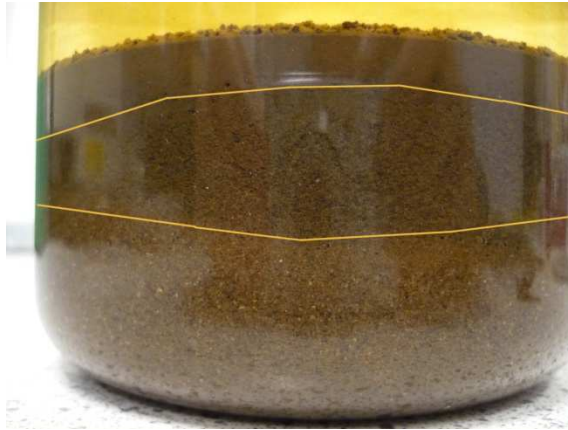


Figure 5. Particle layering following sedimentation

Using a ruler to measure the ratio of sand, silt and clay it was found that the total soil was found to be approximately 4.8cm from the bottom of the beaker, to the top of the clay layer. The sand layer was measured to be 2cm, silt 2cm and clay 0.8cm. Therefore, the soil texture is made up from approximately 42% sand, 42% silt, and 16% clay [38]. According to the soil texture triangle the soil sample falls into the sandy silt loam category.

3.1.3 Saturated Hydraulic Conductivity

Saturated hydraulic conductivity is a quantitative measure of a saturated soil's ability to transmit water when subjected to a hydraulic gradient. It can be thought of as the ease with which pores of a saturated soil permit water movement. Darcy's law describes the one dimensional movement of water through soil under saturated conditions and can be expressed as:

$$J = -K_s i \quad (3.2)$$

Where saturated hydraulic conductivity (K_s) is a constant of proportionality that defines the linear relationship between the two variables flux (J), i.e. the quantity of water moving in the direction of, and at a rate proportional to, the hydraulic gradient through a cross sectional area per unit of time, and hydraulic gradient (i). Solving Darcy's equation for K_s yields the saturated hydraulic conductivity.

Hydraulic gradient describes the effectiveness of the driving force behind water movement and is defined as:

$$i = \frac{\Delta H}{l} \quad (3.3)$$

Where ΔH is the change in total water potential between the inflow and outflow in the soil core and l is the distance between the inflow and outflow. Hydraulic head represents soil water potential. The hydraulic gradient is the difference in total hydraulic head per unit distance. For saturated flow the two primary driving forces are the submergence component of pressure head and the gravitational head. Thus, total soil water potential, also known as total hydraulic head (H), can be expressed as:

$$H = H_g + H_p \quad (3.4)$$

where H_g is the gravitational head and H_p is the pressure head due to submergence. For a soil core encased in a vessel as shown in Figure 6 there is both a constant cross-sectional area and a one-dimensional vertical saturated flow. Total hydraulic head at both the inflow ($H_i = H_g + H_p$) and outflow ($H_o = 0$) are determined relative to the plane of outflow. The total head difference ($\Delta H = H_i - H_o$) between the inflow and outflow is the driving force for water flow. The effectiveness of this driving force depends on the distance (l) between the inflow

and outflow. An increase in the total head difference or a decrease in the distance (l) increases the hydraulic gradient. The result is an increase in flux or flow rate. Variations in H_p can regulate flux. Increasing H_p increases the hydraulic gradient, which in turn increases flux.

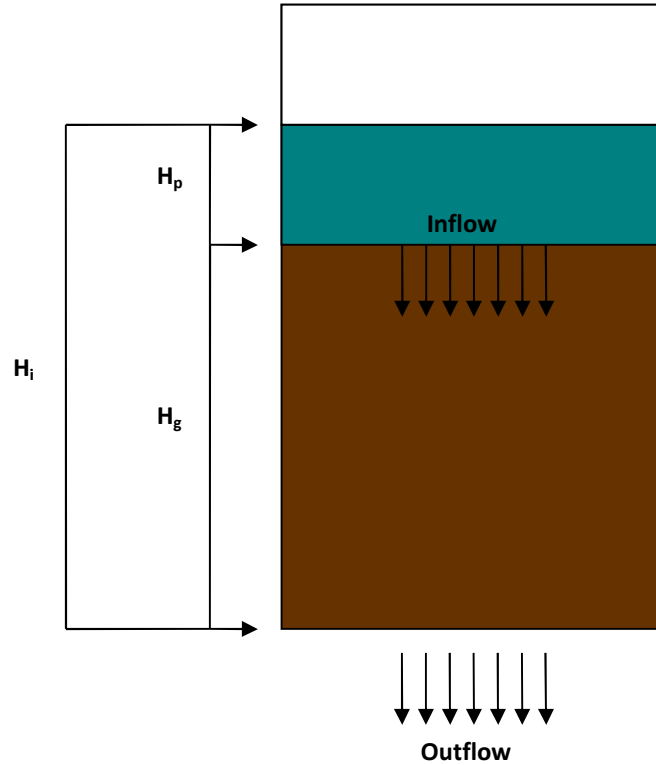


Figure 6. Diagram of the variables involved in the determination of the hydraulic gradient.

If the same hydraulic gradient is applied to two soils, the soil from which the greater quantity of water is discharged i.e. the highest flux is the more conductive as it will exhibit the greatest flow rate.

In order to ascertain the saturated hydraulic conductivity for a soil sample, the flux must be measured experimentally. This can be done by measuring the outflow from a soil sample contained in a uniform vessel over a known period of time. A constant head of water must be maintained at the inflow. If the surface area of the soil is known the flux can be calculated from the following expression:

$$J = \frac{Q}{At} \quad (3.5)$$

Where the Flux (J) is the quantity of water (Q) moving through a cross-sectional area (A) per unit of time (t).

Additional soil water potentials may appreciably influence water flow under specific conditions. The most notable is the matric potential, a pressure component attributed to soil matrix capillary and adsorptive forces. Matric head is also called tension or suction. Matric head is an important factor in unsaturated flow and imparts a negative pressure head value. However for the case of saturated flow this force need not be considered as all pore available space will be occupied by water, in the subsequent section regarding soil water retention characteristics, this will be discussed in more detail.

Standard Operating Procedure for Saturate Hydraulic Conductivity Measurement

A core of sieved, oven dried soil was contained in a tall acrylic vessel providing a soil core of approximately 15.3 cm in height with a diameter of 7cm as shown in Figure 7. The base of the vessel allows water to flow out uninhibited while keeping the fine particles of soil within the vessel.

This soil core was then subject to a wetting procedure using a Heidolph PD5001 pump drive such that the soil reached saturation with minimal disturbance to the surface. This wetting procedure was recorded using a Panasonic Lumix DMC-L570 7.2 megapixel digital camera. Once the soil had reached a state of saturation, the inflow was regulated to balance a simple overflow mechanism such that the head of water remained constant. This head of water was then measured.

Once the head of water had stabilised and the soil was saturated, the amount of water collected from the outflow over a period of 15 minutes was measured. From this the flux can be calculated using equation (3.5). The hydraulic gradient can be calculated based on the fill level of the soil and the height of the head of water using equation (3.3). Darcy's law, i.e. equation (3.2), is then solved yielding the saturated hydraulic conductivity for the soil sample.



Figure 7. Experimental setup

Initial Tests

Two soil cores of differing levels of compaction were subjected to the standard operating procedure. Soil 1 was non-compacted. Soil 2 was compacted by dropping the vessel onto a hard surface 15-20 times. The saturated hydraulic conductivity of the soil cores was then compared.

The resulting experimental data is plotted in Figure 8, as expected the least compacted soil yields a higher flux than the compacted soil for the same hydraulic gradient and hence exhibits the highest saturated hydraulic conductivity. This is due to the larger fraction of pore space in a non-compacted soil core. The results of this experiment show that for a greater level of compaction, saturated hydraulic conductivity is reduced; this is due to reduced pore size. The data for these initial experiments is lacking in data points, so cannot be used to accurately parameterise the soil cores, however the results demonstrate that the experimental setup can distinguish between the hydraulic conductivity of two soil cores with mildly varying levels of compaction.

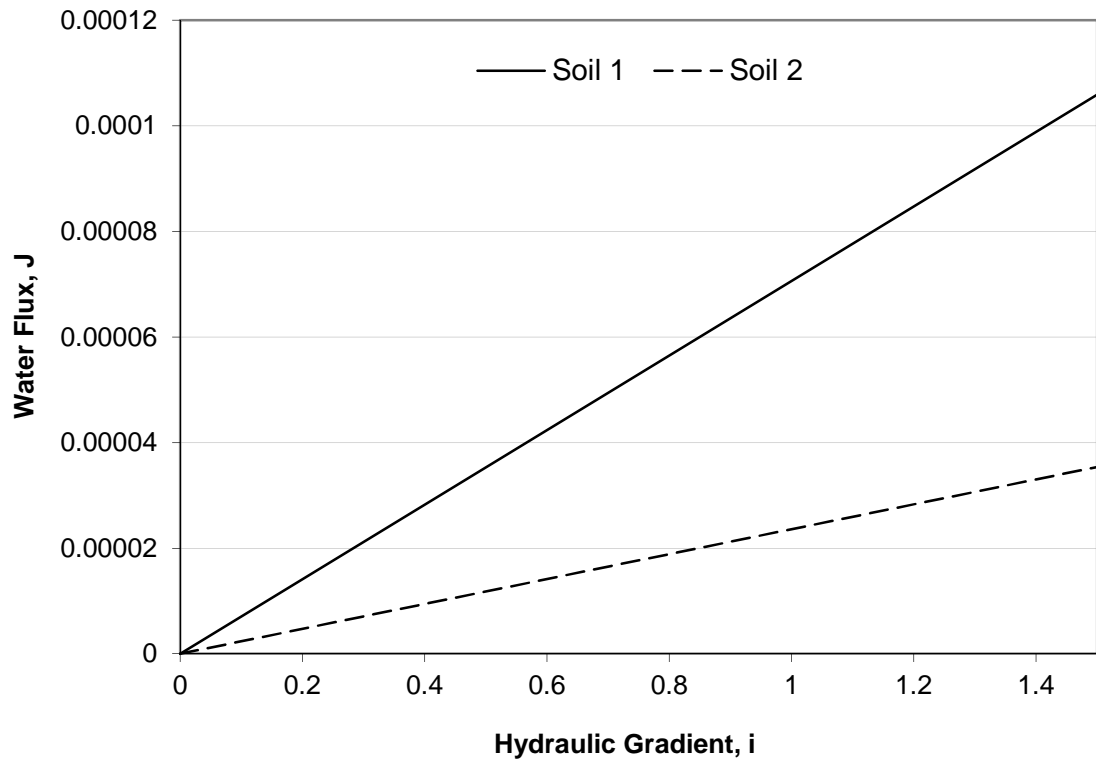


Figure 8. A plot of Flux against Hydraulic conductivity for both compacted and non-compacted soil cores.

Varying Hydraulic Gradients

To better estimate the saturated hydraulic conductivity for a given soil core, it is beneficial to measure the flux for varied heads of water. The flux vs. hydraulic gradient plot should exhibit a linear relationship. As stated by Darcy's law, the saturated hydraulic conductivity is given by the gradient of this curve.

With the experimental equipment in Figure 7, four different hydraulic gradients are achievable. To measure the flux for a number of hydraulic gradients, the standard operating procedure was repeated. After the initial 15 minutes the water collected was measured and then emptied. The water level was then increased by selecting the next overflow valve. The water level then increases until level with this overflow valve and stabilises. Once the water level was stable, the height of the head of water was measured. Then the amount of water collected over 15 minutes was measured as before.

This process was repeated two more times for the remaining two possible heads of water. Following this measurement, the same process was repeated in descending order with decreasing heights of water. This ensured that any compaction or particle rearrangement in the soil due to the head of water was observed. It was anticipated that this progressive compaction or particle

rearrangement as the head of water was increased would result in non-linearity in the flux vs. hydraulic gradient curve. The descending measurements were expected to result in a more linear relationship and provide a measure of repeatability. The effect of compaction was able to be evaluated in parallel with the effect of varying hydraulic gradients.

As anticipated, measurements of flux for varying hydraulic gradients exhibited a non-linear relationship as the hydraulic gradient was increased as described above. This suggests that as the water level is increased some compaction or particle rearrangement occurs in the soil core. When measurements are repeated in a descending order a much more linear relationship is observed. The second plot for a decreasing water level provides the most accurate measurement of saturated hydraulic conductivity. Figure 9 shows the typical characteristics observed for varying hydraulic gradients. From the results of this experiment the saturated hydraulic conductivity for the soil was estimated to be between 1.1 and 1.85. Poor repeatability is observed, most clearly on the ascending measurements, this is likely due to increasing levels of compaction due to particle rearrangement as the head of water is increased.

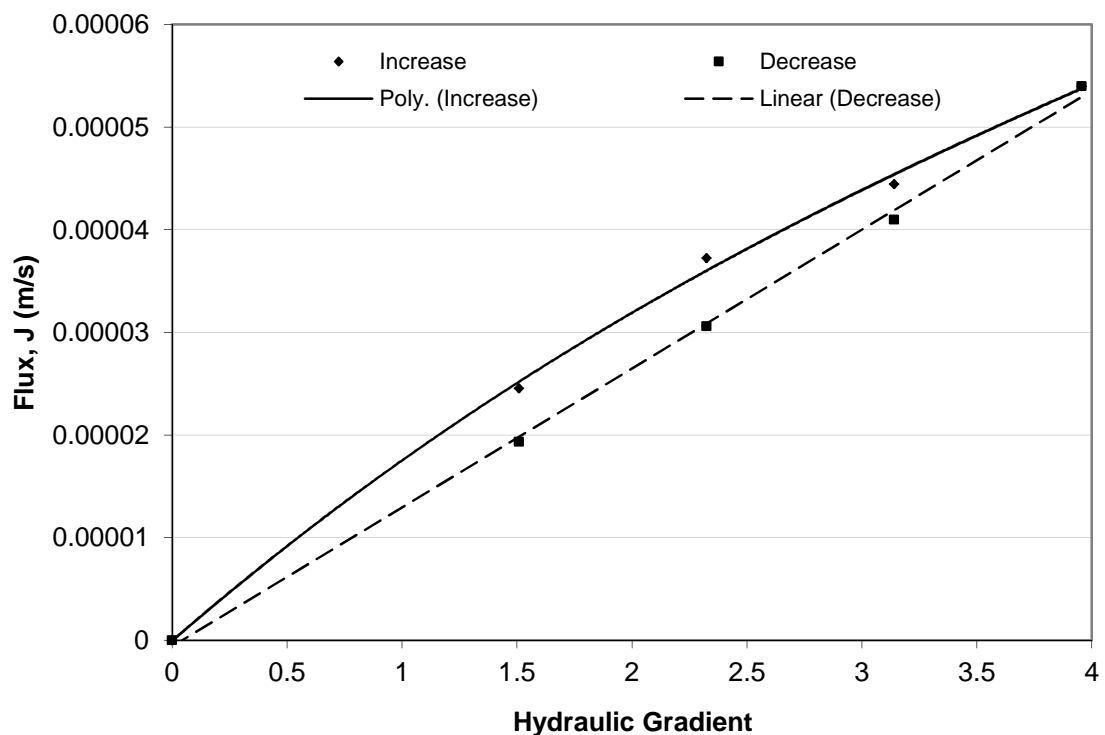


Figure 9. A plot of Flux against Hydraulic conductivity for both increasing and decreasing hydraulic gradients.

Repeatability Testing

6 different soil cores with approximately equal levels of compaction were subjected to the standard operating procedure. The saturated hydraulic conductivities were be calculated and compared; the results are presented in Table 1. It is clear from these results that there is considerable inconsistency between the obtained results. This is likely due to random nature of the arrangement of soil particles at the filling stage, i.e. soil packing may not be uniform between experiments or may be affected by moving the apparatus. The standard deviation was calculated to be 0.48.

Table 1. Repeatability Testing Data

Soil Height (m)	Water Height (m)	Water Collected (ml)	Hydraulic Gradient, i	Water Flux, J (m/s)	Saturated Hydraulic Conductivity, k (m/d)
0.1533	0.078	142	1.508806262	4.09977E-05	2.347686692
0.1533	0.078	85	1.508806262	2.45409E-05	1.405305414
0.1533	0.076	131	1.495759948	3.78219E-05	2.184714381
0.1533	0.078	67	1.508806262	1.9344E-05	1.107711326
0.1533	0.078	112	1.508806262	3.23362E-05	1.851696546
0.1533	0.078	93	1.508806262	2.68506E-05	1.537569453

Wetting Phase: Video to Simulation Comparisons

For each soil core used, the wetting phase was recorded using a Panasonic Lumix DMC-L570 digital camera to record the progression of the incident wetting front. The measured saturated hydraulic conductivity for each soil core was then substituted into a FEM implemented in COMSOL Multiphysics and the Richards equation solved to simulate the wetting front.

A comparison between simulated and observed wetting fronts was carried out. For the case in Figure 10 the saturated hydraulic conductivity was measured as 2.35 m/d. The progression of the simulated wetting front had an estimated average error of 11.1% relative to the observed wetting front.

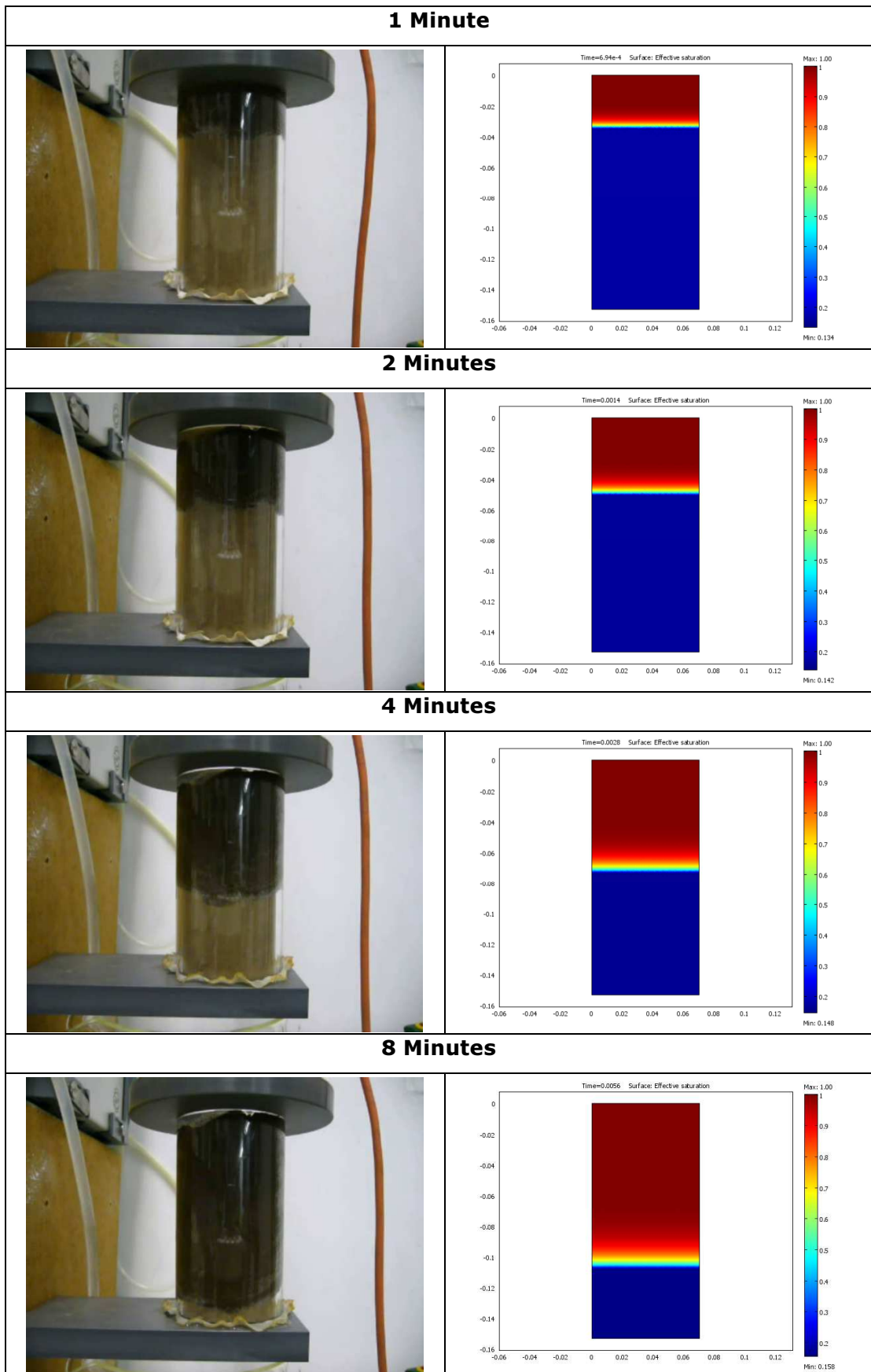


Figure 10. A comparison between experimental and simulated wetting fronts incident on a cylindrical soil core.

3.1.4 Soil Water Retention Characteristics

The Richards equation (3.1) used to predict fluid flow in a soil core is influenced by soil hydraulic conductivity which varies both spatially and with soil moisture contents. The relationship describing hydraulic conductivity with respect to water content is given by a soil retention curve. This curve must be obtained experimentally via controlled drying, logging both soil matric potential, or tension and moisture contents, either using a moisture content probe or gravimetrically, throughout the drying period. Having obtained the experimental data over a drying period of approximately 14-25 days as dictated by the soil texture there are two well established models in the literature that can be fitted to this characteristic curve to describe the soil hydraulic behaviour mathematically. These two equations are known as the Brooks and Corey model and the Van Genuchten equation [69]. Soil retention curves can typically be described by one or both of these models, the model best suited is dependent on individual soil structure.

The van Genuchten equation describes the variation of hydraulic conductivity, with water content and is given by

$$K = Se^l \left(1 - \left(1 - Se^{\frac{1}{m}} \right)^m \right)^2 \quad (3.6)$$

where $m=1-1/n$ and l , m and n are fitting parameters and vary according to soil type.

In this study, it is assumed that the spatial variation of hydraulic conductivity is negligible, this is not truly the case in the field, however in the laboratory, soil is sieved and packed according to an established workflow thus spatial variation of compaction and other influencing factors such as the inclusion of rocks, roots or large lumps of soil is minimal. This assumption can be validated by placing more than one tensiometer in the same soil core at 2 alternative locations and observing the output, presuming the difference between both instruments outputs is acceptably small, spatial variation of hydraulic conductivity may be neglected.

Once one or both of the chosen models have been fitted to the data, the fitting parameters can then be entered into the fluid flow simulation implemented using COMSOL Multiphysics finite element modelling package. The experiment and fitting process must be repeated for each new type of soil that is to be observed, this is time consuming but provides the most reliable measure of soil retention characteristics, less accurate but less time consuming methods

may be based on soil texture obtained via experimental means such as sieving or settling.

Standard Operating Procedure for Obtaining a Soil Water Retention curve

Each soil sample was sieved to 2mm and then poured into a plastic pot. The soil was packed according to Retzlaff and South's simple guide for determining a partial soil water retention curve [70] i.e. by gently dropping the pot from a height of 5cm onto a laboratory bench. This was done in several stages until the plastic pot was filled. The drainage holes in the bottom of the pot were covered with a fine filter fabric to prevent the soil from falling through whilst still allowing the effluent to drain away. De-ionised water was added using a measuring cylinder taking care to disturb the soil as little as possible. In keeping with the guide referred to above, the soil was then saturated with tap water until excess liquid ran freely from the drainage holes in the pot. The soil core was then left until no more excess liquid freely dripped from the core and then was moved to an environmental chamber set at a constant temperature of 24 degrees Celsius. The soil core was placed on a set of laboratory scales so that water loss via evaporation could be monitored in addition to the soil moisture sensor measurements. Two tensiometers (Delta-T SWT5) were installed according to the manufacturer's instructions; both tensiometers were installed vertically to a depth of 10cm. The soil moisture probe was also inserted according to the manufacturer's instructions; this was installed to a depth where the entirety of the metallic electrodes was beneath the soil surface. Three complete drying cycles were logged for each soil sample. Figure 11 shows the experimental setup as installed in the environmental chamber. In addition to monitoring the soil tension as a function of moisture contents, a number of other parameters were logged in parallel, these include: Weight, Soil temperature and Bulk electrical conductivity. The procedure was repeated between 3 and 4 times per soil type.

Three soils were characterised, these soils include:

1. Highfied (Fallow) Rothamsted - Silty soil
2. Warren Field (Arable) Rothamsted (Woburn) - Clay soil
3. Butt Close (Arable) Rothamsted (Woburn) - Sandy soil



Figure 11. Experimental Setup.

The resulting soil retention curves obtained over 3 drying cycles for a silty soil type are shown in Figure 12.

From the soil retention curves in Figure 12 there appears to be a poor level of repeatability between experiments 1 and 2 (which agree well) and experiment 3. The cause for this is believed to be due to air bubbles entering the tensiometers during the very dry period of the previous 2 experiments. Air bubbles in the shaft of the tensiometers will compromise the performance of the tensiometer. The tensiometers were refilled according to the manufacturer's instructions and their response tested before commencing any further experiments.

Disregarding the compromised data set, the soil retention curves in Figure 13 appear to exhibit a good level of repeatability over 2 drying cycles. The mismatch between experiment 1 and experiment 2 can be explained as follows. In experiment 1, the soil was freshly sieved and had not been through a complete drying cycle whereas in experiment 2, the soil had been subject to 1 complete drying cycle. As a result there will have been a change in soil compaction/particle arrangement following the 1st drying cycle as demonstrated previously in regard to saturated hydraulic conductivity.

In all 3 experiments (including in the compromised data), tensiometer 1 and tensiometer 2 agreed closely, furthermore, if the soil tension measured using Tensiometer 1 is plotted against that measured with tensiometer 2 as in Figure 14 the gradient is very close to 1:1 thus the assumption that “spatial variation of hydraulic conductivity is negligible” can be considered valid.

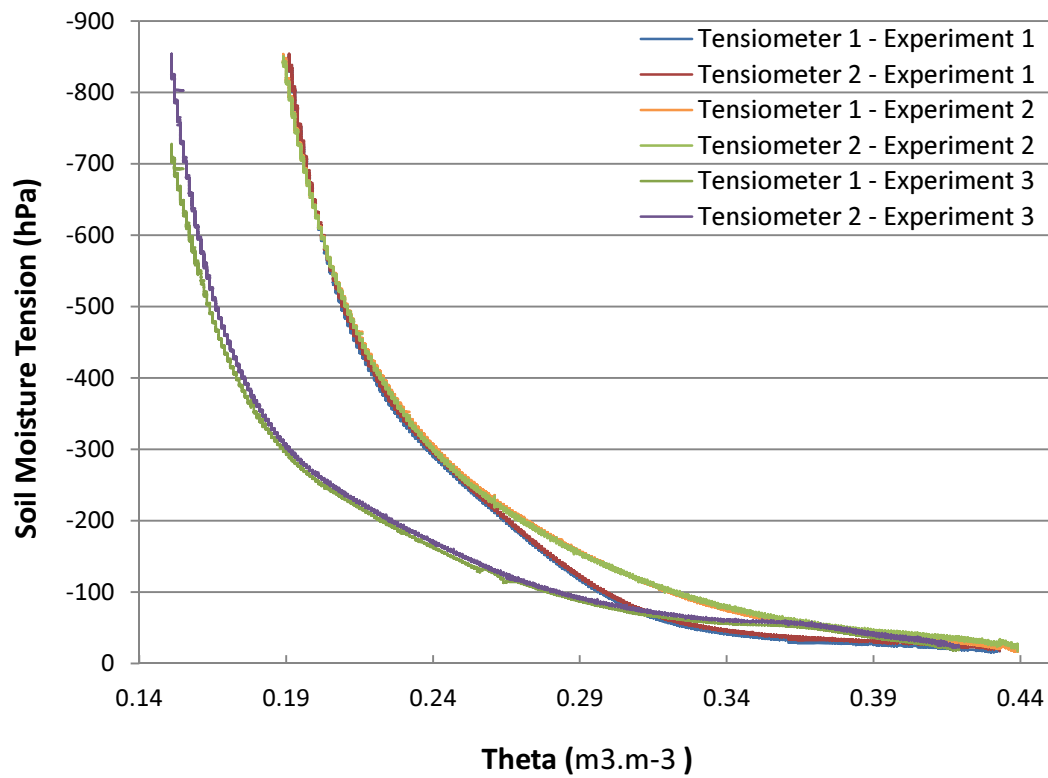


Figure 12. Poor repeatability of soil water retention curve for a single soil core.

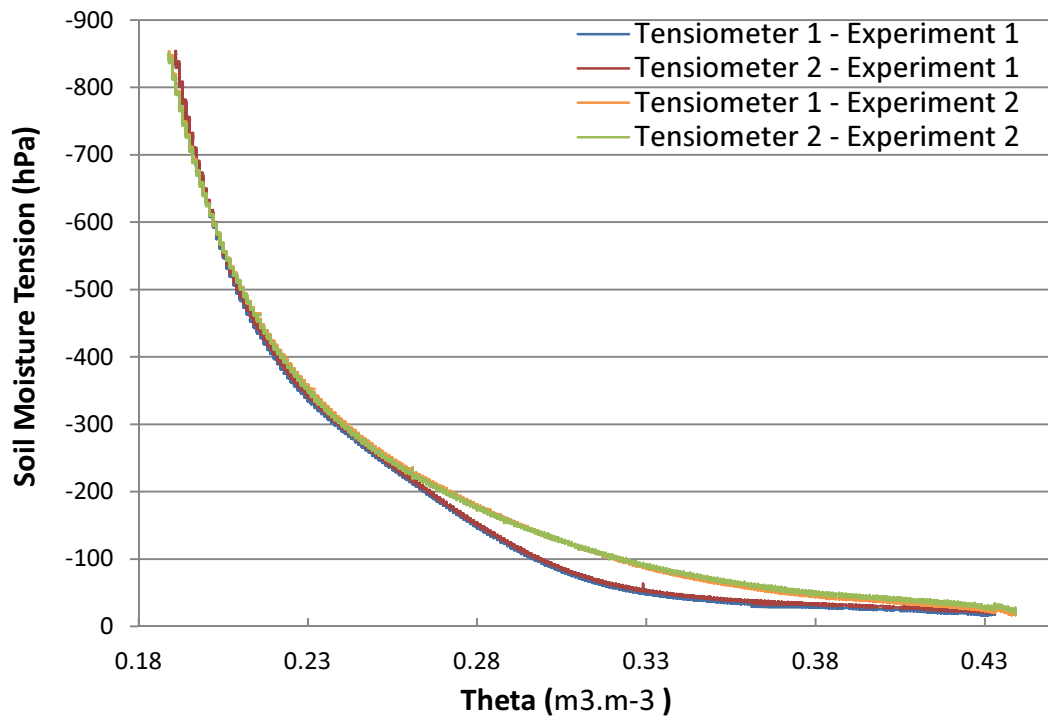


Figure 13. Soil water retention curves for a single soil core.

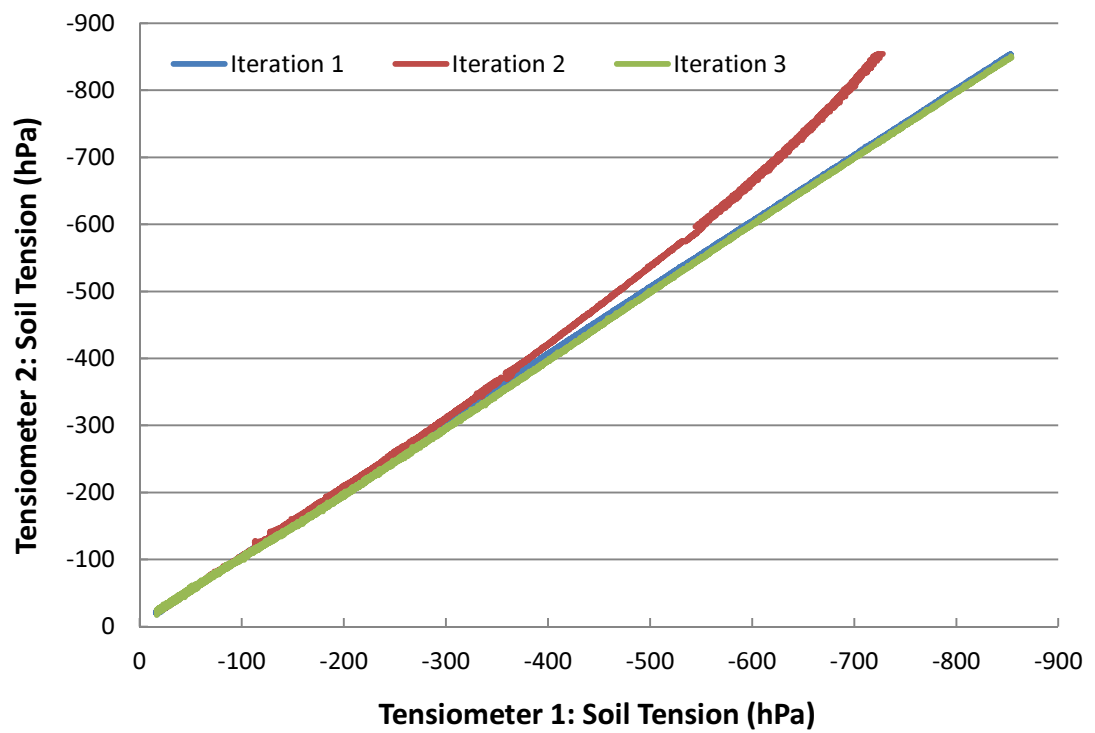


Figure 14. Verification that spatial variation of hydraulic conductivity is negligible

Based on the soil retention curve data the van Genuchten parameters were computed. In the case of the silty soil above an alpha parameter of 0.065 was calculated, this value is in accordance with the literature reported values of between 0 and 0.13 for a silty soil [123]. The 'n' parameter was calculated as 1.58, this too was in accordance with the ranges found in the literature for a silty soil, i.e. between 1.15 and 1.6 [123].

The results from an additional study of temperature as a function of water content are shown in Figure 15. The relationship between soil temperature and water content show that in the initial stages of the experiment, the soil core undergoes a cooling phase. This is due to the wetting process, the soil was wetted using de-ionised water at ambient temperature, thus the soil core will initially be at approximately ambient temperature. As moisture begins to evaporate in the early stages of the experiment, the temperature of the soil core begins to reduce. Following this initial cooling phase, the soil temperature remains relatively constant and below that of the environmental chamber for a large portion of the saturation range. This is attributed to the evaporation of moisture from the soil surface reducing the extent to which soil is warmed. Some warming due to sunlight and elevated ambient temperatures is inevitable, especially as the soil dries, as observed in the dry stages of the experiment. When the soil becomes very dry, the soil temperature begins to rise and equilibrate with the ambient temperature within the environmental chamber.

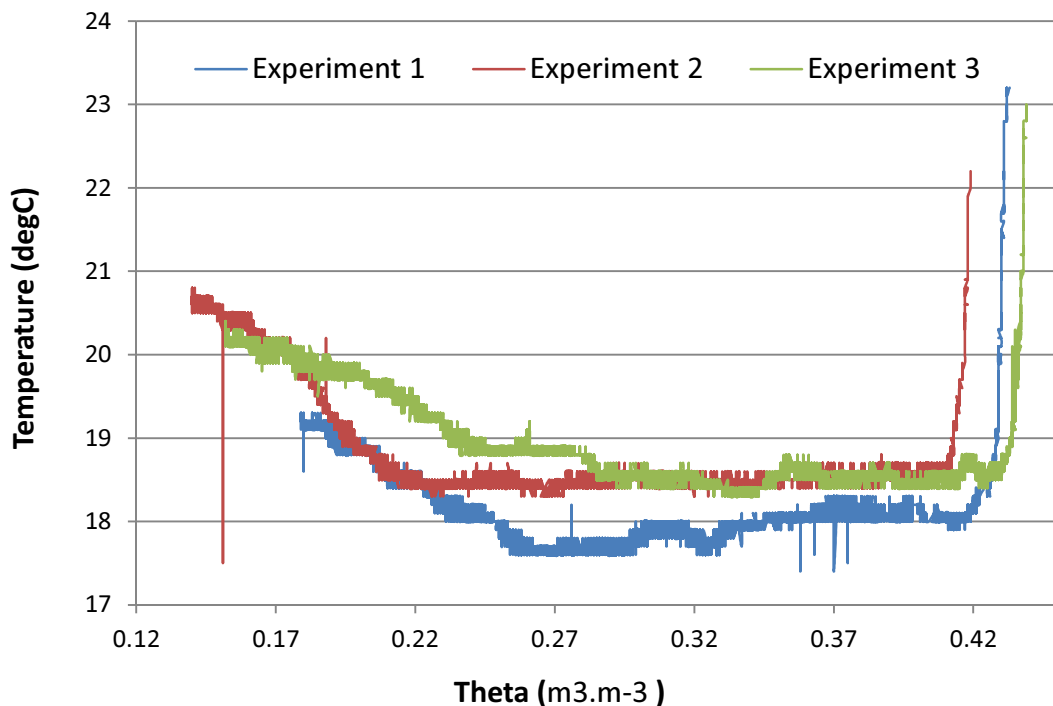


Figure 15. Temperature with respect to soil water content.

3.2 Electrostatics

Simulation of electrical impedance measurements in this application is a multiphysics problem combining flow through a porous media to describe the movement of water through a soil column as discussed in the previous sections and electrostatics for the calculation of the electrical field distribution and subsequently the boundary voltage measurements resulting from the moisture distribution. In order to validate the electrostatic model a parallel plate arrangement was used to compare simulated and experimental electrical measurement data for varying heights of water. Furthermore, the model was implemented for a typical tomographic sensor array and the resulting boundary measurement data for a homogenous conductivity distribution compared with that predicted by the forward solution in EIDORS with an equivalent geometry.

3.2.1 Parallel Plate Arrangement

In order to validate an electrostatic simulation implemented in COMSOL Multiphysics, the capacitance of a rectangular vessel as described in Figure 16 was used. The vessel walls were manufactured to include two parallel plate electrodes of dimension 130mm x 85mm as shown in Figure 17. These electrodes were insulated from the medium using a solder mask layer of 75 μ m thickness. Measurements were carried out using a Hewlett Packard 4192A Impedance analyser.

The dielectric constant of the solder mask layer was set to 3.56 (as defined by the manufacturer) in the FEM. For the following experiments, the dielectric constant of air was taken as 1.00059 [140] and the dielectric constant of water was taken as 79 at 20 degrees Celsius [141][142].

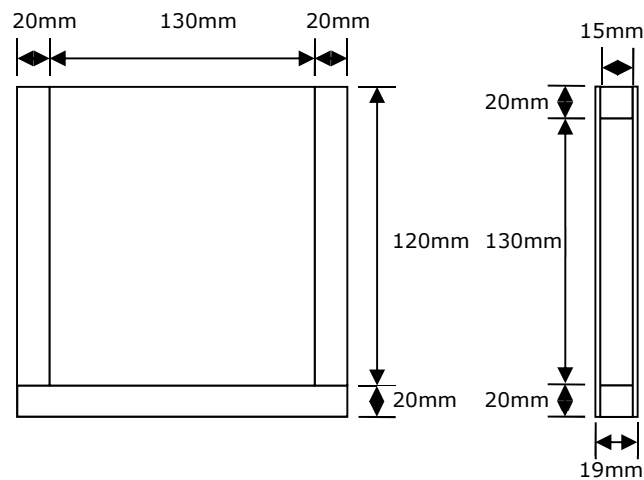


Figure 16. Schematic diagram of the rectangular vessel. Left: Front view, Right: Top view.

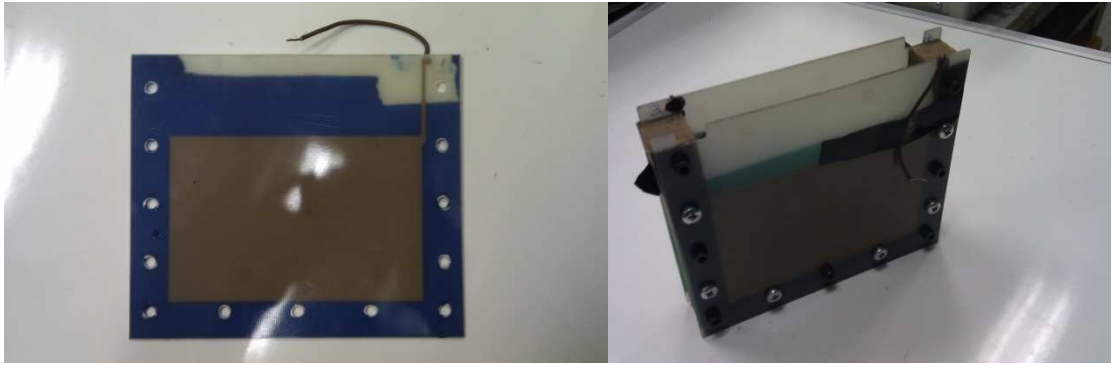


Figure 17. Left: Vessel wall showing electrode Right: Constructed measurement vessel

3.2.2 Varied Heights of Water

Simulations were carried out for fill levels ranging from 0mm (100% air) to 120mm (100% water) in 10mm steps. A comparison between measured and simulated capacitance data is shown in Figure 18. The point at which both measurement sets cease to increase linearly is the point at which the water fill level exceeds the height of the electrodes. Beyond this level, the change is in the fringing field only and variations were of $\sim 11\text{pF}$ corresponding to approximately 3% of the total measured capacitance. The maximum error between simulation and measurement was 44% corresponding to a difference of 5.26 pF. This error occurred when the vessel was empty, i.e. filled with air. This point corresponds to the lowest measured capacitance, hence the most sensitive to measurement error. The average error was 8.88%. Possible sources of error include experimental error and the absence of temperature data in order to account for the temperature dependency of the dielectric constant of water. Analysis of the potential sources of error is presented in section 3.3.5.

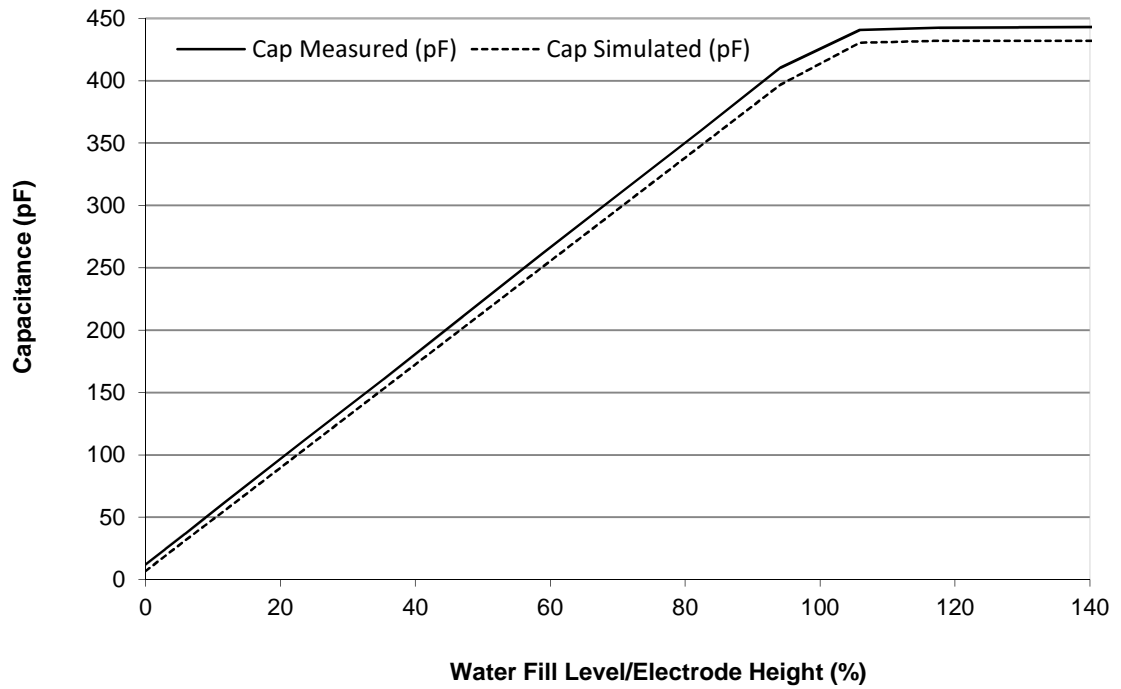


Figure 18. Plot of capacitance vs. fill level for measured and simulated capacitance data.

Figure 19 shows the simulated electric field distribution for a half filled vessel. Note the electric field is highest in the region of higher dielectric constant (i.e. the water) as represented by the largest arrows. The smaller arrows represent the weaker electric field in the air filled region.

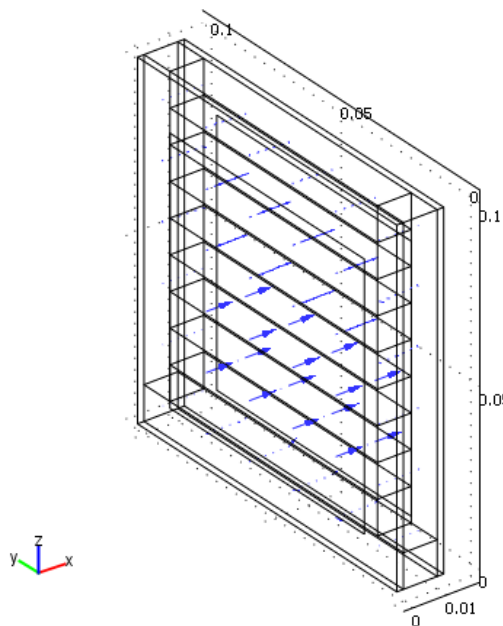


Figure 19. Simulated electric fields for a half filled rectangular vessel.

3.2.3 Comparison with EIDORS

In order to verify the implementation of the proposed electrostatic model for a conductive media an ERT sensor geometry based on the work of Alme [143] and with the properties shown in Table 2 was created in the COMSOL Multiphysics CAD environment (Figure 20) and also within EIDORS using NETGEN (Figure 21). The predicted boundary voltage measurements using COMSOL were compared with those predicted using EIDORS. In this experiment a dipole-dipole adjacent strategy was used and all recipricals were retained. An excitation current of 8mA and a background conductivity of 0.085 S/m was used.

Table 2. Vessel geometry details

ERT sensor	Specification
Number of electrodes	16
Electrode length and width	15mm x 15mm
Electrode thickness	1mm
Inner/outer pipe diameter	140/150mm

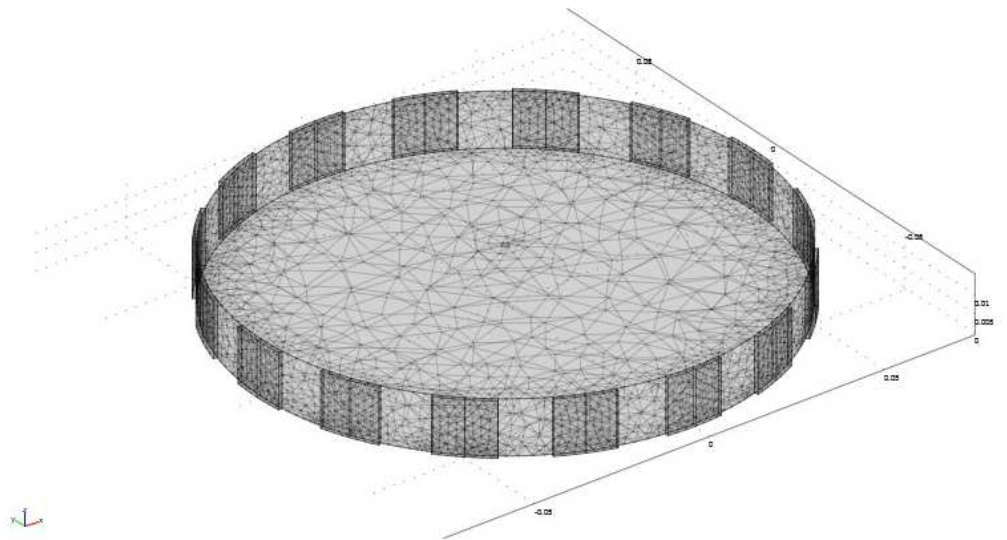


Figure 20. COMSOL Model/Mesh

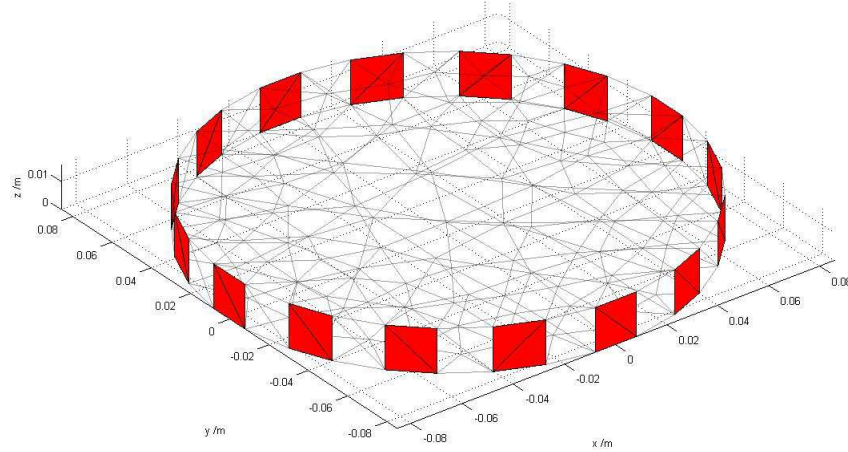


Figure 21. EIDORS/NETGEN Mesh with Electrodes Highlighted in Red

Having computed the boundary measurements using COMSOL and EIDORS, the results were compared. The predicted boundary voltages are shown in Figure 22. An average error of 2.3% was observed between the COMSOL and EIDORS solutions. The worst case absolute error was 7.4% which occurs when exciting and measuring on adjacent electrode pairs. It is believed that this error is likely due in large part to what is termed contact impedance, which occurs at the electrode-medium interface. The rationale for this is that EIDORS includes an implementation of the complete electrode model which takes into account this contact impedance. At this stage, the contact impedance is not yet accounted for in the COMSOL model. This may account for the mismatch between EIDORS and COMSOL solutions.

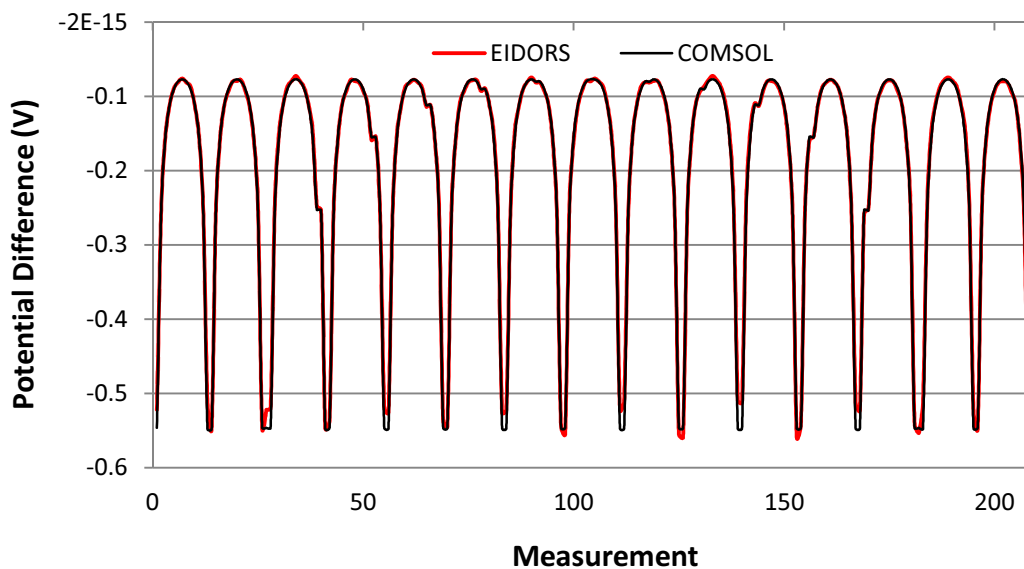


Figure 22. Simulated boundary voltage comparison between EIDORS and COMSOL Multiphysics.

3.2.4 Complex Impedance Implementation using COMSOL

Additional work, not directly related to the main body of this thesis, was carried out using capacitively coupled electrodes. During a two electrode impedance measurement, a measurement is made between two metallic electrodes separated from the media by an insulating layer, i.e. capacitively coupled electrodes. These insulating layers have an associated capacitance that is dependent on the thickness of the layer and the dielectric permittivity of the layer. These two capacitances can be added in reciprocal to provide a single measure of wall capacitance. This leaves the impedance of the media to be measured as an unknown. The frequency dependant analytical model of Dr Frank Podd [15] can be applied to calculate the unknown impedance given the known parameters of the insulating wall over a range of frequencies. Given a wall capacitance of 7.06 nF and a wall resistance of $>1 \times 10^{12}$ Ohms, the analytical model of Dr Frank Podd was used to predict the measurements for a range of frequencies, these predictions were compared with measured values obtained experimentally by Dr Frank Podd. Further to this, a COMSOL model capable of simulating frequency dependant complex impedance measurement data was implemented. Using this model a second set of predictions was made. As can be seen in Figure 23 overleaf, the general shape of the simulated and analytical solutions is very similar, some divergence can be observed at low frequencies, however at high frequencies the trend is very well matched, however an offset of observed throughout the whole frequency range. It was suspected that fringing fields may be the cause of this offset as they are not accounted for in the analytical model, however simulations were carried out both with and without the inclusion of a fringing region and the effect of fringing fields was negligible, causing some only some minor error at low frequencies, i.e. when the wall capacitance is dominant. This error was not large enough to account for the offset between the two models throughout the frequency range. The measured data shows a very similar trend however it diverges at high frequencies this is most likely due to measurement equipment limitations at high frequencies.

Beyond the above, further work was carried out utilising these techniques in a tomographic context, this led to the publication [21].

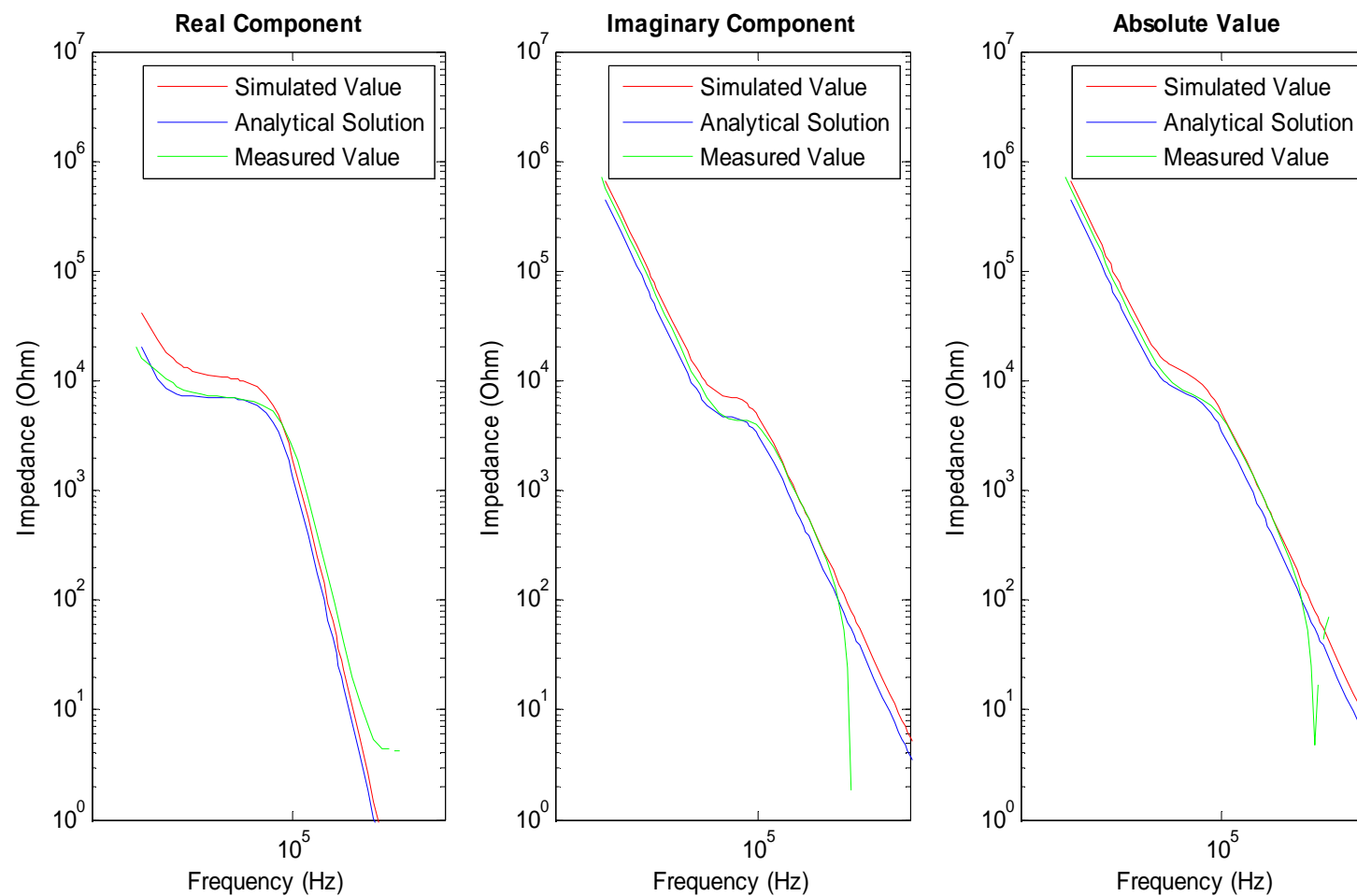


Figure 23. Simulated, Analytical and Measured complex spectroscopic impedance data.

3.3 Coupling Mechanisms

The bulk electrical conductivity and bulk dielectric permittivity of a partially saturated soil matrix varies as a function of water content. The implication of being able to describe this relationship mathematically is the ability to infer the water content in a soil sample via electrical measurement.

Electromagnetic techniques for inferring soil moisture content, such as time domain reflectometry (TDR) and capacitance methods [40] rely on this strong dependence of electrical signals on dielectric permittivity [43] whilst measurement techniques such as ERT depend heavily on bulk conductivity. The bulk conductivity and dielectric permittivity can be related to soil water content using a calibration curve [44].

This consists of establishing the relationship between the signal provided by the instrumentation and the soil moisture content by using a reference method. This relationship is comprised of two subsequent relationships. Firstly the relationship between the probes output signal and the soil bulk conductivity and/or dielectric permittivity, which may be determined experimentally. Secondly the relationship between soil bulk conductivity and/or dielectric permittivity and soil water content. This may be determined using theoretical models or empirically [49].

One further interesting property of being able to mathematically model the relationship between soil moisture content and bulk conductivity and/or dielectric content is the potential to estimate electrical measurements (i.e. resistivity or capacitance measurements) for a given soil sample based on a simulated soil moisture distribution. This provides a basis for the implementation of a multi-physics simulation.

Fluid flow and electrostatics models can be coupled via the bulk conductivity or dielectric constant, if the bulk conductivity or dielectric constant can be predicted based on effective soil saturation.

A number of methods have been proposed to predict the electrical properties of water saturated soils at varying soil saturation levels. Archie's law is formulated to predict bulk electrical conductivity whilst the Topp model [130] and the Complex Refractive Index Method (CRIM) [131] are formulated to predict the dielectric constant of soil at varying soil saturation levels. These methods have been tested extensively [132][133] and are commonly used in the calibration of electrical soil moisture probes [43].

3.3.1 Archie's Law

Since most soils are formed by non-conducting materials, Archie's law assumes that the electric currents are mainly passed by ionic content in the pore space rather than through the soil particulate. Originally, Archie's law was valid only for the effective conductivity of a fully-saturated rock or soil, but it can be extended to variably saturated porous media.

Archie's law relates the effective or bulk conductivity to the fluid conductivity σ_L , fluid saturation S_L and porosity ε_p :

$$\sigma = S_L^n \varepsilon_p^m \sigma_L \quad (3.7)$$

Where, m is the "cementation" exponent, which describes pore connectivity. $m = 1$ represents a volume average of the conductivities of a fully saturated, insulating porous matrix and a conductive fluid. The saturation coefficient n is normally close to 2. The ratio:

$$F = \frac{\sigma_L}{\sigma} \quad (3.8)$$

is referred to as the formation factor.

As Archie's Law does not take into account the relative permittivity's of either the wetting fluid or the solid. The relative permittivity of the porous medium is typically considered to be that of air.

3.3.2 Topp Model

The popular empirical model known as the Topp model was developed by Topp et al by compiling data for many soils under varying moisture conditions [134]. This model is given by the third-order polynomial equation

$$\varepsilon = 3.03 + 9.3\theta + 146\theta^2 - 76.7\theta^3 \quad (3.9)$$

where ε denotes the effective dielectric constant of the soil mixture and θ denotes the water content. Extensive testing has shown the Topp model to be reasonably accurate for many soils [48]. However its validity has not been demonstrated over a full range of possible water contents and porosities [47].

3.3.3 Complex Refractive Index Model (CRIM)

The complex refractive index method (CRIM) involves using simple mixing laws to calculate the dielectric constant of a material (ϵ_T) given the dielectric constant (ϵ_i) and the volume fraction (V_i) as given by

$$\sqrt{\epsilon_T} = \sum_i V_i \sqrt{\epsilon_i} \quad (3.10)$$

This can be expanded for the case of a soil sample at a given level of water saturation (θ), where θ is the volume fraction of the pore space that is filled with water, the remainder being filled with air [137]. The system is composed of soil (ϵ_s), water (ϵ_w) and air (ϵ_a). Porosity is given by Φ and the dielectric constant for a given soil saturation level is expressed as

$$\sqrt{\epsilon_T} = (1 - \Phi)\sqrt{\epsilon_s} + \theta\Phi\sqrt{\epsilon_w} + (1 - \theta)\Phi\sqrt{\epsilon_a} \quad (3.11)$$

Assuming that the soil and air components have negligible conductivity, the dielectric constants of both soil and air can be assumed to be entirely real[137][138].

An obvious limitation of both models is that they assume localised homogeneity and complete mixing. They also do not take into account electro-chemical interactions amongst the constituent components [137].

3.3.4 Experimental Validation and Comparison

Archie's Law

Due to the proliferation of the use of said model in relating bulk conductivity to water content, it was decided that verification of Archie's law was not an appropriate use of the time available.

Topp and CRIM Model

Due to varying opinions in the literature surveyed regarding the most suitable model for relating dielectric properties of soil to water content, it was decided that the two most prolific methods should be compared on the soil samples that were to be studied. As such the Topp and CRIM models were verified using a Hewlett Packard 4192A impedance analyser to measure the capacitance of the previously described rectangular vessel (section 3.2.1) when filled with soil of varying levels of saturation. The dielectric constant of the soil

matrix was predicted for the corresponding saturation levels using both the Topp and CRIM models. For the CRIM model porosity was calculated from data provided by a soil analysis service offered by Forest Research Surrey using the following equation

$$\Phi = 1 - \frac{\rho_{bulk}}{\rho_{particle}} \quad (3.12)$$

Where Φ is the porosity, ρ_{bulk} is the bulk density, defined as the average density of dry soil. $\rho_{particle}$ is the particle density, defined as the density of the particles that the soil consists of. It is equal to the dry density of the solid material comprising the soil matrix i.e. the mass of air is negligible [139]. The particle density of a soil may be estimated using the weighted average of the solid components [139] and is given by

$$\rho_{particle} = \rho_m X_m + \rho_{om} X_{om} \quad (3.13)$$

where $\rho_{particle}$ is total soil density, ρ_m and ρ_{om} are the mineral fraction density and organic matter fraction density respectively, X_m and X_{om} are the mineral volume fraction and the organic matter volume fraction respectively. The porosity was calculated as 0.54. This value is consistent with values for silty soils [113].

The predicted dielectric constants from the Topp and CRIM models were substituted into the FEM and the respective capacitance measurements were calculated by simulation.

As the soil water content was increased, the capacitance measurements had two distinct regions of linearity, as can be seen in Figure 24. Any non-linearity is likely to be caused by inconsistencies in the level of compaction of soil and/or any bowing of the vessel wall between subsequent measurements.

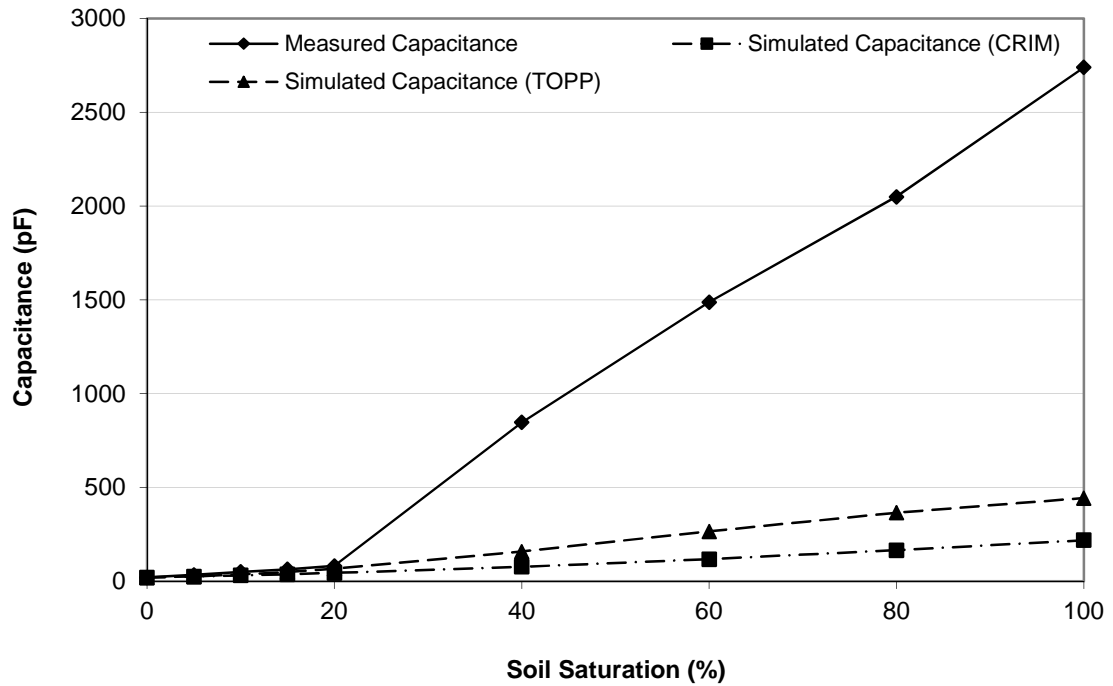


Figure 24. Measured and simulated capacitance measurements vs. soil saturation level.

Beyond a saturation level of $\sim 20\%$ there is a sudden increase in the slope for the measured data. This discrepancy to the FEM model is believed to be the result of resistive coupling on the reading from the impedance analyser for conductivities greater than 0.48 mS. Distilled water was used to wet the soil, however the mineral content of the soil increased the conductivity of the water from 0 mS to 0.75 mS as determined by measuring the conductivity of the run off. This hypothesis was investigated by repeating the procedure using a non-conductive liquid (Rapeseed oil) to saturate the soil. It is assumed that the ions present in the soil are not oil soluble and do not increase the conductivity of the oil. An equivalent experiment using "washed" sand and distilled water was also carried out.

The CRIM equation was used to predict the dielectric constant of the soil/sand matrix for varying saturation levels and substituted into the FEM to simulate the expected capacitance measurement data. This simulated data was compared with measured data. In this case, the dielectric constant of rapeseed oil was taken as 3.1 [114]. The Topp model was not considered in these experiments as it is formulated for a soil-water matrix and can not be modified to describe other components.

As can be seen in Figure 25 and Figure 26, the change of slope is no longer present. This suggests that the hypothesis of instrumentation limitations for high conductivities appears valid. Any non-linearity in the measured data is likely due to variations in the level of compaction between subsequent measurements. Predictions based on the CRIM model had an average error of 3.77% and 5.25% for the soil-oil and sand-water experiments respectively as compared to measured data.

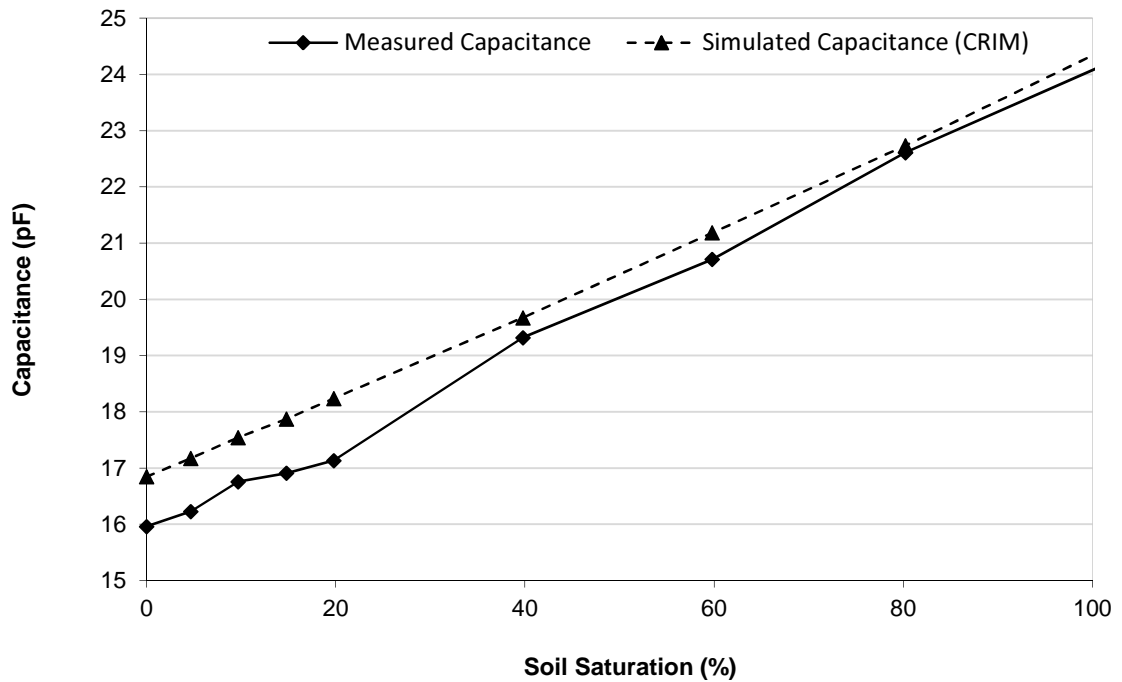


Figure 25. Measured and simulated capacitance measurements vs. level of soil saturation using rapeseed oil.

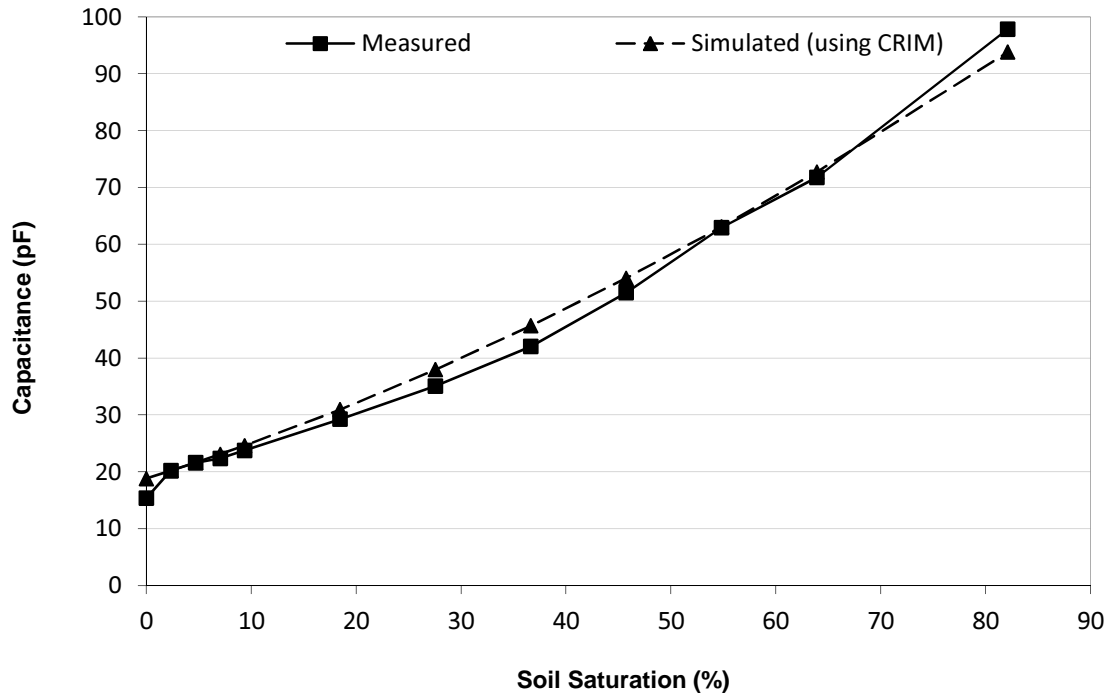


Figure 26. Measured and simulated capacitance measurements vs. level of sand saturation using distilled water

It is thought that at lower measurement frequencies the effects of soil type and soil conductivity are prevalent. The result is a requirement for higher excitation frequencies, this is due to decreased conductive losses at higher frequencies hence reducing the effect of soil conductivity [116]. The result of using a higher frequency is a simplification of the calibration process. In many cases a single calibration curve may be used for numerous soil types [53]. The literature suggests that using suitable calibration curves capacitance measurements can provide reliable results over the full typical range of saturation levels (0-60%) [40][54]. Typically soil dielectric measurement instruments operate in the 10-200 MHz region [40].

3.3.5 Investigating the source of error

In order to determine the sensitivity of measurement data with respect to temperature, the variability of the dielectric constant of water vs. temperature was investigated. The variation of dielectric constant of water with respect to temperature was modelled using the polynomial equation [115]

$$\epsilon_w = 5321T^{-1} + 233.76 - 0.9297T + 0.1417 \times 10^{-2}T^2 - 0.8292 \times 10^{-6}T^3 \quad (3.14)$$

where ϵ_w is the dielectric constant of water and T is the temperature in Kelvin. The modelled dielectric constant of water for the temperature range of 0 to 100 degrees Celsius is shown in Figure 27.

The standard parallel plate capacitor equation was then used to calculate analytically the capacitance for the vessel fully filled with distilled water over a range of temperatures. The thickness and dielectric constant of the dielectric layer were taken to be as described in section 3.2.1. The dielectric constant of water was taken as 79 at 20 degrees Celsius [115] for a reference point. To determine the extent to which the measurements were sensitive to temperature changes of water, the dielectric constant of water was varied until the resulting expected capacitance varied by 10% from the reference, this corresponds approximately to the degree of average error observed in section 3.2.2. Figure 28 shows the change in capacitance calculated for the temperature induced variation in the dielectric constant of water. The result was a change of 12.6% in the value of the dielectric constant of water which is equivalent to a temperature rise of approximately 25-30 degrees Celsius. This corresponds to a temperature of approx 50 degree Celsius. It is unlikely that such an increase in temperature occurred during experimentation.

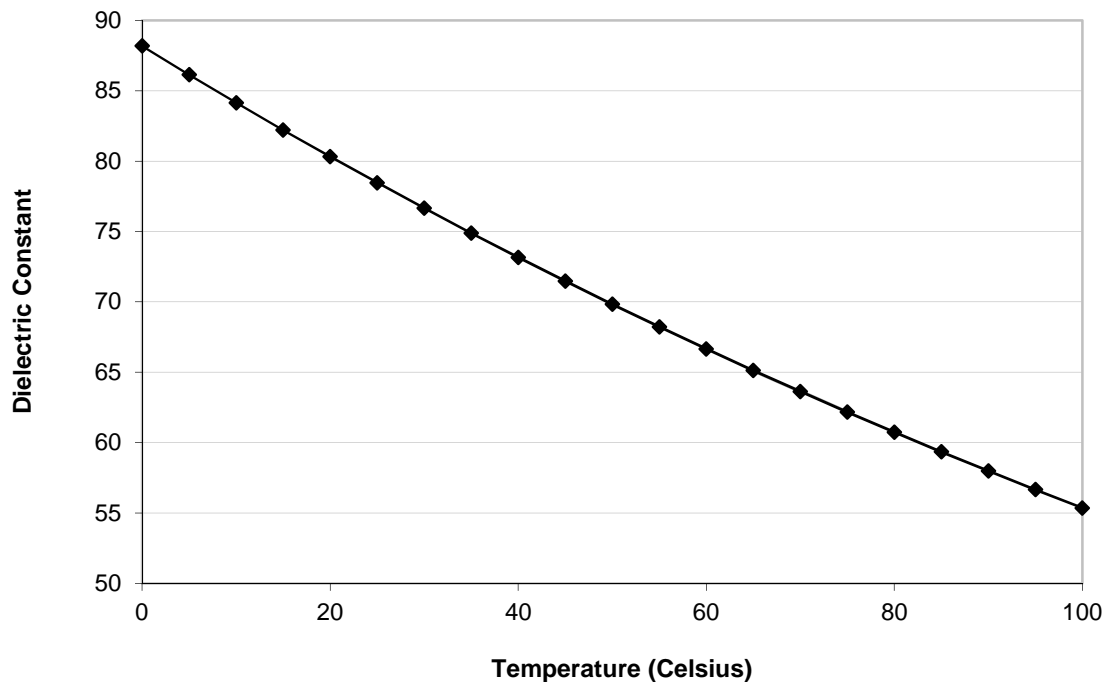


Figure 27. Variation of the dielectric constant of water with respect to temperature.

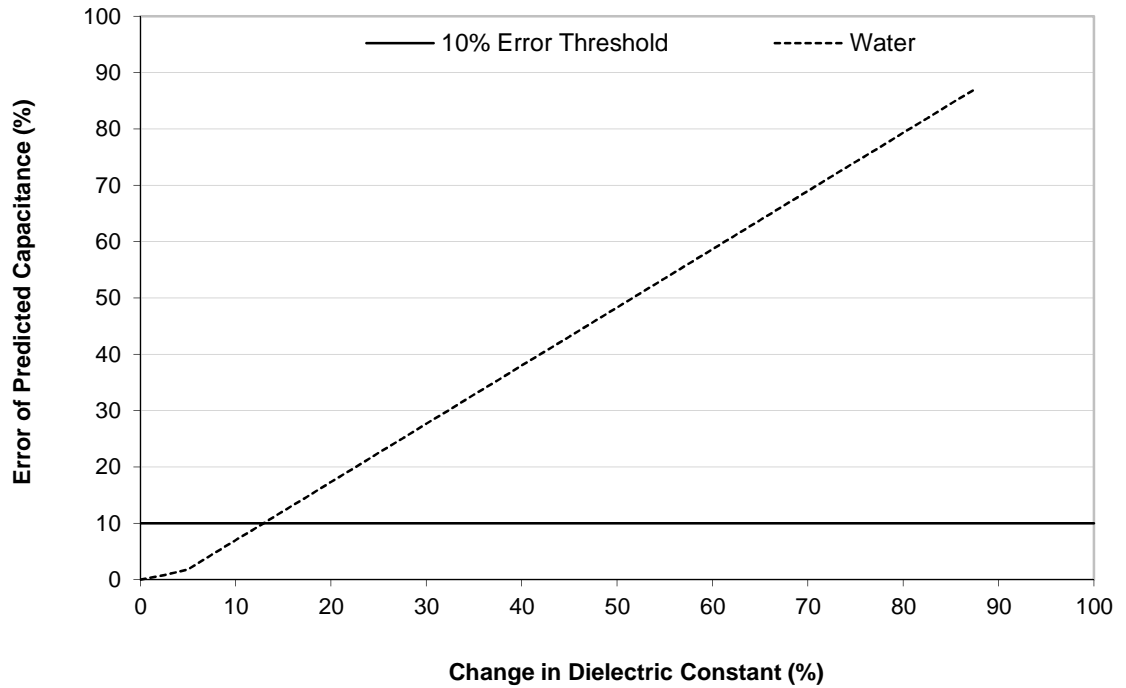


Figure 28. Error in predicted capacitance vs. temperature induced drift in dielectric constant of water for determining the extent to which the temperature dependence of the dielectric constant of water contributes to measurement error.

3.4 Multiphysics

A time varying soil saturation scenario, based on experimental data and data found in the literature, was generated using COMSOL Multiphysics. For each time step, the spatial soil saturation distribution was predicted using the Richards equation with a central irrigation point. From this saturation prediction the electrical properties of each element in the finite element mesh was modelled using Archie's law. Finally electrical boundary measurements were estimated using Poisson's equations based on the conductivity distribution in the soil core. The same vessel dimensions as in Table 2 were used and an injection current of 8 mA between adjacent electrodes and an adjacent measurement strategy, maintaining all reciprocal measurements was used. Figure 29 shows the moisture distribution and the conductivity distribution resulting from the time varying time series. Figure 30 shows the subsequent boundary voltage measurements for each time step. As evident in the plot, as the water content increases the potential difference between adjacent pairs of measurement electrodes decreases, this is due to an increase in bulk conductivity.

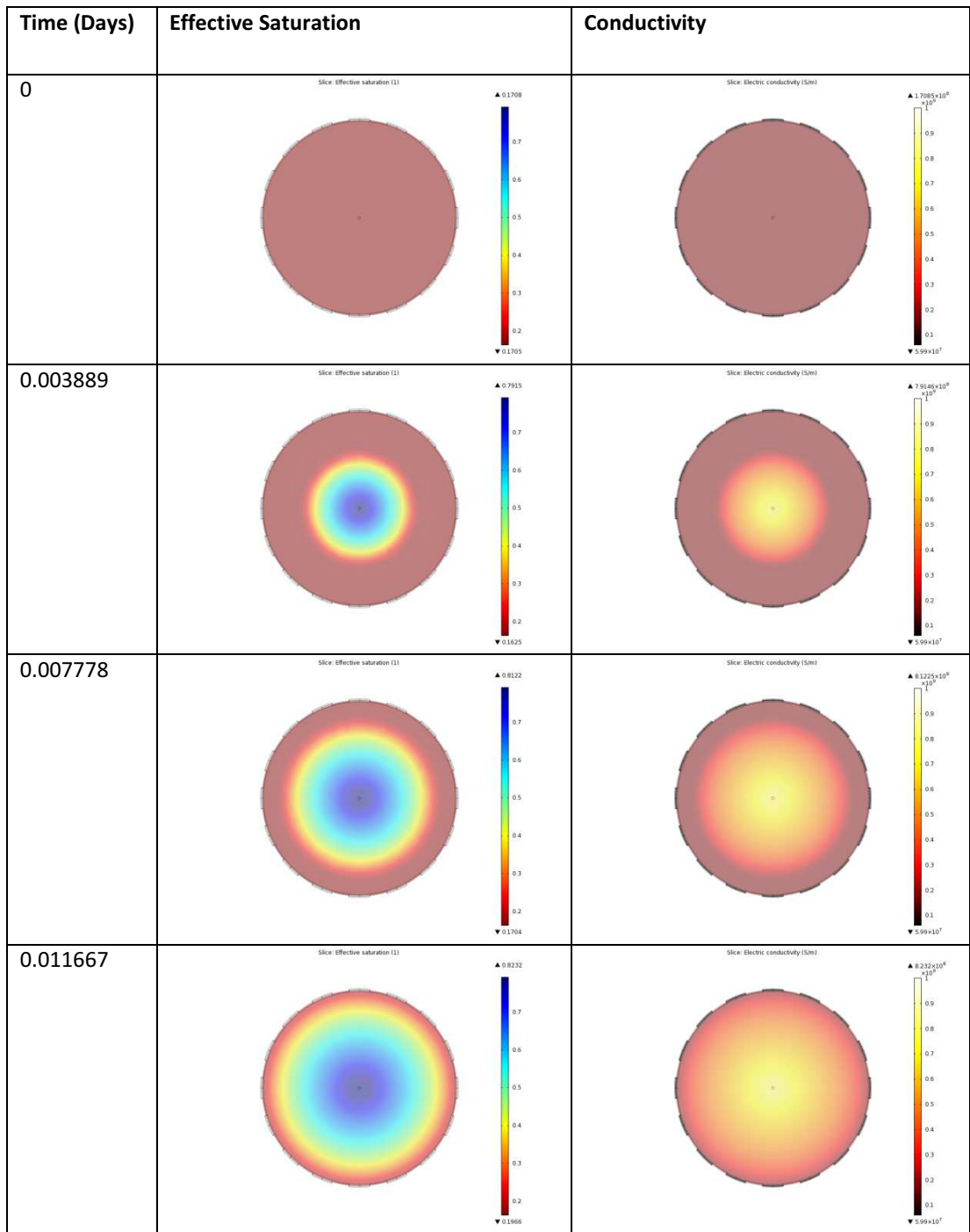


Figure 29. Simulated effective saturation using the Richards equation and subsequent conversion to conductivity distribution using Archie's law for a series of time steps.

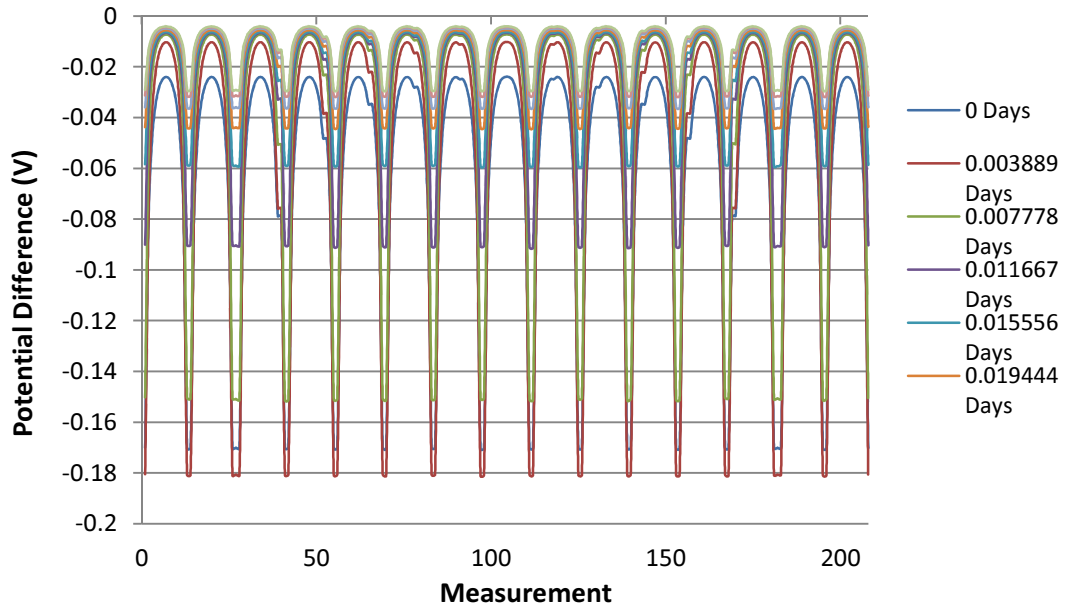


Figure 30. Predicted boundary voltages for a time dependant fluid flow scenario.

3.5 Summary

Fluid flow in a porous media and electrostatics models have been implemented in isolation. These models have been validated and coupled through the bulk electrical conductivity or dielectric constant vs. soil saturation curve as predicted by a mixture model. This allows the simulation of electric fields due to varying soil water distributions hence facilitating the implementation of a multiphysics based forward solver in COMSOL multiphysics.

3.5.1 Fluid Flow

A survey of the literature has yielded several methods for monitoring soil water content and root water uptake, these methods range from entirely simulation based soil transport and root water uptake models. Existing literature indicates that the Richards equation is the most commonly used soil transport model. The Richards equation was implemented in COMSOL Multiphysics and the average error between simulated and observed data was calculated to be less than 10%. Any discrepancies between the shape of the simulated and observed wetting fronts is attributed to the varying spatial compaction in the experimental case, as despite all efforts to create a uniformly packed soil, it is unlikely that a homogenous packing density was indeed achieved.

This experiment shows that the solution to the Richards equation can be used to accurately simulate a wetting front incident on a soil sample given relevant soil parameters. Furthermore the error in the estimated soil

parameterisation would have contributed to this error. The extent of this error may be reduced by prior parameterisation of a sub-sample of the soil sample being observed, as such a series of soil parameterisation experiments were carried out.

3.5.2 Soil Parameterisation

Saturated Hydraulic conductivity was measured for a number of soil cores. It was found that saturated hydraulic conductivity is highly dependent on soil packing density, as a result poor repeatability was found between “equivalent” soil cores with values ranging from 1.1 m/d to 2.34 m/d. This is attributed to the random nature of the particle packing within the soil. Simulated wetting fronts based on measured saturated hydraulic conductivity values were accurate with approximately 11% error relative to the observed wetting front for the corresponding soil core.

Furthermore, the non-saturated hydraulic conductivity was evaluated by way of experimentally obtained soil water retention curves. Parameters derived from these curves agree with the existing literature for a silty soil, however, the sensitivity of the measurement instrumentation to correct filling has been apparent. Spatial variation of saturated hydraulic conductivity was assumed to be negligible, the observed results have shown that this is a valid assumption for a soil packed following the outlines standard operating procedure. Furthermore two additional soil types were parameterised.

3.5.3 Electrostatics and Coupling Mechanisms

An electrostatic model was implemented in COMSOL multiphysics and experiments have shown that the electrostatics simulation is able to predict changes in capacitance due to varying heights of water and varying levels of soil saturation based on two methods for predicting the dielectric constant of soil at varying soil water saturation levels.

The electrostatic model has been shown to exhibit an average error of <9% for varying water fill levels in comparison to measured data. Predictions generated using both the Topp and CRIM models were compared to measured data for varying soil saturation levels. It has been noted that beyond 20% soil saturation, there are difficulties in measuring the capacitance of the wetted soil. This has been attributed to the limitations of the measurement instrumentation for highly conductive media.

The CRIM model was evaluated for two further matrices in addition to water wet soil. This was not possible with the Topp model as this relation is only valid for a matrix of water wet soil. Predictions based on the CRIM model had an

average error of between 3.77% and 5.25% for the soil-oil and sand-water experiments respectively compared to measured data. As a result, the CRIM model was implemented in COMSOL multiphysics to couple the electrostatic simulation to the soil transport simulation to allow for multiphysics simulations.

Experiments have shown that the temperature dependency of the dielectric constant of water will not contribute substantial error over the normal operating temperature range of the instrument. However temperature correction may be easily integrated using a simple mathematical model [115].

3.5.4 Multiphysics

The individual elements identified and verified have been combined within a FEM implemented in COMSOL Multiphysics to produce a multiphysics based forward solver that predicts fluid flow using Richards' equation, converts the resulting soil moisture distribution to equivalent soil electrical properties and then predicts boundary voltage measurements.

4 Inverse Problem

In the context of this thesis the term inverse problem refers to a mathematical method employed for estimating the current state of a time varying system given a series of indirect noisy observations. The state refers to the physical state as described by a number of dynamic variables. In this context such variables may include pressure head, soil water content, soil hydraulic properties, electrical conductivity etc. The indirect and noisy nature of measurements introduces a certain degree of uncertainty surrounding observations. Furthermore as the dynamic system evolves as a function of time and there is also noise in the dynamics of the system, referred to as process noise, the dynamic system cannot be modelled entirely deterministically. In this context the term filtering, as implied by the use of the Kalman filter, refers to the filtering out such noise in the measurements and providing an optimal estimate of the state given the observations and the assumptions made regarding the observed system [151].

This chapter will present image reconstructions utilising some traditional inverse solvers included in the EIDORS suite. It will then introduce the Kalman filter (KF) and two extensions of this method, the Extended Kalman filter (EKF) and the Ensemble Kalman filter (EnKF), which are applicable for state estimation in non-linear dynamic systems such as the one being studied, as the basis for a proposed inverse solver which utilises the multiphysics forward solver described in the previous chapter. It is hypothesised that this suggested method will increase the fidelity of images or metrics extracted from the data acquired using the LCT2 instrument.

4.1 Basic Image Reconstruction

An ERT sensor geometry with the properties shown in Table 2 was created in the COMSOL Multiphysics CAD environment and also within EIDORS using NETGEN (Figure 20 and Figure 21 respectively). This geometry was based on the work of Alme [54] In this experiment a dipole-dipole adjacent strategy was used and all reciprocals were retained for use in the inversion. An excitation current of 8mA and a background conductivity of 0.085 S/m was used. A series of inclusions were inserted into the COMSOL model and the corresponding ERT data sets simulated, Figure 31 shows the resulting simulated potential distribution for a single excitation. These were then inverted using the EIDORS code. The inclusions included:

- A single centralised rod with a conductivity higher than the background conductivity.

- A single off centre rod with a conductivity higher than the background conductivity.
- Two asymmetrically placed rods, of identical conductivity, both higher conductivity than that of the background.
- Two asymmetrically placed rods, one with higher conductivity than the background and one with lower conductivity than the background.

These data sets were then reconstructed using the following algorithms:

- Linear back projection(LBP) with a smoothing factor of $1e-5$ (as determined to be optimal by trial and error)
- Nonlinear Gauss-Newton (NLGN) with a smoothing factor of $1e-5$ (as determined to be optimal by trial and error) for 1,5 and 10 iterations.
- Generalised singular value decomposition (GSVD) with optimal smoothing values as determined by data driven methods implemented in EIDORS.

The results of the inversion can be seen in Figure 32 overleaf. As can be seen in all cases the location of the inclusions can be identified. A qualitative analysis of all cases shows that LBP located the position and approximate size of the inclusion for all cases; however it lacks the ability to accurately identify the true conductivity of the inclusion. On the other hand GSVD more accurately identified the true conductivity values, but exhibits a poor ability to extract the size of the inclusion; however it does show the approximate location for all cases. Non-linear Gauss-Newton showed decreasing spatial identification of the inclusions as iterations were increased, however absolute conductivity values improved from 1 iteration to 5 iterations. Greater than 5 iterations produced poor spatial resolution and poor absolute conductivity values.

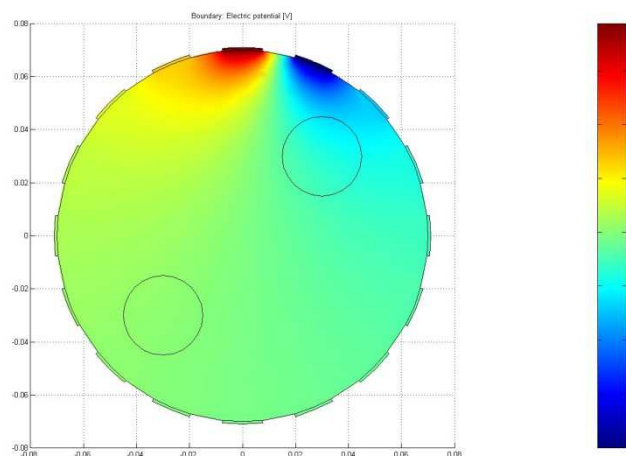
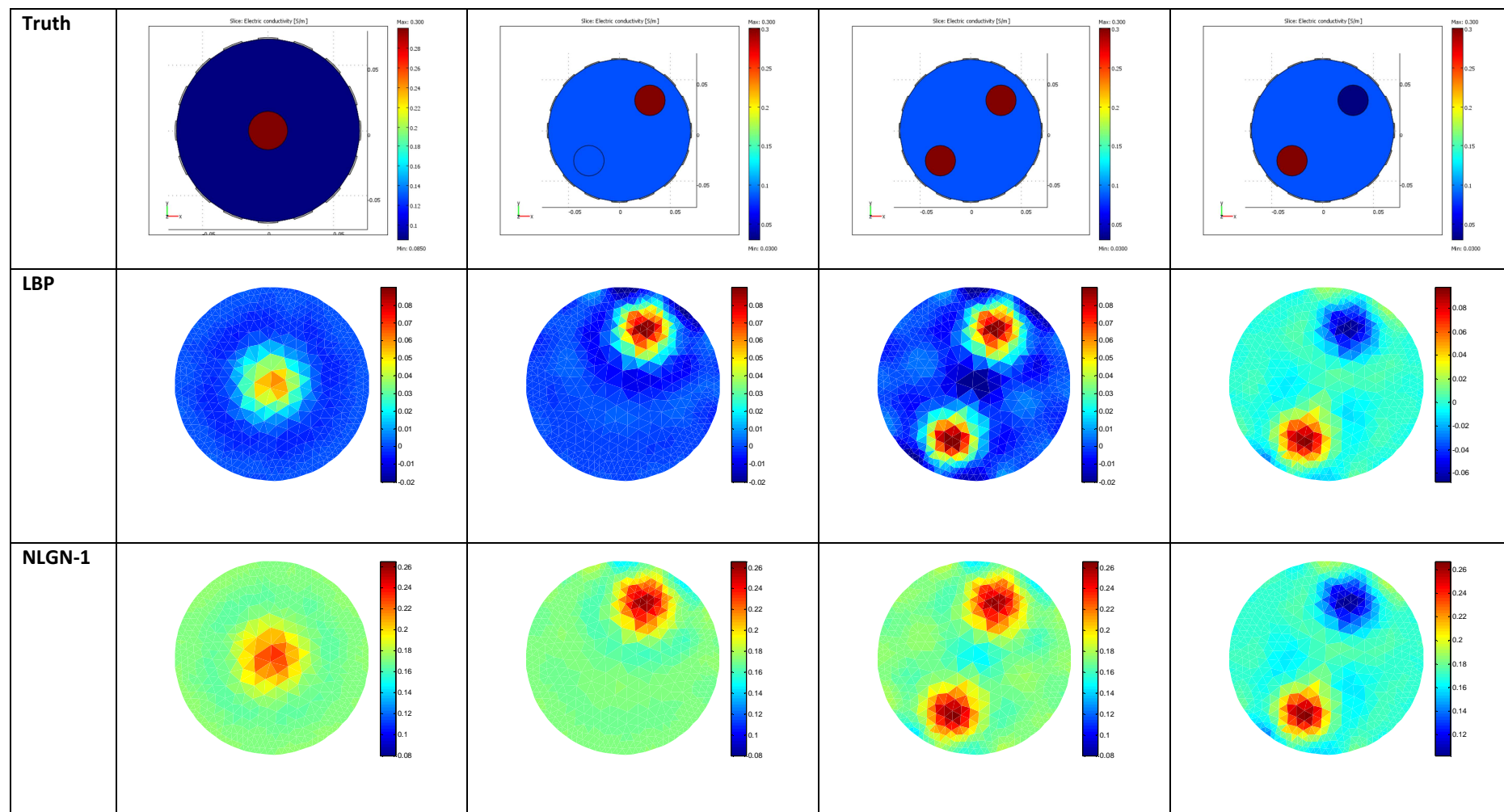


Figure 31. Simulated potential distribution for a single excitation pattern in COMSOL Multiphysics



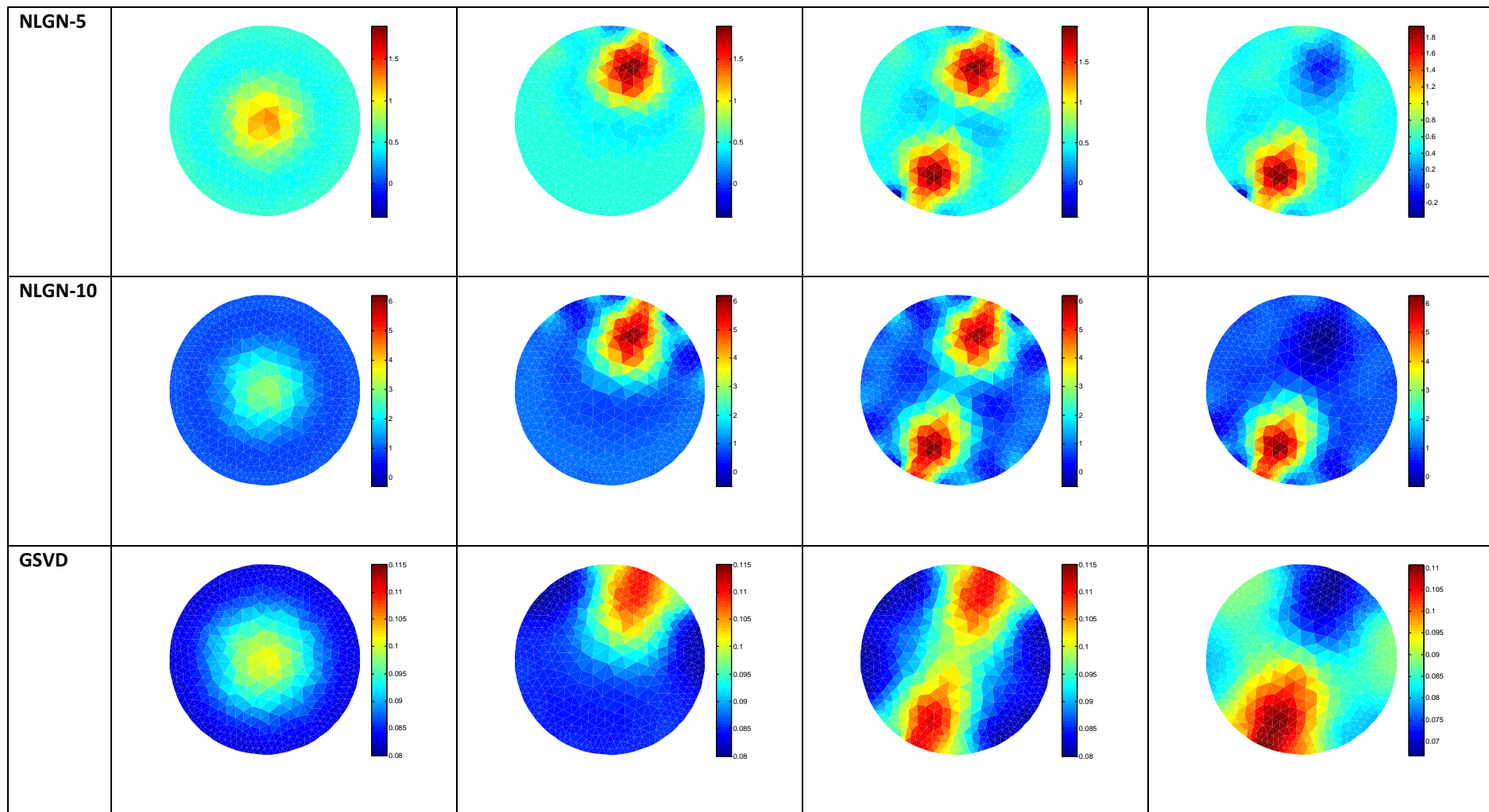


Figure 32. Reconstructed conductivity distributions for a number of basic inclusions.

4.2 Image Reconstruction of Simulated Soil Moisture Distribution

Based on the data shown in Figure 29 and Figure 30, EIDORS was used to reconstruct the conductivity distribution resulting from the fluid flow model using basic reconstruction algorithms, LBP, NLGN and GSVD. Figure 33 shows the reconstructed conductivity distributions using LBP for time steps of 0.003889, 0.007778, 0.011667, 0.015556 and 0.031111 days. The spreading of the wetting front following the irrigation event can be clearly observed. By the final time step, the reconstructed image has reached a near homogenous state and the soil core is saturated. The images below can be compared to the images in Figure 29. In doing so, a qualitative inspection suggests that there is a close correspondence between the truth (as simulated using COMSOL Multiphysics) and the reconstructed distributions.

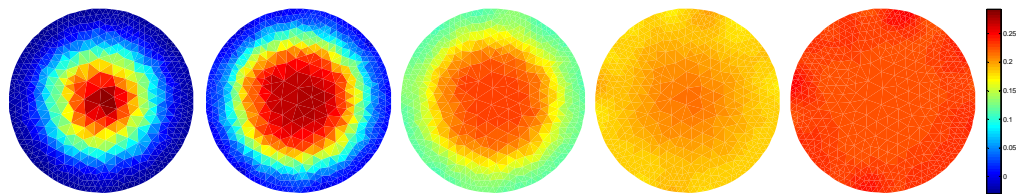


Figure 33. Reconstructed conductivity distributions for a number of time steps using LBP

4.3 Image Reconstruction of Experimental Soil Moisture Distributions

A completely saturated soil core contained in a cylindrical vessel with 2 planes of 16 electrodes, as shown in Figure 34, was monitored throughout the drying cycle. As the vessel was fully enclosed bar the top surface, it was anticipated that drying would occur through surface evaporation only. This is both a highly repeatable and controllable experiment since the soil would be uniformly wet and thus have a homogenous resistivity distribution at the start of data acquisition. Note the actual vessel used has circular electrodes of 16mm diameter, in the model used for reconstruction, see Figure 35, square electrodes were simulated, this was for computational reasons. Data was collected for single rings of electrodes, using an adjacent strategy, in turn and then using a 3D planar adjacent measurement strategy. This provides enough data for 2D, planar and 3D image reconstruction. A MATLAB function was written to separate data into 2D, planar and 3D measurement sets post-acquisition. Measurements were carried out every 5 minutes until the soil was deemed to be dry.

In this iteration of the experiment only 2D reconstruction was carried out. This was done for both the upper and lower electrode planes individually. Reconstructions were carried out using the LBP, NLGN and GSVD algorithms within the EIDORS suite. A selection of reconstructed images, reconstructed using the NLGN algorithm with 5 iterations are shown in Figure 36.



Figure 34. Photograph of Experimental Setup

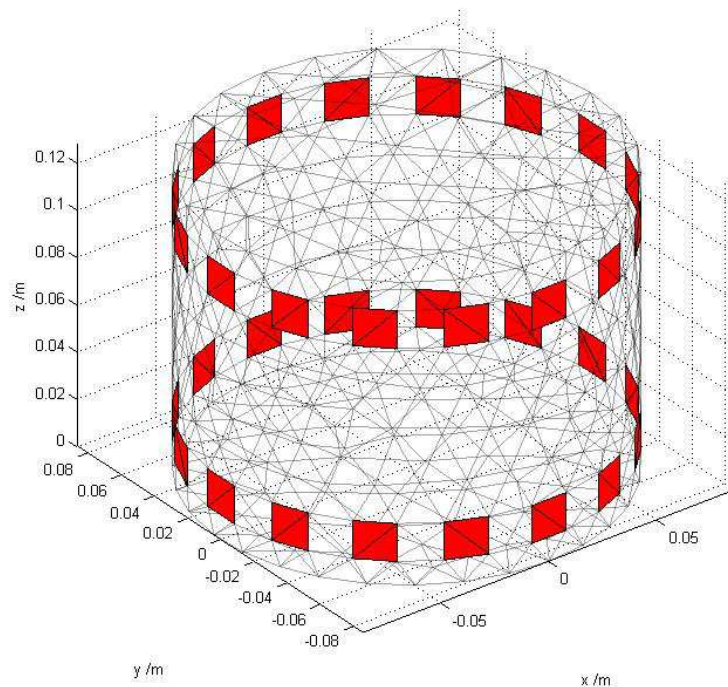


Figure 35. Two Plane ERT Vessel Geometry

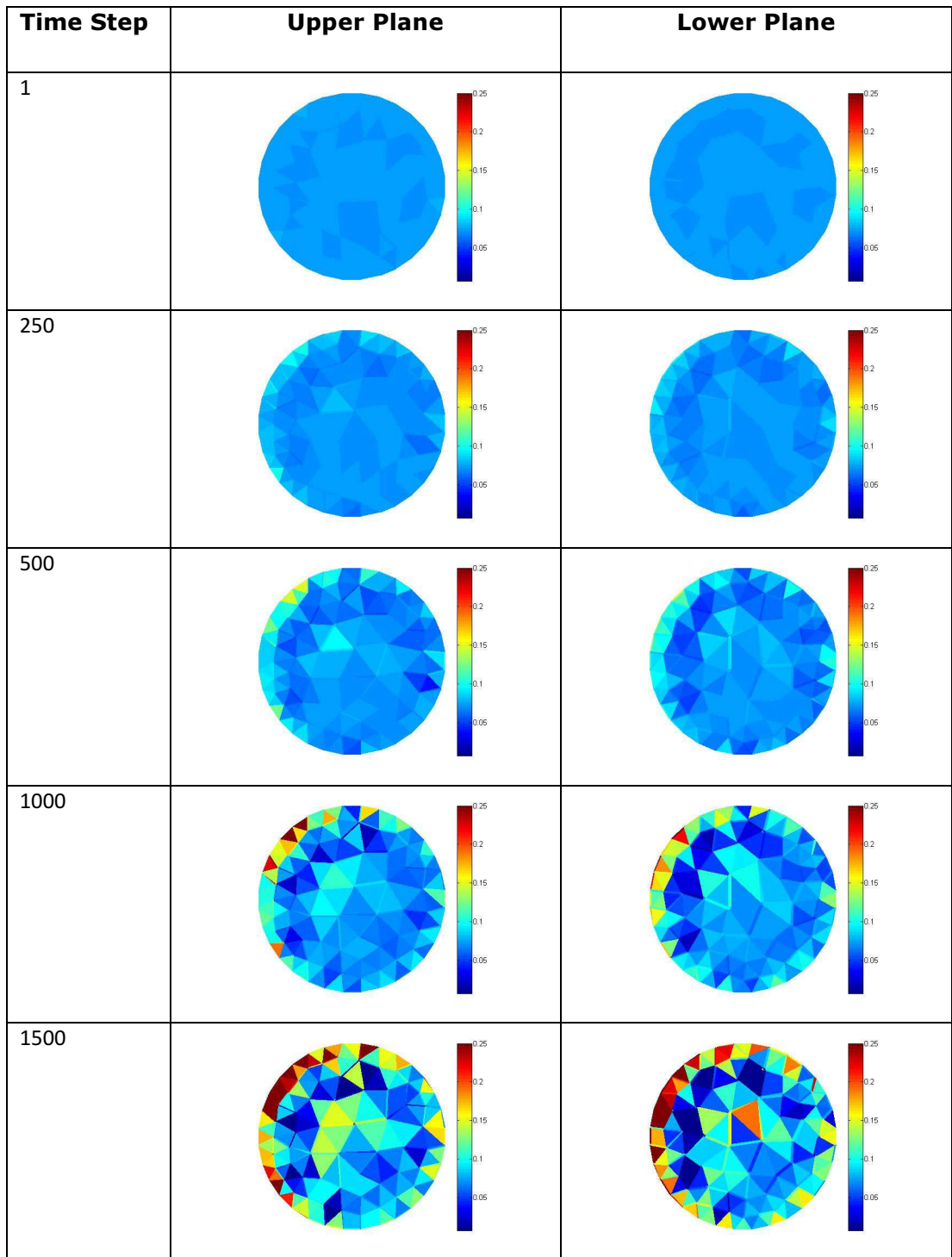


Figure 36. Reconstructed resistivity (Ω/m) distributions using NLGN, 5 iterations, for upper and lower electrode planes for a section of time steps throughout a drying cycle. Blue indicates low resistivity, red indicates high resistivity

In general the reconstructed images are poor and show very little, indeed there are many artefacts. However there are some features that are of interest. For example it can be observed that the average resistivity increases with each time step, this is indicative of the soil drying as resistivity increases with decreasing water content. The average resistivity was calculated and plotted for each time step, as shown in Figure 37. Further, there is a notable increase in resistivity around the periphery of the vessel, particularly around the 11 o'clock position. This may be attributed to shrinkage of the soil core during the later stages of drying, thus pulling away from the electrodes and causing a very high resistivity region. The photograph in Figure 38 provides evidence that the soil did indeed pull away from the electrodes in the experiment.

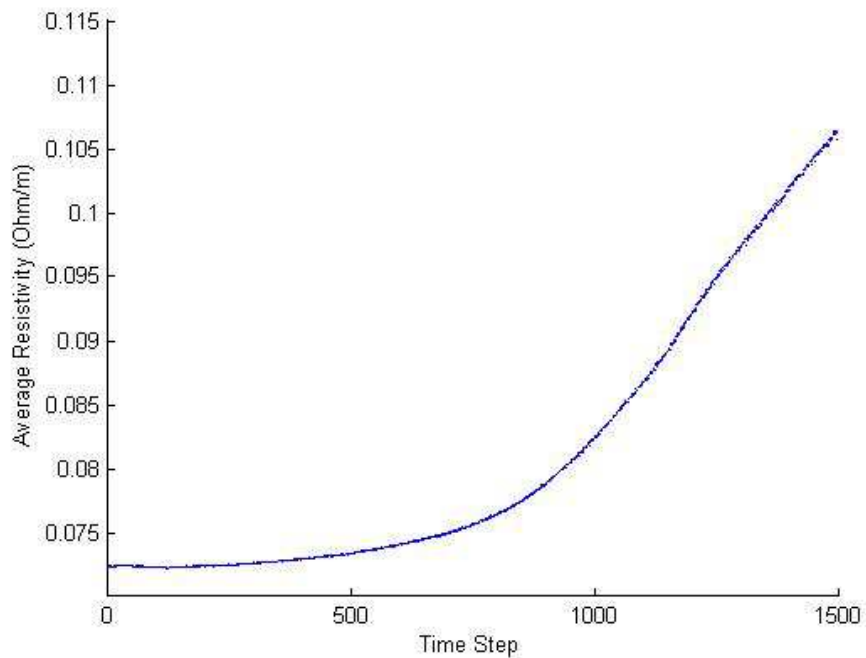


Figure 37. Plot of average resistivity vs Time Step (Each Step being 5 minutes)



Figure 38. Shrinkage caused the soil to pull away from the wall electrodes

4.4 The Kalman Filter

As this section will conclude with the proposal of an Kalman filter based reconstruction, it is appropriate to first introduce the basic Kalman filter and its mode of operation.

The Kalman filter is set of mathematical equations that provide an efficient computational means to estimate the state of a process. It provides a closed form recursive solution for estimating linear discrete-time dynamic systems. R. E. Kalman published his original paper describing a recursive solution to the discrete-data linear filtering problem in 1960[152][151]. His method reduces noise by assuming a pre-defined system model. As a result, the Kalman filter requires a meaningful model of the dynamic system to be observed, it is proposed that the state space representation of the forward model presented in the previous sections would fulfil this role.

4.4.1 Basic Mode of operation

On order to understand the Kalman filter algorithm it is useful to consider the high-level operation of the algorithm before looking at the specific equations. The Kalman filter estimates a process by utilising a form of feedback control, the filter estimates the process state at some time utilising a state-space model and then obtains feedback in the form of (noisy) measurements in order to correct the state estimate. As such, the operation of the Kalman filter can be conveniently considered to have two distinct steps:

1. The prediction
2. The correction/update

The prediction step predicts the next state and error covariance estimates using a dynamic state space model. In the correction/update step, the state estimate and error covariance is corrected with respect to the observation model such that the error covariance of the estimator is minimised. The process is repeated at each time step taking the previous state as initial values. Figure 39 illustrates the high-level operation of the discrete Kalman filter.



Figure 39. Operation of the discrete Kalman Filter [153]

The following pages will discuss the formulation of the dynamic model and the specific equations of Kalman filter algorithm.

4.4.2 State Vector

The state vector, x_t contains all of the uncertain and dynamic variables of interest, it describes the state of the dynamic system and represents its degrees of freedom. The variables contained in the state vector can not be measured directly but they can be inferred from parameters that are measureable[154]. In this application, elements of the state vector may include pressure head, soil water content, soil hydraulic properties etc.

4.4.3 Dynamic & Observation Models

The dynamic model describes the evolution of the state vector over time and is usually expressed in the form:

$$x_t = Ax_{t-1} + Bu_{t-1} + w_{t-1} \quad (4.1)$$

Where A is a constant $n \times n$ matrix that relates the state of the previous time step $t - 1$ to the state at the current time step t , in the absence of either an input function or process noise. B is an $n \times 1$ matrix that relates an optional control input, u_{t-1} , to the state x . w_t is the process noise, i.e. the noise in the dynamics of the system.

The observation model describes the relationship between the state and the measurements. Usually measurements or observations are made at discrete time steps, t , and the observation model is given by:

$$z_t = Hx_t + v_t \quad (4.2)$$

Where H is a constant $m \times n$ matrix that relates the state to the measurement z_t . v_t is the measurement noise.

Both w_t and v_t are assumed to be independent of each other, white and with normal probability distributions i.e.

$$p(w) \sim N(0, Q) \quad (4.3)$$

$$p(v) \sim N(0, R) \quad (4.4)$$

Where Q is the process noise covariance and R is the measurement noise covariance.

4.4.4 The Discrete Kalman Filter Algorithm

As stated previously the Kalman filter has two distinct steps, the prediction and the update/correction step and each step has its own set of equations which are applied sequentially.

Firstly the next state and error co-variance are predicted by the time update equations given by:

$$\hat{x}_t^- = A\hat{x}_{t-1} + Bu_{t-1} \quad (4.5)$$

$$P_t^- = AP_{t-1}A^T + Q \quad (4.6)$$

Where equation (4.5) is the state update equation and equation (4.6) is the co-variance update equation. Note that the equations project the state and co-variance estimates forward in time from $t - 1$ to t .

Following this a set of measurements are obtained and the state and error co-variance predictions are corrected using the measurement data. In the measurement update, first the Kalman gain, K_t is computed using:

$$K_t = P_t^- H^T (HP_t^- H^T + R)^{-1} \quad (4.7)$$

From this *a posteriori* state estimate is generated using:

$$\hat{x}_t = \hat{x}_t^- + K_t(z_t - H\hat{x}_t^-) \quad (4.8)$$

In this equation the estimated state and measurements are weighted and combined to calculate the true state. This means that if the measurement covariance is much smaller than that of the predicted state, the measurement's

weight will be high and the projected state's will be low thus the uncertainty can be reduced[154].

Finally the *a posteriori* error covariance matrix is computed using:

$$P_t = (I - K_t H) P_t^- \quad (4.9)$$

After each time and measurement update, the process is repeated with the previous *a posteriori* estimates to predict new *a priori* estimates.

The recursive nature of the Kalman filter is a very appealing feature as the filter recursively conditions the current estimate on all past measurements without the need to operate on all of the data directly for each step. Figure 40 expands on the diagram in Figure 39 to give a more complete illustration of the operation of the Kalman filter algorithm including the equations applied at each step.

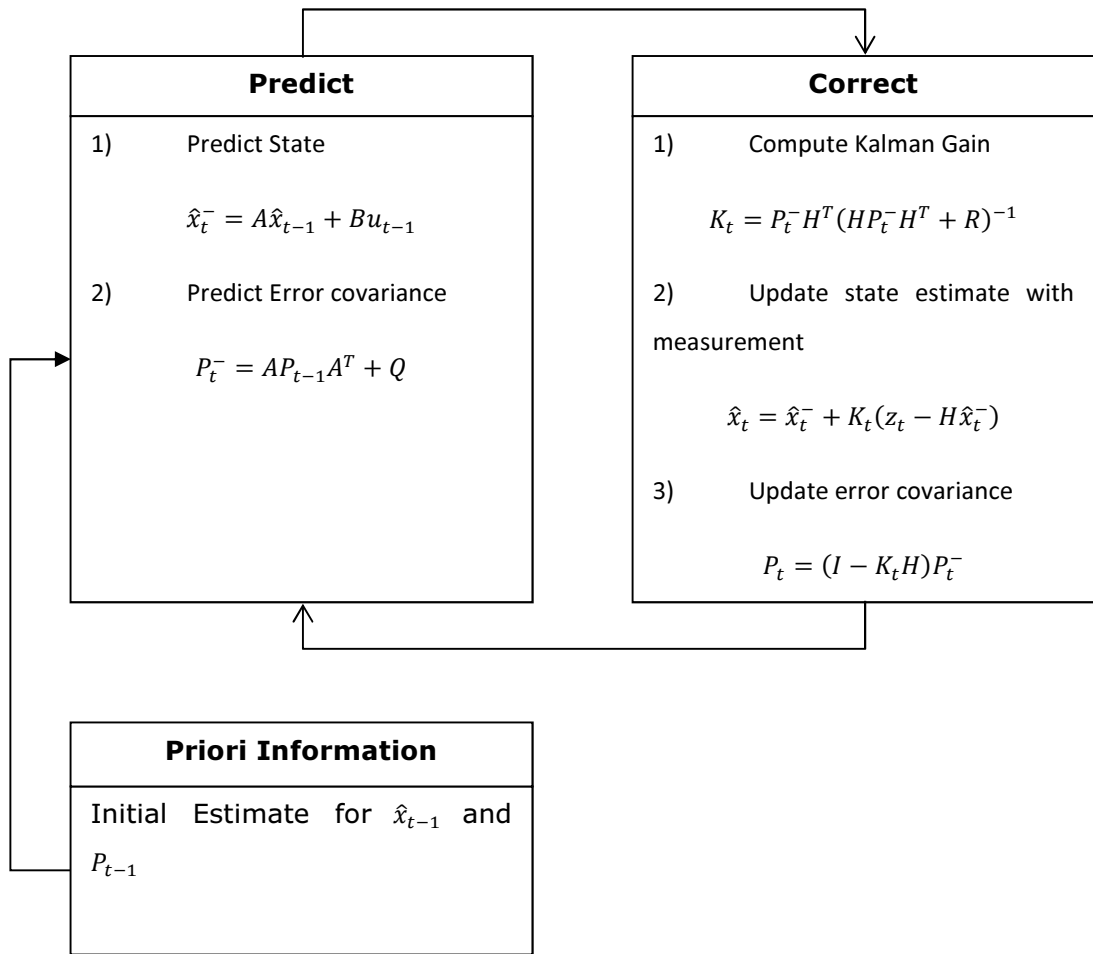


Figure 40 . Schematic diagram of the operation of the Kalman filter [153]

4.5 Extended Kalman Filter (EKF)

As described previously the traditional Kalman filter is a set of equations for estimating the state of a discrete time dynamic system governed by a linear stochastic difference equation. In many cases, such as the application this thesis is concerned with, the dynamic system to be observed is not naturally linear, in such cases it is possible that either the dynamic and/or measurement model are nonlinear. As a result, the traditional Kalman filter must be modified in order to be applied to such systems. The Extended Kalman filter extends the traditional Kalman filter by forming a Gaussian approximation of the joint distribution of state, x_t , and measurements, z_t , using a Taylor series based approximation. This facilitates the application of the Kalman filter algorithm in nonlinear cases by linearising about the current mean and covariance using the partial derivatives of the process and measurement functions the computer estimates in the face of non-linear relationships.

4.5.1 State Vector

As with the traditional Kalman filter the state vector, x_t contains all of the variables of interest, it describes the state of the dynamic system and represents its degrees of freedom.

4.5.2 Dynamic & Observation Models

The dynamic model describes the evolution of the state vector over time, much the same as in the case of the traditional Kalman filter, however in the non-linear case; the dynamic model is usually expressed in the form of a non-linear stochastic difference equation:

$$x_t = f(x_{t-1}, u_{t-1}, w_{t-1}) \quad (4.10)$$

Where the non-linear function f relates the state at the previous time step, $t - 1$ to the state at the current time step, t . It includes any input parameters u_{t-1} and the zero-mean process noise, w_t .

The observation model is given by:

$$z_t = h(x_t, v_t) \quad (4.11)$$

Where the non-linear function h in equation (4.11) relates the state x_t to the measurement z_t taking into account measurement noise, v_t .

4.5.3 Linearisation

As stated above the dynamic models describing the time evolution of the system are written as in equation (4.10). If the relationship is only weakly non-linear this can be approximated as:

$$x_t \approx A_t x_{t-1} + w_t \quad (4.12)$$

Where A_t is the Jacobian matrix of $f(x_{t-1}, u_{t-1}, w_{t-1})$. Similarly if the observation model is given by:

$$z_t = h(x_t, v_t) \quad (4.13)$$

Then it can be approximated by the linearised relationship:

$$z_t \approx H_t x_t + v_t \quad (4.14)$$

Where H_t is the Jacobian matrix of $h(x_t, v_t)$.

In addition to the computational expense of computing the posterior covariance matrix at every time step, the use of the EKF requires that G_t is also computed at each step. This is prohibitively expensive when there are many data [155].

4.5.4 Extended Kalman Filter Algorithm

Like the traditional Kalman filter, the extended Kalman filter can be considered as two distinct steps, again these are a prediction step and an update/correction step. As with the traditional Kalman filter the time update equations project both the state and covariance estimates forward in time from $t - 1$ to t and are given by:

$$\hat{x}_t^- = f(\hat{x}_{t-1}, u_{t-1}, 0) \quad (4.15)$$

$$P_t^- = AP_{t-1}A_t^T + W_tQ_{t-1}W_t^T \quad (4.16)$$

Where the A_t and W_t are the process Jacobians at time, t . Q_t is the process noise covariance at time, t .

Following the prediction step a set of measurements are obtained and the state and error co-variance predictions are corrected using the measurement data. In the measurement update, first the Kalman gain, K_t is computed using:

$$K_t = P_t^- H_t^T (H_t P_t^- H_t^T + V_t R_t V_t^T)^{-1} \quad (4.17)$$

Where H_t and V_t are the measurement Jacobians at time, t and R_t is the measurement noise covariance at time, t .

From this *a posteriori* state estimate is generated using:

$$\hat{x}_t = \hat{x}_t^- + K_t(z_t - h(\hat{x}_t^-, 0)) \quad (4.18)$$

Finally the *a posteriori* error covariance matrix is computed using:

$$P_t = (I - K_t H_t) P_t^- \quad (4.19)$$

After each time and measurement update, the process is repeated with the previous *a posteriori* estimates to predict new *a priori* estimates.

The basic operation of the EKF is the same as the linear Kalman filter as shown in Figure 39. Figure 41 expands on the diagram in Figure 39 to give a more complete illustration of the operation of the EKF algorithm including the equations applied at each step.

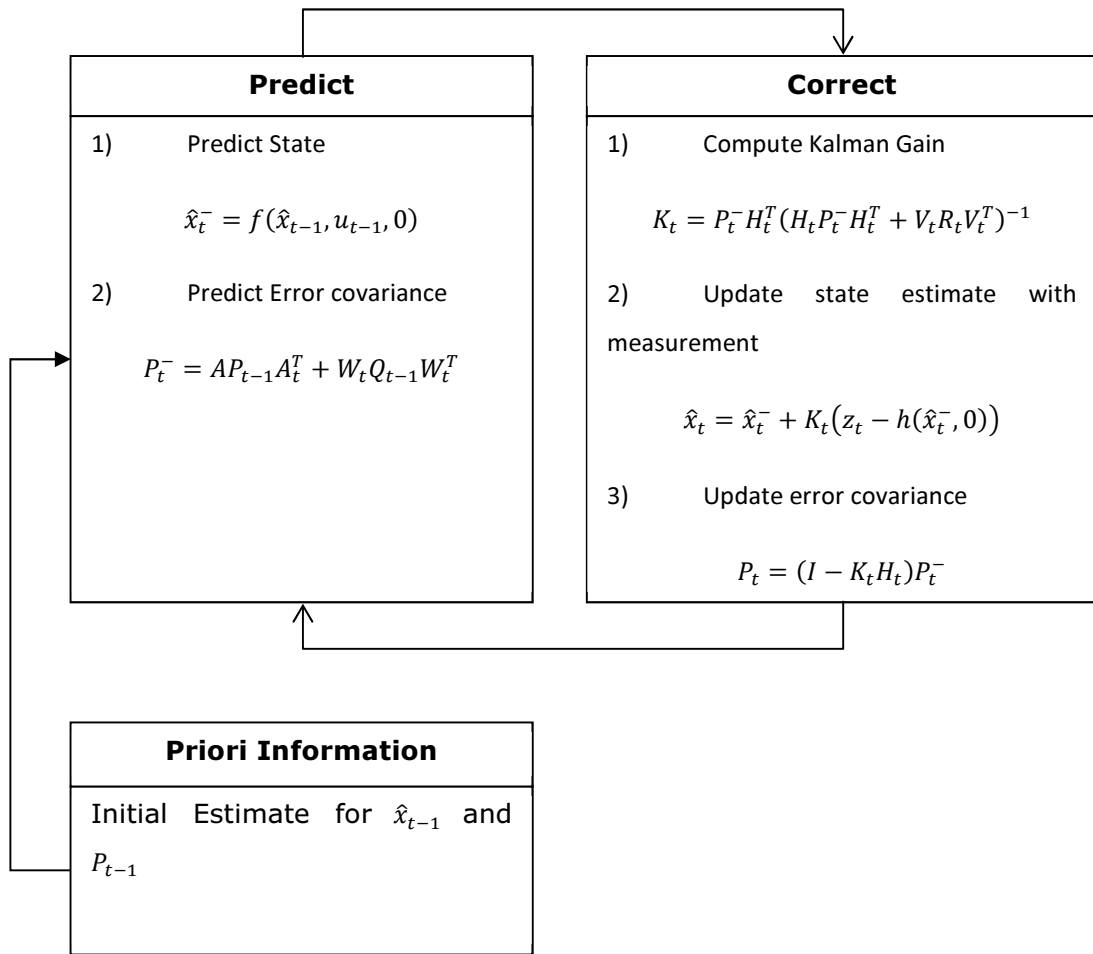


Figure 41. Schematic diagram of the operation of the EKF [153]

4.5.5 Limitations of the Extended Kalman Filter

The EKF has a number of limitations in comparison with the traditional Kalman filter, it is computationally expensive as the dynamic and observation matrix can not be pre-computed as these are functions of the state and thus may vary with each time step. Further the filter only produces reliable results if the error propagation can be well approximated by a linear or quadratic function. When this is not the case, the performance of the EKF can be very poor. It is also true that the filter can only be applied when the Jacobian matrices exist so that the linearisation can be applied [151].

4.6 Ensemble Kalman Filter (EnKF)

"The ensemble Kalman filter (EnKF) method is a Monte Carlo implementation of the Kalman filter in which the mean of an ensemble of realisations provides the best estimate of the population mean and the ensemble itself provides an empirical estimate of the probability density" [155]. The EnKF avoids several of the limitations of the Kalman filter and the EKF. In particular there is no need to linearise the dynamic or the observation models. "There is also no need to compute and update the estimated covariance so the method is practical for very large models" [155].

4.6.1 State Vector

The ensemble Kalman filter propagates an ensemble of initial models through time in order to assimilate data, the information carried by the models at each time step is used to update the model covariance. The ensemble of state estimates is denoted by Y and the EnKF generates an ensemble of N_e initial models consistent with prior knowledge of the initial state and its probability distributions:

$$X = \{x_1, x_2, \dots, x_{N_e}\} \quad (4.20)$$

Where x_i for $i = 1, \dots, N_e$ are state vectors. As with the traditional Kalman filter and the EKF, the state vectors in the EnKF contain all of the dynamic variables of interest that define the state of the dynamic system and represent its degrees of freedom.

4.6.2 Ensemble Kalman Filter Algorithm

As with the traditional and EKF, the EnKF consists of two distinct and sequential steps, the prediction and the correction/update step. In the prediction step the EnKF projects the state estimates in each member of the ensemble forward in time from $t - 1$ to t as in:

$$x_{t,i}^- = f(x_{t-1,i}) \quad (4.21)$$

For $i = 1, N_e$.

However the covariance is no longer calculated as in the traditional Kalman filter, instead it is estimated from the mean of the ensemble members.

$$P_X^- = \frac{1}{\sqrt{N_e - 1}} \sum_{i,j=1}^{N_e} (x_i^- - \bar{x}^-)(x_j^- - \bar{x}^-)^T \quad (4.22)$$

Where \bar{x}^- is the mean of the ensemble members at the current time step and i and j refer to ensemble members. It is not practical to compute and store P_X^- for large problems, fortunately the computation of P_X^- is rarely necessary. Instead L_e is computed and stored, L_e is given by:

$$L_e = \frac{1}{\sqrt{N_e - 1}} (X - \bar{x}^-) \quad (4.23)$$

Following from this, the correction step utilises L_e to provide a much more computationally efficient form of the Kalman gain as given by:

$$K_e = L_e (H L_e)^T [(H L_e)(H L_e)^T + R]^{-1} \quad (4.24)$$

Each ensemble member is thus updated using the following:

$$x_{ti} = x_{ti}^- + K_e (z_t - H x_{ti}^-) \quad (4.25)$$

Where z_t is the measurement data.

Figure 42 shows the steps of the EnKF in schematic form.

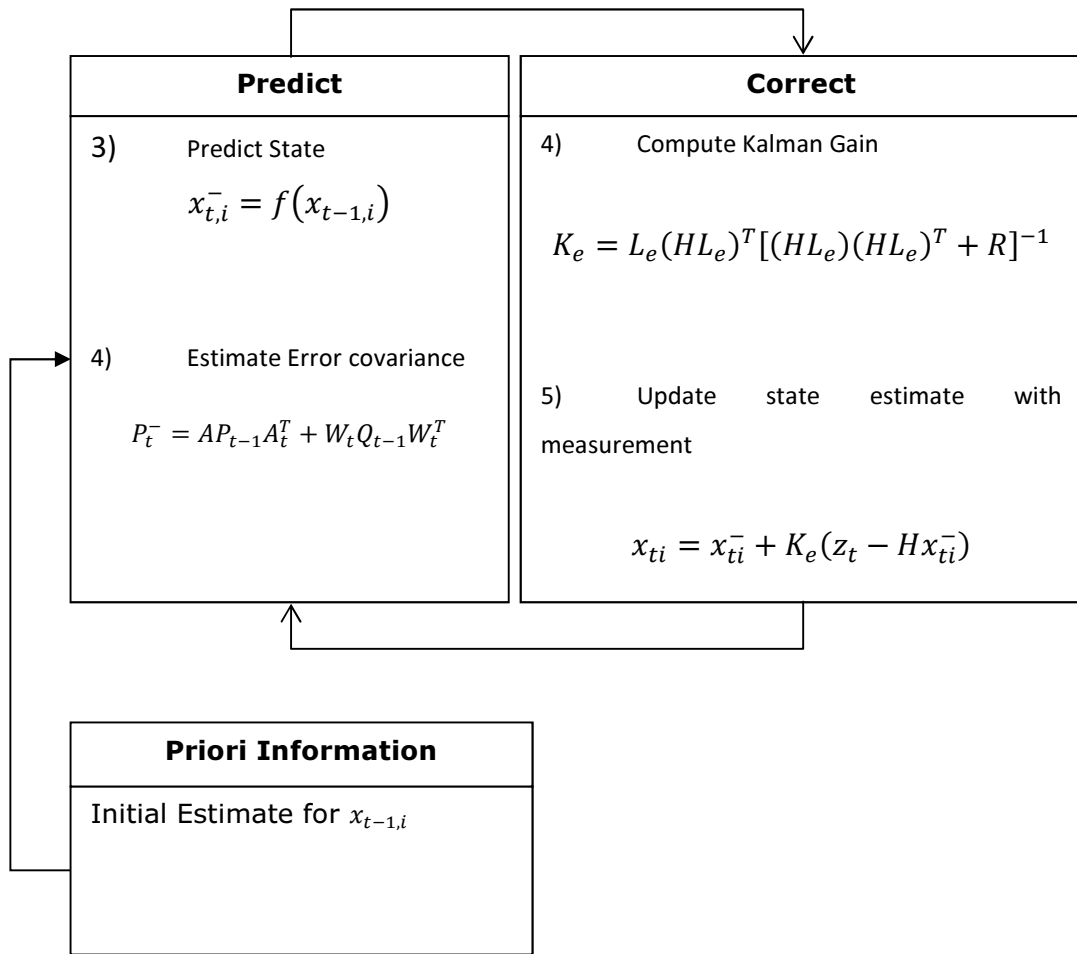


Figure 42. Schematic diagram of the operation of the Ensemble Kalman Filter

4.7 Kalman Filter Based Inverse Solver

Having considered the basic operation of the Kalman filter and its various forms, as relevant to the application with which this thesis is concerned, there are a number of ways in which the algorithm may be implemented in the context of reconstruction of ERT data, as acquired utilising the LCT2 instrument.

4.7.1 Hybrid Reconstruction

It is proposed that a hybrid reconstruction scheme may be implemented utilising the Kalman Filter in combination with traditional reconstruction schemes, such as those supplied within the EIDORS suite. Any appropriate formulation of the Kalman filter may be used, such as the EKF or the EnKF. In this case, at each time step:

1. The propagation of moisture in the soil core is estimated using COMSOL Multiphysics.
2. Boundary data is acquired using the LCT2 instrument.
3. The boundary data is reconstructed using any appropriate reconstruction scheme.
4. The resulting resistivity map is converted to a moisture content map using Archie's law, this provides an indirect measurement of the moisture content within the soil core.
5. A sub-domain (such as to avoid the most artefact prone regions of the traditional inversion, e.g. very close to the electrodes, see Figure 36 and Figure 38) of both the COMSOL estimation and the reconstructed moisture content are mapped onto a common mesh.
6. The two data sets (estimation and measurement) are compared and the flow parameters of the COMSOL model are updated as according to the operation of the Kalman Filter.

Refer to Figure 43 for a schematic diagram that reflects the above mode of operation.

Advantages of this method are that the final reconstruction is given by the current state of the forward solver i.e. the COMSOL Multiphysics based forward model, as such, even despite the reliance on traditional inverse solvers and their subsequent limitations, the final reconstruction may be of a higher resolution. Additionally the dynamic model representation of the forward model is relatively simple as it is essentially the state space representation of the Richards equation. Further to this, due to the ability to update the forward model

based on a sub-domain the impact of being reliant on traditional inversing algorithms may be negated.

Disadvantages are of course the reliance on traditional inversing methods, as such the effectiveness of this method will not only be influenced by the typical limitations of said algorithms but in practical terms also by the computational demands of the traditional algorithms in addition to the Kalman filter operation.

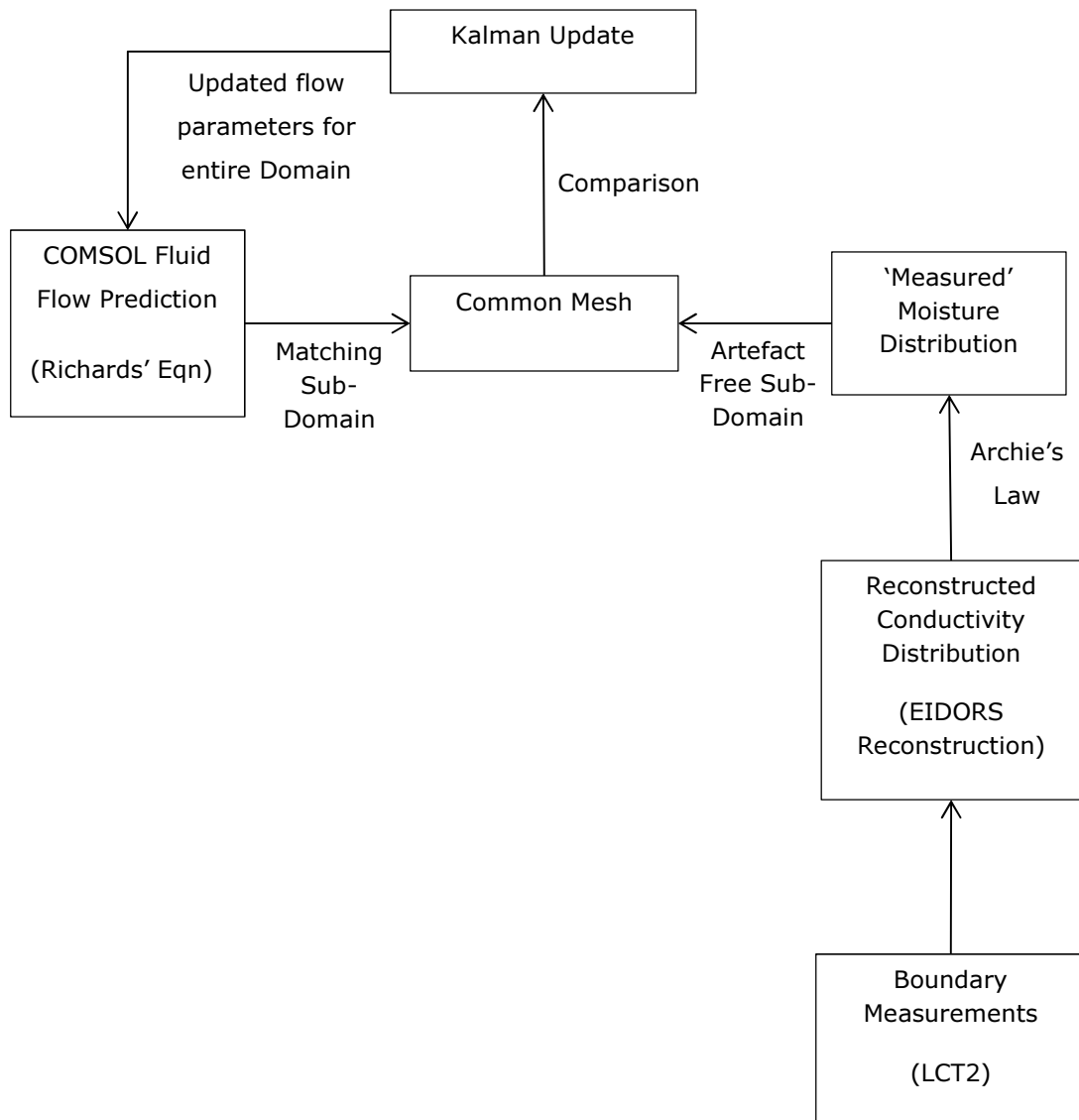


Figure 43. Hybrid Reconstruction

4.7.2 Kalman Filter Only

An alternative approach to the above would be to eliminate the reliance on traditional inverse techniques and perform a Kalman filter only based optimisation. Any appropriate Kalman filter formulation may be utilised, such as the EKF or the EnKF. In this case, at each time step:

1. The propagation of moisture in the soil core is estimated using COMSOL Multiphysics.
2. This predicted moisture distribution is converted to a predicted electrical resistivity distribution using Archie's law.
3. The resultant predicted boundary data, as based on the above electrical resistivity distribution is generated.
4. Boundary data is acquired using the LCT2 instrument.
5. The two data sets (estimated boundary data and measured boundary data) are compared and the flow parameters of the COMSOL based forward model are updated as according to the operation of the Kalman Filter.

Note, steps 1,2,3 are essentially one step, as one run of the multiphysics based forward model presented in the previous section carries out these 3 steps.

Refer to Figure 44 for a schematic diagram that reflects the above mode of operation.

Advantages of this method are that the final reconstruction is given by the current state of the forward solver i.e. the COMSOL Multiphysics based forward model. Further, the solution in this case is not reliant on traditional inverse solvers, in fact no inversion is carried out and the solution is a culmination of many runs of the forward model with increasingly refined input parameters, as such the limitations of traditional inverse techniques are eliminated. Additionally, unlike the hybrid method proposed above there is no additional computation time attributed to that of a traditional inverse technique contained within the algorithm. It is yet unclear whether this would produce a faster algorithm, since where computation time is shed by eliminating the need for a traditional inverse solver, computation time is added due to the increased complexity of the forward solver and the dynamic model. The dynamic model representation of the forward model required for the operation of the Kalman filter in this case is much more complex, this is one distinct disadvantage of this particular reconstruction scheme.

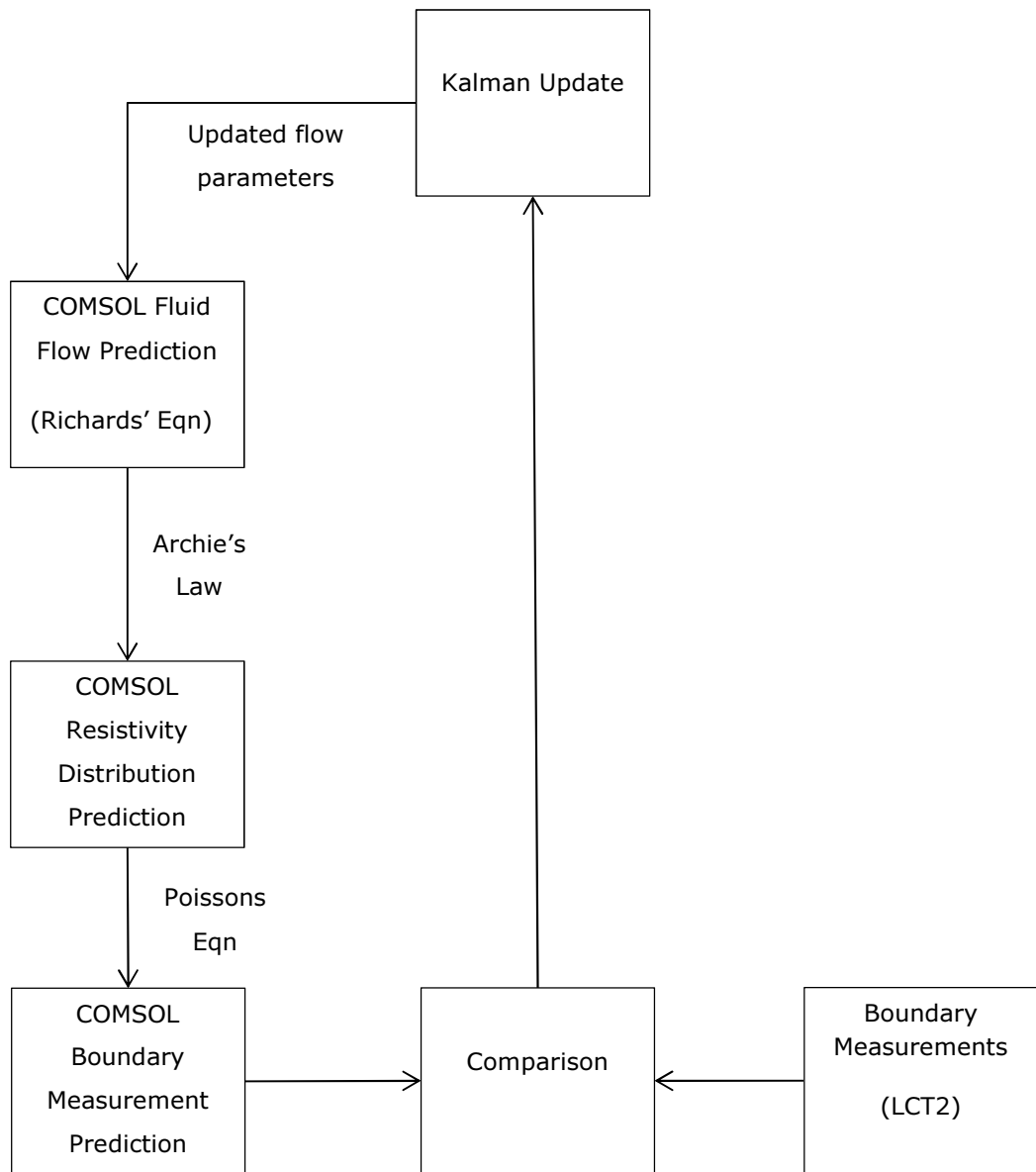


Figure 44. Kalman Filter Only

4.8 Summary

A series of traditional inversion techniques have been used to reconstruct both simulated and experimental data and the subsequent images presented. Further to this, this chapter has introduced a series of parameter estimation tools for estimating the state variables of a dynamic system in a number of scenarios ranging from the linear case where the traditional Kalman filter can be applied, through non-linear cases, where the Kalman filter is extended by utilising an additional linearisation step and also large model case, where an ensemble implementation of the Kalman filter may be optimal. From this, two potential reconstruction schemes based on the use of the Kalman filter, for the reconstruction of ERT data collected using the LCT2 instrument on a soil core, have been proposed and their merits debated.

5 Conclusions and Future Work

5.1 Literature Review & Decisions Made

Based on the literature survey it was abundantly clear that tomographic techniques were highly appropriate for inferring the 3D spatial moisture distribution on the lysimeter scale, i.e. around the root zone of a maize plant as contained in a cylindrical vessel of 3-6 litres in volume. In particular electrical tomographic methods were favourable for in-situ monitoring of crops due to relatively low power requirements, instrument size and component costs hence allowing mass deployment in the field or industrial greenhouse environment.

Ideally an EIT instrument capable of measuring complex impedance would be utilised however for this research it was decided that the LCT2 instrument would be used for data acquisition, this decision was made for logistical reasons. However the proposed inversion techniques may be applied to both ERT and ECT in insolation or as part of complex impedance EIT imaging system.

It was also noted that the Richards' equation is universally accepted as the governing equation for soil water movement in the unsaturated zone and thus the most appropriate soil transport model to use in a forward model that would include a fluid flow component. This model has been extensively tested over the previous 30 years and stands as the most widely used soil transport model to date. Furthermore there were several commercially available solvers for the solution of the Richards' equation, of these COMSOL Multiphysics was chosen.

COMSOL Multiphysics costs approximately £3580 (2012) including both the AC-DC module and the Earth Sciences module allowing both the simulation of electric fields, as per the traditional EIT forward problem, and soil hydrology. In addition COMSOL Multiphysics interfaces with MATLAB via the included LiveLink™ for MATLAB module allowing post-processing of generated data, editing and visualisation within the popular MATLAB environment. MATLAB was already available on the current workstation and is widely used in both research and academic institutions thus the developed techniques may propagate efficiently within the scientific community where appropriate.

Three well documented coupling mechanisms between electrical properties and soil water content were identified, i.e. the Topp model, CRIM equation and Archie's law. These equations were tested experimentally to determine the most appropriate model for the soil samples available.

Finally, it was decided that statistical methods and/or iterative parameter estimation techniques such as the Kalman filter offered distinct advantages over traditional inversing techniques, particularly for the study of dynamic processes. As such, it was proposed that statistical methods in particular the Kalman filter would be utilised to propose a new reconstruction scheme.

5.2 Difficulties Faced

During the literature review recent developments in coupled root water uptake and root growth modelling were investigated and it was decided that the L-system based root growth model RootBox, implemented in the popular programming language MATLAB, would be used to model root inclusions. This decision was made as the toolbox includes meshing functions for meshing the soil domain around the generated root structure which could then imported into COMSOL Multiphysics and coupled with arbitrary root water uptake and soil transport models. However as experimental work was undertaken, it quickly became apparent that the medium, soil, was far more complex than anticipated and even when strict test procedures are adhered to, the inherent properties of the soil meant that experimental difficulties were experienced. As such it was considered that adding a plant specimen at this stage would complicate matters beyond the scope and time constraints of the project. As such this work focused a soil core, without the presence of a plant specimen. However, due to the extensible framework of this body of work, it would be possible, in future work to add root inclusions and model their behaviour in tandem with the fluid dynamics observed in soil.

Furthermore it should be noted that a major portion of this work consists of the identification, experimental validation and implementation of physical models and coupling mechanisms suitable for predicting soil water distributions and the resulting electrical measurement data at the boundary such that the forward problem, which is critical to both traditional inversing techniques and the proposed inversion techniques, could be implemented. As such, substantial effort was placed in characterising 5 common agricultural soils as found in the United Kingdom such that the models could be calibrated and initialised appropriately. This work was not undertaken without difficulty, the instrumentation used in the characterisation of the soils, namely the tensiometers, despite careful handling as per the manufacturers guidance, the operation of the devices was questionable and delays were incurred through substantial time spend trouble shooting and eventually returning them to the manufacturer for servicing.

5.3 Forward Problem

Fluid flow in a porous media and electrostatics models were implemented and validated in isolation and subsequently coupled through the bulk electrical conductivity or dielectric constant vs. soil saturation relationship determined by a mixture model. As such a multiphysics based forward solver was implemented in COMSOL multiphysics. The following sub-sections provide brief conclusions on the individual elements and the finally multiphysics based forward solver.

5.3.1 Fluid Flow

The Richards equation was implemented in COMSOL Multiphysics and the average error between simulated and observed data, based on visual inspection was calculated to be less than 10%. Any discrepancies between the shape of the simulated and observed wetting fronts was attributed to two main causes:

1. Varying spatial compaction of the soil in the experimental case, as despite all efforts to create a uniformly packed soil, it is unlikely that a homogenous packing density was indeed achieved, see 5.2
2. In this experiment the soil parameterisation was estimated based on the literature, rather than from measured data on the specific soil sample, thus the error in the estimated soil parameterisation would have contributed to this error. The extent of this error may be reduced by prior parameterisation of a sub-sample of the soil sample being observed, as such a series of soil parameterisation experiments were carried out.

5.3.2 Soil Parameterisation

Saturated Hydraulic conductivity was measured for a number of soil cores. It was found that saturated hydraulic conductivity is highly dependent on soil packing density, as a result poor repeatability was found between "equivalent" soil cores with values ranging from 1.1 m/d to 2.34 m/d. This is attributed to the random nature of the particle packing within the soil. Simulated wetting fronts based on measured saturated hydraulic conductivity values were accurate with approximately 11% error relative to the observed wetting front for the corresponding soil core. This was consistent with previous experiments.

Furthermore, the non-saturated hydraulic conductivity was evaluated by way of experimentally obtained soil water retention curves. Parameters derived from these curves agree with the existing literature, the sensitivity of the measurement instrumentation to correct filling has been apparent and the reliability questionable, see 5.2.

Spatial variation of saturated hydraulic conductivity was assumed to be negligible, the observed results show that this is a valid assumption for a soil packed following the outlined standard operating procedure. Furthermore two additional soil types were parameterised.

5.3.3 Electrostatics and Coupling Mechanisms

An electrostatic model was implemented in COMSOL multiphysics and experiments show that the electrostatics simulation is able to predict changes in capacitance due to varying heights of water and varying levels of soil saturation.

The electrostatic model has been shown to exhibit an average error of <9% for varying water fill levels in comparison to measured data and an average error of 2.3% was observed between COMSOL and EIDORS solutions for a homogeneous background conductivity. The worst case absolute error was 7.4% which occurs between adjacent electrode pairs.

Archie's law was chosen to couple the electrostatics and fluid flow models, this was not verified experimentally as it did not seem to be an appropriate use of time, given it is almost universally accepted as correct.

However the Topp and CRIM models were experimentally validated. Capacitance predictions generated using both the Topp and CRIM models to calculate dielectric constants of a wet soils were compared to measured data for corresponding soil saturation levels. It was found that beyond 20% soil saturation, there were difficulties in measuring the capacitance of the wetted soil. This has been attributed to the limitations of the measurement instrumentation for highly conductive media.

The CRIM model was evaluated for two further matrices in addition to water wet soil. This was not possible with the Topp model as this relation is only valid for a matrix of water wet soil. Predictions based on the CRIM model had an average error of between 3.77% and 5.25% for experiments where a soil was wetted with rapeseed oil and a sand was wetted with deionised water. As a result, the CRIM model was implemented in COMSOL multiphysics to couple the electrostatic simulation to the soil transport simulation to allow for multiphysics simulations.

Experiments have shown that the temperature dependency of the dielectric constant of water does not contribute substantial error over the normal operating temperature range of the instrument.

5.3.4 Multiphysics

The individual elements identified and verified have been combined within a FEM implemented in COMSOL Multiphysics to produce a multiphysics based forward solver. The forward solver predicts fluid flow using Richards' equation, converts the resulting soil moisture distribution to equivalent soil electrical properties using either Archie's law or the CRIM equation, depending on the modality, and then predicts boundary voltage measurements.

5.4 Inverse Problem

A series of traditional inversion techniques found in the EIDORS suite were used to reconstruct both simulated and experimental data. Further to this, two potential reconstruction schemes based on the use of the Kalman filter, for the reconstruction of ERT/EIT data collected using the LCT2 instrument on a soil core, have been proposed and their merits debated.

5.4.1 Hybrid Reconstruction

Advantages of this method are that the final reconstruction is given by the current state of the forward solver i.e. the COMSOL Multiphysics based forward model, as such, even despite being reliant on a traditional inverse solver and the subsequent limitations, the final reconstruction may be of a higher quality. Further, it is proposed that since the whole system model can be updated based on a sub-domain of the measurement, the impact of typical ERT/EIT reconstruction artifacts may be minimised. Additionally the dynamic model representation of the forward model is relatively simple as it is essentially the state space representation of the Richards equation.

Disadvantages are of course the reliance on traditional inverting methods, as such the effectiveness of this method will not only be influenced by the typical limitations of said algorithms but in practical terms also by the computational demands of the traditional algorithms in addition to the Kalman filter operation.

5.4.2 Kalman Filter Only

Advantages of this method are, as per with the hybrid method, that the final reconstruction is given by the current state of the forward solver i.e. the COMSOL Multiphysics based forward model. However, the solution in this case is not reliant on traditional inverse solvers, in fact no inversion is carried out at all and the solution is a culmination of many runs of the forward model with increasingly refined input parameters, as such the limitations of traditional inverse techniques are eliminated. Additionally, unlike the hybrid method

proposed above there is no additional computation time attributed to that of a traditional inverse technique contained within the algorithm. It is yet unclear whether this would produce a faster algorithm, since where computation time is shed by eliminating the need for a traditional inverse solver, computation time is added due to the increased complexity of the forward solver and the dynamic model.

The dynamic model representation of the forward model required for the operation of the Kalman filter in this case is much more complex, this is one distinct disadvantage of this particular reconstruction scheme.

5.5 Future Work

As with any research project, the time granted was not sufficient to carry out all of the work desired, as such several possibilities for future work are presented in the following sub-sections.

5.5.1 Implementation of Proposed Algorithms

A great deal of the research programme consisted of the identification, experimental validation and implementation of physical models and coupling mechanisms suitable for predicting soil water distributions and the resulting electrical measurement data at the boundary such that the forward problem, which is critical to both traditional inversing techniques and the proposed inversion techniques, could be implemented. The culmination of which meant that the proposed algorithms have not yet been implemented. As such future work should include the implementation of the proposed algorithms using MATLAB. This will allow for the interfacing and exchange of data between EIDORS, which is also written in MATLAB, COMSOL Multiphysics which can be interfaced with MATLAB and also Rootbox (the inclusion of which would be an additional future task, as detailed in 5.5.4) which is also written in MATLAB. This would also allow for the propagation of the algorithm in the scientific community.

The most substantial portion of this future work would be to derive the dynamic model, or state space representation, of both the Richards' equation (for implementation of the hybrid reconstruction) and the Multiphysics forward model which includes electrostatics, fluid flow and mixture model physics (for the Kalman Filter only reconstruction). For the latter case, this is not an insubstantial task as the forward model is very complex and features many parameters.

5.5.2 Validation of Proposed Algorithms

Following the implementation of the proposed algorithms it would be essential to validate them using simulated and experimental data, validation via simulation is fairly simple however experimental validation is more challenging, as such a number of experiments are proposed.

1. Observe a completely saturated soil core throughout a drying cycle, drying will occur through surface evaporation only. This is anticipated to be the most repeatable and controllable experiment since the soil could be uniformly wet and thus a homogenous distribution at the beginning. Variations may be carried out such as leaving the entire top surface open to allow uniform drying or by covering the majority of the top surface but with a known opening to allow for evaporation, this will produce none uniform drying.
2. Observe a wetting event from a point source.
3. The above may be combined whereby a wetting event is long enough to fully saturate the soil core and then the drying phase is subsequently observed.

Given that one can not see into the soil core to know if the computed solution is indeed correct at each time step, it is therefore proposed that 3 laboratory scales and a triangular support are used to monitor the centre of gravity of the soil core throughout any experiments. This will allow comparison to reconstructed images since the centre of gravity will move to where the soil is most wet. Therefore this point can be compared to reconstructed images. A triangular support has been manufactured and data acquisition software for acquiring the weight from 3 individual laboratory scales has been written. A function for determining the centre of gravity, given the dimensions of the support and the 3 weight values has also been written. In addition to this, the total weight, as determined from the sum of the three laboratory scale readings, may be used to calculate the gravimetric water content, this can be compared to the total moisture contents calculated from the reconstructed images.

5.5.3 Complex Impedance Measurement

Given that medium, soil, exhibits both conductive, wet, dominating phases and dielectric, dry, dominating phases, there are a potential problems arising from the formation or breaking of conducting paths between measurement electrodes and a transition between the dominance of the real and imaginary impedance components. As a result of water loss, soil is prone to shrinking and cracking which further complicates the measurement process due to the quality of the connection at the boundary points between the medium and the electrodes. As a result it may be beneficial to track complex impedance, as such both phases can be accounted for and comparison between resistance and capacitance data may offer some interesting insights. Future work may be to replace the current measurement instrument with an alternative instrument. This may also involve some consideration of electrode construction, for example capacitively coupled electrodes and modified measurement protocols, for example spectroscopic measurements. Some work on capacitively coupled electrodes was carried out in tandem with this research project, the reader is encouraged to refer to [21] and section 3.2.4.

5.5.4 Plant Soil Interactions

It would be desirable to include plant soil interactions within the forward model, this is possible using the L-system based root growth model RootBox, implemented in the popular programming language MATLAB. This toolbox includes meshing functions for meshing the soil domain around a generated root structure. These meshes can then be imported into COMSOL Multiphysics and coupled with arbitrary root water uptake and soil transport models and in theory with the electrostatic models detailed in this thesis to expand the forward model.

5.6 Final Words

This research project has presented a multiphysics based forward model, incorporating a fluid flow model for soil water interactions, mixture models for the conversion of moisture contents to electrical properties and electrostatics models for the prediction of boundary measurements. The individual constituents of the forward model have been implemented and validated prior to their integration and the integrated model has been demonstrated.

Further to this, two reconstruction schemes, based on the use of this forward model, in combination with traditional inversion techniques and statistical techniques have been proposed.

It is envisaged that the work contained within this thesis will contribute to the delivery of a new tool for seed breeders utilising electrical impedance tomography (EIT) technology. This tool will indicate how efficiently a plant specimen utilises the water and nutrients available in the surrounding soil. It will be used in greenhouses and/or field trials during seed breeding programmes as an on-line, in-situ tool for monitoring root water uptake for the purpose of sub-surface phenotyping and early detection of desirable genetic traits. This will facilitate the identification and delivery of drought tolerant food crops and securing the food supply of tomorrow. Further implications of the research programme include increased control in maintaining soil health by ensuring excessive water is not used in agricultural food production.

6 References

- [1] Wang G 2005 Agricultural drought in a future climate: results from 15 global climate models participating in the IPCC 4th assessment *Climate Dynamics* **25** 739-753
- [2] Loaiciga H A et al 1996 Global warming and the hydrological cycle *Journal of Hydrology* **174** 83-127
- [3] Postel S L 1998 Water for food production: Will there be enough in 2025? *BioScience* **48** 8 629-37
- [4] Sivakumar M V K, Das H P & Brunini O 2005 Impacts of present and future climate variability and change on agriculture and forestry in the arid and semi-arid tropics, *Climatic Change* **70** 31-72
- [5] Lange M D 2001 Water law and human rights – roles and responsibilities *Water Science and Technology* **43** 4 143-50
- [6] Kendall H W and Pimentel D 1994 Constraints on the expansion of the global food supply *Ambio* **23** 3 198-205
- [7] Burke I C et al 1998 Plant-Soil interactions in temperate grasslands *Biogeochemistry* **42** 121-143
- [8] Grieve B D, Murphy S, Burnett-Thompson A and York T A 2010 An accessible electrical impedance tomograph for 3D imaging, *Transactions of the Institute of Measurement and Control* **32** 1 31-50
- [9] Grieve B D et al 2010 Towards subsoil imaging of 'Root Function' as a phenotype, for accelerated breeding of climate tolerant crops 6th *World Congress on Industrial Process Tomography*
- [10] Garré S et al 2011 Three-Dimensional Electrical Resistivity Tomography to Monitor Root Zone Water Dynamics *Vadose Zone j.* **10** 412-424
- [11] Tapp H S, Kemsley E K, Wilson R H and Holley ML 1998 Image improvement in soft-field tomography through the use of chemometrics *Meas. Sci. Technol.* **9** 592-598
- [12] Borcea L 2002 Electrical Impedance Tomography *Inverse Problems* **18** 99-136
- [13] Reichle R H, McLaughlin D B and Entekhabi D 2002 Hydrologic Data Assimilation with the Ensemble Kalman Filter *Monthly Weather Review* **130** 103-114
- [14] Camporese M, Cassiani G, Deina R and Salandin P 2011 Assessment of local hydraulic properties from electrical resistivity tomography monitoring of a three-dimensional synthetic tracer test experiment *Water Resources Research* **47** 12 W12508 doi:10.1029/2011WR010528
- [15] Podd F 2010 Analytical Solution for Insulating Electrodes *SSUIC Internal Report*
- [16] Koestel J et al 2009 Imaging brilliant blue stained soil by means of electrical resistivity tomography *Vadose Zone J.* **8** 963-975
- [17] Koestel J et al 2008 Quantitative imaging of solute transport in an unsaturated and undisturbed soil monolith with 3-D ERT and TDR *Water Resources Research* **44** W12411
- [18] Garré et al 2010 Comparison of heterogeneous transport processes observed with electrical resistivity tomography in two soils *Vadose Zone J.* **9** 336-349
- [19] Garré et al 2011 Three-Dimensional Electrical Resistivity Tomography to Monitor Root Zone Water Dynamics *Vadose Zone J.* **10** 412-424

- [20] R R Hayes *et al* 2010 An investigation into the use of a mixture model for simulating the electrical properties of soil with varying effective saturation levels for sub-soil imaging using ECT *J. Phys.: Conf. Ser.* **255** 012002
- [21] R. Hayes *et al* 2012 Capacitively-Coupled Impedance Measurements for ERT, 6th International Symposium on Process Tomography, Cape Town, South Africa, 26-28 March 2012
- [22] Wang G 2005 Agricultural drought in a future climate: results from 15 global climate models participating in the IPCC 4th assessment *Climate Dynamics* **25** 739-753
- [23] Loaiciga H A *et al* 1996 Global warming and the hydrological cycle *Journal of Hydrology* **174** 83-127
- [24] Postel S L 1998 Water for food production: Will there be enough in 2025? *BioScience* **48** 8 629-37
- [25] Maracchi G, Siroenko O & Bindi M 2005 Impacts of present and future climate variability on agriculture and forestry in the temperate regions: Europe *Climatic Change* **70** 117-135
- [26] Riha S J, Wilks D S & Simoens P 1996 Impact of temperature and precipitation variability on crop model predictions *Climatic Change* **32** 293-311
- [27] Burke I C *et al* 1998 Plant-Soil interactions in temperate grasslands *Biogeochemistry* **42** 121-143
- [28] Pohlmeier A *et al* 2008 Changes in soil water content resulting from Ricinus root uptake monitored by magnetic resonance imaging *Vadose Zone J.* **7** 1010-1017
- [29] Pierret A, Kirby M & Moran C 2003 Simultaneous X-ray imaging of plant root growth and water uptake in thin-slab systems *Plant and Soil* **255** 361-373
- [30] Leitner D and Schnepf 2009 Root growth simulation using L-systems *Proceedings of Algoritmy* 313-20
- [31] Schnepf A and Leitner D 2009 FEM simulation of below ground processes on a 3-dimensional root system geometry using Distmesh and COMSOL Multiphysics, *Proceedings of Algoritmy* 321-30
- [32] Lynch J P, Nielsen K L, Davis R D and Jabllokow A G 1997 SimRoot: Modelling and visualization of root systems *Plant and Soil* **188** 139-51
- [33] Javaux M, Schröder T, Vanderborght J and Vereecken H 2008 Use of a three-dimensional detailed modelling approach for predicting root water uptake *Vadose Zone J.* **7** 1079-88
- [34] Šimůnek J, van Genuchten M T and Šejna M 2008, Development and applications of the HYDRUS and STANMOD software packages and related codes *Vadose Zone J.* **7** 587-600
- [35] Knight R & Endres A 1990 A new concept in modelling the dielectric response of sandstones: Defining a wetted rock and bulk water system *Geophysics* **55** 5 586-594
- [36] Topp G C, Davis J L & Annan A P Electromagnetic determination of soil water content: measurements in coaxial transmission lines *Water Resources Research* **16** 3 574-582
- [37] White R E 1979 *Introduction to the Principles and Practice of Soil Science* Blackwell Scientific Publications
- [38] Newill P 2010 Soil Basics *SSUIC Internal Report*

- [39] Garner C M K et al. 1991 Soil Water Content, In: Smith K A & Mullins C E (editors), *Soil and Environmental Analysis: Physical Methods* 2nd ed, p6-7
- [40] Eller H and Denoth A 1996 A capacitive soil moisture sensor *Journal of Hydrology* **185** 137-146
- [41] Cosh M H 2005 Calibration of an impedance probe for estimation of surface soil water content over large regions *Journal of Hydrology* **311** 49-58
- [42] Stangl R, Buchan G D and Loiskandl W 2009 Field use and calibration of a TDR-based probe for monitoring water content in a high-clay landslide soil in Austria *Geoderma* **150** 23-31
- [43] Seyfried M S, Grant LE, Du E & Humes K 2005 Dielectric Loss and Calibration of the Hydra Probe Soil Water Sensor *Vadose Zone* **4** 1070-1079
- [44] Bogaen H R, Huisman J A, Oberdörster & Vereecken H 2007 Evaluation of a low-cost soil water content sensor for wireless network applications *Journal of Hydrology* **344** 32-42
- [45] Rosenbaum U et al 2009 Sensor-to-sensor variability of ECH2O EC-5, TE and 5TE sensors used for wireless sensor networks
- [46] Seyfried M S & Murdock M D 2003 Measurement of Soil Water Content with a 50-MHz Soil Dielectric Sensor *Soil Sci. Soc. Am. J.* **68** 394-403
- [47] Roth K, Schulin R, Flüßler H and Attinger W 1990 Calibration of time domain reflectometry for water content measurement using a composite dielectric approach *Water Resources Research* **26** 4 2267-2273
- [48] Noborio K 2001 Measurement of soil water content and electrical conductivity by time domain reflectometry: A review *Computers and Electronics in Agriculture* **31** 213-237
- [49] Dobson M C, Ulaby F T, Hallikainen M T & Mohamed A ER 1985 Microwave dielectric behaviour of wet soil – part II: Dielectric mixing models *IEEE Transactions on Geoscience and Remote Sensing* **GE-23** 1 35-46
- [50] Chanzy A et al. 1998 Soil moisture monitoring at the field scale using automatic capacitance probes *European Journal of Soil Science* **49** 637-648
- [51] Inoue Y, Watanabe T and Kitamura K 2002 Prototype time-domain reflectometry probes for measurement of moisture content near the soil surface for applications to "on-the-move" measurements *Agricultural Water Management* **50** 41-52
- [52] Dean T J, Bell J P & Betty A J B 1987 Soil moisture measurement by an improved capacitance technique, part 1. sensor design and performance *Journal of Hydrology* **93** 67-78
- [53] Kizito CS et al 2008 Frequency, electrical conductivity and temperature analysis of a low-cost capacitance soil moisture sensor *Journal of Hydrology* **352** 367-378
- [54] Robinson M & Dean T J 1993 Measurement of near surface soil water content using a capacitance probe *Hydrological Processes* **7** 77-86
- [55] Grieve B D, Murphy S, Burnett-Thompson A and York T A 2010 An accessible electrical impedance tomograph for 3D imaging, *Transactions of the Institute of Measurement and Control* **32** 1 31-50
- [56] Grieve B D et al 2010 Towards subsoil imaging of 'Root Function' as a phenotype, for accelerated breeding of climate tolerant crops 6th *World Congress on Industrial Process Tomography*

- [57] Koestel J et al 2009 Imaging brilliant blue stained soil by means of electrical resistivity tomography *Vadose Zone J.* **8** 963-975
- [58] Koestel J et al 2008 Quantitative imaging of solute transport in an unsaturated and undisturbed soil monolith with 3-D ERT and TDR *Water Resources Research* **44** W12411
- [59] Koestel J et al 2009 Noninvasive 3-D transport characterization in a sandy soil using ERT: 1. Investigating the validity of ERT-derived transport parameters *Vadose Zone J.* **8** 711-722
- [60] Garré et al 2010 Comparison of heterogeneous transport processes observed with electrical resistivity tomography in two soils *Vadose Zone J.* **9** 336-349
- [61] Garré et al 2011 Three-Dimensional Electrical Resistivity Tomography to Monitor Root Zone Water Dynamics *Vadose Zone J.* **10** 412-424
- [62] Zimmermann E, Kemna A, Berwix J, Glaas W and Vereecken H 2008 EIT measurement system with high phase accuracy for the imaging of spectral induced polarization properties of soils and sediments *Meas. Sci. Technol.* **19** 1-9
- [63] Dahlin T 2000 Short note on electrode charge-up effects in DC resistivity data acquisition using multi-electrode arrays *Geophysical Prospecting* **48** 181-87
- [64] Ozier-Lafontaine H and Bajazet Thierry 2005 Analysis of root growth by impedance spectroscopy (EIS) *Plant and Soil* **277** 229-313
- [65] Pierret A, Kirby M and Moran C 2003 Simultaneous x-ray imaging of plant root growth and water uptake in thin-slab systems *Plant and Soil* **255** 361-73
- [66] Nachabe M H, Islas A L and Illangasakare T H 1995 Analytical solutions for water flow and solute transport in the unsaturated zone *Ground Water* **33** 304-10
- [67] Šimůnek J, Jarvis N K, van Genuchten M T, Gärdenäs A 2003 Review and comparison of models for describing non-equilibrium and preferential flow and transport in the vadose zone *Journal of Hydrology* **272** 14-35
- [68] Richards L A 1931 Capillary conduction of liquids through porous mediums *Physics* **1** 318-33
- [69] van Genuchten M Th 1980 A closed-form equation for predicting hydraulic conductivity of unsaturated soils *Soil Sci. Soc. Am. J.* **44** 892-98
- [70] Retzlaff W A and South D B 1985 A Simple Method for Determining a Partial Soil Water Retention Curve *Reprinted from Tree Planters' Notes* **36** 4 20-23
- [71] Milly P C D 1988 Advances in modeling of water in the unsaturated zone *Transport In Porous Media* **3** 491-514
- [72] Othmer H, Diekkrüger B and Kutilek M 1991 Bimodal porosity and unsaturated hydraulic conductivity *Soil Sci.* **152** 3 139-50
- [73] Durner W 1994 Hydraulic conductivity estimation for soils with heterogeneous pore structure *Water Resour. Res.* **30** 211-33
- [74] COMSOL Ltd. <http://www.uk.comsol.com/>
- [75] MathWorks: <http://www.mathworks.co.uk/index.html>
- [76] COMSOL: Earth Science Module [cited 2010 Feb 23] Available from: <http://www.comsol.com/products/es/>
- [77] Passioura J B and Frere M H 1967 Numerical analysis of the convection and diffusion of solutes to roots *Australian J. Soil Res.* **5** 149-59

- [78] Somma F, Hopmans J W and Clausnitzer V 1998 Transient three-dimensional modelling of soil water and solute transport with simultaneous root growth, root water and nutrient uptake *Plant and Soil* **202** 281-93
- [79] Nye P H and Marriot F H C 1969 A theoretical study of the distribution of substances around roots resulting from simultaneous diffusion and mass flow *Plant and Soil* **3** 459-72
- [80] Roose T, Fowley A C and Darrah P R 2001 A mathematical model of plant nutrient uptake *J. Math. Bio.* **42** 347-60
- [81] Barley K P 1970 The configuration of the root system in relation to nutrient uptake *Advances in Agronomy* **22** 159-201
- [82] Baldwin J P Tinker P B and Nye P H 1972 Uptake of solutes by multiple root systems from soil. II. The theoretical effects of rooting density and pattern on uptake of nutrients from soil *Plant and Soil* **36** 693-708
- [83] Alm D M, Cavelier J and Nobel P S 1992 A finite-element model of the radial and axial conductivities for individual roots: Development and validation for two desert succulents *Annals of Botany* **69** 87-92
- [84] Hackett C and Rose D A 1972 A model of the extension and branching of a seminal root of barley, and its use in studying relations between root dimensions. I. The model *Aust. J. Biol. Sci.* **25** 669-79
- [85] Hackett C and Rose D A 1972 A model of the extension and branching of a seminal root of barley, and its use in studying relations between root dimensions. II. Results and inferences from the model *Aust. J. Biol. Sci.* **25** 681-90
- [86] Lungley D R 1973 The growth of root systems – a numerical computer simulation model *Plant and Soil* **38** 145-59
- [87] Diggle A J 1988 ROOTMAP – a model in three-dimensional coordinates of the growth and structure of fibrous root systems *Plant and Soil* **105** 169-78
- [88] Pagès L, Jordan M O and Picard D 1989 A simulation of the three-dimensional architecture of the maize root system *Plant and Soil* **119** 147-54
- [89] Shibusawa S 1994 Modelling the branching growth fractal pattern of the maize root system *Plant and Soil* **165** 339-47
- [90] Clausnitzer V and Hopmans J W 1994 Simultaneous modelling of transient three-dimensional root growth and soil water flow *Plant and Soil* **164** 299-314
- [91] Seelinger B and Claassen N 1990 A method for determining Michaelis-Menten kinetic parameters of nutrient uptake for plants growing in soil *Journal of Plant Nutrition and Soil Science* **153** 301-03
- [92] Doussan C, Pagès L and Vercambre G 1998 Modelling of the Hydraulic Architecture of Root System: An Integrated Approach to Water Absorption – Model Description *Annals of Botany* **81** 213-223
- [93] Leitner D, Klepsch S, Bodner G and Schnepf A 2010 A dynamic root system growth model based on L-Systems: Tropisms and coupling to nutrient uptake from soil *Plant and Soil* **332** 177-92
- [94] Persson P-O and Strang G 2004 A simple mesh generator in MATLAB *SIAM Review* **46** 329-45
- [95] Borcea L 2002 Electrical impedance tomography *Inverse Problems* **18** R99-136

- [96] Zhang L, Tian P, Jin X and Tong W 2010 Numerical simulation of forward problem for electrical capacitance tomography using element-free Galerkin method *Engineering Analysis with Boundary Elements* **34** 477–82
- [97] Isaacson D and Cheney M 1991 Effects of measurement precision and finite number of electrodes on linear impedance imaging algorithms *SIAM J. Appl. Math.* **51** 6 1705-31
- [98] Sommersalo E, Cheney M and Isaacson D 1992 Existence and uniqueness for electrode models for electric current computer tomography *SIAM J. Appl. Math.* **52** 4 1023-40
- [99] ANSYS: <http://www.ansys.com/>
- [100] Adler A and Lionheart W R B 2006 Uses and abuses of EIDORS: An extensible software base for EIT *Physiol. Meas.* **27** 25-42
- [101] Polydorides N and Lionheart W R B 2002 A Matlab toolkit for three-dimensional electrical impedance tomography: a contribution to the EIDORS project *Measurement Science and Technology* **13** 12 1871-1883
- [102] Polydorides N 2002 Image Reconstruction Algorithms for Soft-Field Tomography Ph.D. Thesis UMIST, Manchester
- [103] Kowalsky M B and Rubin Y 2004, The use of ground-penetrating radar for characterizing sediments under transient flow conditions *Aquifer Characterization, SEPM Special Publication* **80** 107-127
- [104] Knight R and Abad A 1995 Rock/water interaction in dielectric properties: Experiments with hydrophobic sandstones *Geophysics* **60** 2 431-436
- [105] Archie G E 1942 The Electrical Resistivity Log as an Aid in Determining Some Reservoir Characteristics *Petroleum Technology* 54-62
- [106] Cardiff M and Kitanidis P K 2008 Efficient solution of nonlinear, underdetermined inverse problems with a generalized PDE model *Computers & Geosciences* **34** 1480-1491
- [107] Reichle R H, McLaughlin D B and Entekhabi D 2002 Hydrologic Data Assimilation with the Ensemble Kalman Filter *Monthly Weather Review* **130** 103-114
- [108] Camporese M, Cassiani G, Deina R and Salandin P 2011 Assessment of local hydraulic properties from electrical resistivity tomography monitoring of a three-dimensional synthetic tracer test experiment *Water Resources Research* **47** 12 W12508 doi:10.1029/2011WR010528
- [109] Irving J and Singha K 2010 Stochastic inversion of tracer test and electrical geophysical data to estimate hydraulic conductivities *Water Resources Research* **46** W11514 doi:10.1029/2009WR008340
- [110] Pollock D and Cirpka O A 2010 Fully coupled hydrogeophysical inversion of synthetic salt tracer experiments *Water Resources Research* **46** W075501 doi:10.1029/2009WR008575
- [111] Yang W Q and Peng L 2003 Image reconstruction algorithms for electrical capacitance tomography *Meas. Sc. Technol.* **14** R1-13
- [112] William A J and Horton R 2004 *Soil Physics 6th Edition* John Wiley and Sons, Inc. Hoboken New Jersey 29-30
- [113] Sasal M C, Andriulo A E, Taboada M A 2006 Soil porosity characteristics and water movement under zero tillage in silty soils in Argentinian Pampas *Soil & Tillage Research* **87** 9–18

- [114]Kusdiana D and Saka S 2004 Two-Step Preparation for catalyst-free biodiesel fuel production hydrolysis and methyl esterification *Applied Biochemistry and Biotechnology* **113–116** 781-791
- [115]Catenaccio A, Daruich Y and Magallanes C 2003 Temperature dependence of the permittivity of water *Chemical Physics Letters* **367** 669–671
- [116]Zhang N et al 2004 Simultaneous measurement of soil water content and salinity using a frequency-response method *Soil Sci. Soc. Am. J.* **68** 1515–1525
- [117]Richards L A 1931 Capillary conduction of liquids through porous mediums *Physics* **1** 318-33
- [118]Claude Doussan, Loïc Pagès and Gilles Vercambre 1998 Modelling of the Hydraulic Architecture of Root System: An Integrated Approach to Water Absorption – Model Description *Annals of Botany* **81** 213-23
- [119]White, R.E. 1979 Introduction to the Principles and Practice of Soil Science *Blackwell Scientific Publications*.
- [120]Newill P 2010 Soil Basics *SSUIC Internal Report*
- [121]van Genuchten M Th 1980 A closed-form equation for predicting hydraulic conductivity of unsaturated soils *Soil Sci. Soc. Am. J.* **44** 892-98
- [122]Richards L A 1931 Capillary conduction of liquids through porous mediums *Physics* **1** 318-33
- [123]Retzlaff W A and South D B 1985 A Simple Method for Determining a Partial Soil Water Retention Curve *Reprinted from Tree Planters' Notes* **36 4** 20-23
- [124]Porębska D, Sławiński C, Lamorski K and Walczak R T 2006 Relationship between van Genuchten's parameters of the retention curve equation and physical properties of soil solid phase *Int. Agrophysics* **20** 153-159
- [125]Zhang L, Tian P, Jin X and Tong W 2010 Numerical simulation of forward problem for electrical capacitance tomography using element-free Galerkin method *Engineering Analysis with Boundary Elements* **34** 477–82
- [126]Eller H and Denoth A 1996 A capacitive soil moisture sensor *Journal of Hydrology* **185** 137-46
- [127]Seyfried M S, Grant LE, Du E and Humes K 2005 Dielectric Loss and Calibration of the Hydra Probe Soil Water Sensor *Vadose Zone* **4** 1070-79
- [128]Bogena H R, Huisman J A, Oberdörster and Vereecken H 2007 Evaluation of a low-cost soil water content sensor for wireless network applications *Journal of Hydrology* **344** 32-42
- [129]Dobson M C, Ulaby F T, Hallikainen M T and Mohamed A ER 1985 Microwave dielectric behaviour of wet soil – part II: Dielectric mixing models *IEEE Transactions on Geoscience and Remote Sensing* **GE-23 1** 35-46
- [130]Topp G C, Davis J L and Annan A P 1980 Electromagnetic determination of soil water content: Measurements in coaxial transmission lines *Water Resources Research* **16 3** 574-82
- [131]Whalley W R 1993 Consideration on the use of time-domain reflectometry (TDR) for measuring soil water content *Journal of Soil Science* **44** 1-9
- [132]Seyfried M S and Murdock M D 2003 Measurement of soil water content with a 50-MHz soil dielectric sensor *Soil Sci. Soc. Am. J.* **68** 394-403

- [133]Francisca F M and Rinald V A 2003 Complex dielectric permittivity of soil-organic mixtures (20 MHz – 1.3 GHz) *Journal of Environmental Engineering* 347-57
- [134]Kowalsky M B and Rubin Y 2004 The use of ground-penetrating radar for characterizing sediments under transient flow conditions *Aquifer Characterization, SEPM Special Publication* **80** 107-27
- [135]Noborio K 2001 Measurement of soil water content and electrical conductivity by time domain reflectometry: A review *Computers and Electronics in Agriculture* **31** 213-37
- [136]Roth K, Schuln R, Flüher H and Attinger W 1990 Calibration of time domain reflectometry for water content measurement using a composite dielectric approach *Water Resources Research* **26** 4 2267-73
- [137]Knight R and Endres A 1990 A new concept in modelling the dielectric response of sandstones: Defining a wetted rock and bulk water system *Geophysics* 55 5 586-94
- [138]Knight R and Abad A 1995 Rock/water interaction in dielectric properties: Experiments with hydrophobic sandstones *Geophysics* **60** 2 431-36
- [139]Jury W A and Horton R 2004 *Soil Physics 6th Edition* John Wiley and Sons, Inc. Hoboken New Jersey 29-30
- [140]Hector L G and Schultz H L 1936 The dielectric constant of air at radiofrequencies *Physics* **7** 133-36
- [141]Nightingale N R V, Szwarnowski S, Sheppard J and Grant E H 1981 A coaxial line cell for measuring the permittivity of medium to high loss liquids in the frequency range 2 to 15 GHz *J. Phys. E: Sci. Instrum.* **14** 156-60
- [142]Liebe H J, Hufford G A and Manabe T 1991 A model for the complex permittivity of water at frequencies below 1 THz *International Journal of Infrared and Millimeter Waves* **12** 7 659-75
- [143]Alme K J and Mylvaganam S 2006 Analyzing 3D and Conductivity Effects in Electrical Tomography Systems Using COMSOL Multiphysics EM Module *Exerpt from the Proceedings of the 2006 Nordic COMSOL Conference*
- [144]William A J and Horton R 2004 *Soil Physics 6th Edition* John Wiley and Sons, Inc. Hoboken New Jersey 29-30
- [145]Sasal M C, Andriulo A E and Taboada M A 2006 Soil porosity characteristics and water movement under zero tillage in silty soils in Argentinian Pampas *Soil & Tillage Research* **87** 9-18
- [146]Kusdiana D and Saka S 2004 Two-Step Preparation for catalyst-free biodiesel fuel production hydrolysis and methyl esterification *Applied Biochemistry and Biotechnology* **113-116** 781-91
- [147]Zhang N et al 2004 Simulatioius measurement of soil water content and salinity using a frequency-response method *Soil Sci. Soc. Am. J.* **68** 1515-25
- [148]Kizito CS et al 2008 Frequency, electrical conductivity and temperature analysis of a low-cost capacitance soil moisture sensor *Journal of Hydrology* **352** 367-78
- [149]Robinson M and Dean T J 1993 Measurement of near surface soil water content using a capacitance probe *Hydrological Processes* **7** 77-86
- [150]Catenaccio A, Daruich Y and Magallanes C 2003 Temperature dependence of the permittivity of water *Chemical Physics Letters* **367** 669-71

- [151]Hartikainen J, Solin A & Särkkä S 2011 Optimal Filtering with Kalman Filters and Smoother a Manual for the Matlab toolbox EKF/UKF
- [152]Kalman R E 1960 A new approach to linear filtering and prediction problems *Transactions of the ASME Journal of Basic Engineering* **82** 35-45
- [153]Welch G & Bishop G 2006 An Introduction to the Kalman Filter
- [154]Kleinbauer R 2004 Kalman Filtering Implementation with Matlab
- [155]Oliver D S, Reynolds A C & Liu N 2008 Inverse Theory for Petroleum Reservoir Characterization and History Matching New York, NY, United States: Cambridge University Press ISBN: 978-0-051-88151-7
- [156]Kaipio J P & Somersalo E 2005 Statistical and Computational Inverse Problems *Applied Mathematical Sciences* **160** ISBN: 978-0-387-22073-4 (Print) 978-0-387-27132-3 (Online)
- [157]Liu N 2005 Automatic History Matching of Geological Facies Ph.D. Thesis University of Oklahoma, Norman, Oklahoma, USA
- [158]Van Geer F C 1987 Applications of Kalman Filtering in the analysis and design of groundwater monitoring networks

7 Appendix

Appendix A - EGU2010 Abstract

Verification of a COMSOL Multiphysics based soil model using imaging techniques

R R Hayes^{1*}, P A Newill¹, F J W Podd¹, O Dorn², T A York¹, B D Grieve¹

¹ SSUIC, School of Electrical and Electronic Engineering, University of Manchester, UK

² Inverse Problems Group, School of Mathematics, University of Manchester, UK

* Contact: Robert.hayes@postgrad.manchester.ac.uk

Abstract

In the face of climate change the ability to rapidly identify new plant varieties that will be tolerant to drought, and other stresses, is going to be key to breeding the food crops of tomorrow. Currently, above soil features (phenotypes) are monitored in industrial greenhouses and field trials during seed breeding programmes so as to provide an indication of which plants have the most likely preferential genetics to thrive in the future global environments. These indicators of “plant vigour” are often based on loosely related features which may be straightforward to examine, such as an additional ear of corn on a maize plant, but which are labour intensive and often lacking in direct linkage to the required crop features.

A new visualisation tool is being developed for seed breeders, providing on-line data for each individual plant in a screening programme indicating how efficiently each plant utilises the water and nutrients available in the surrounding soil. It will be used as an in-field tool for early detection of desirable genetic traits with the aim of increased efficiency in identification and delivery of tomorrow's drought tolerant food crops.

Visualisation takes the form of Electrical Impedance Tomography (EIT), a non-destructive and non-intrusive imaging technique. The measurement space is typical of medical and industrial process monitoring i.e. on a small spatial scale as opposed to that of typical geophysical applications. EIT measurements are obtained for an individual plant thus allowing water and nutrient absorption levels for an individual specimen to be inferred from the resistance distribution image obtained. In addition to traditional soft-field image reconstruction techniques the inverse problem is solved using mathematical models for the mobility of water and solutes in soil.


The University of Manchester/Syngenta LCT2 (Low Cost Tomography 2) instrument has been integrated into crop growth studies under highly controlled soil, nutrient and environmental conditions. X-ray imaging has been used to observe the water content of soil for various saturation levels under controlled environmental conditions. The resultant images are compared with those obtained from the Richard's equations solution using a finite element model (FEM). EIT images are also taken under the same controlled conditions to provide an in field replacement for x-rays.

These early studies stand as a proof-of-concept and have given the research team an understanding of the technical challenges that must now be addressed to take the current instrumentation into the world of agri-science and food supply.


¹ SSUIC, School of Electrical and Electronic Engineering, University of Manchester, UK

² Inverse Problems Group, School of Mathematics, University of Manchester, UK

* Corresponding author, contact: Robert.hayes@postgrad.manchester.ac.uk



MANCHESTER
1824



Validation of a COMSOL Multiphysics based soil model using imaging techniques

Robert Hayes, Paul Newill, Frank Podd, Oliver Dorn², Trevor York, and Bruce Grieve
 SSJIC, School of Electrical and Electronic Engineering, University of Manchester, UK
² Inverse Problems Group, School of Mathematics, University of Manchester, UK

Aims

- To image moisture distribution in the sub-soil environment
- To monitor the efficiency of water utilisation
- To provide a new visualisation tool for seed breeders

Motivation

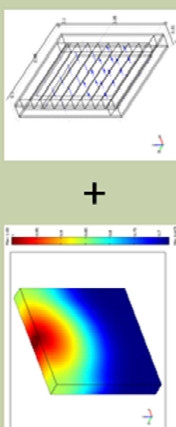
- Climate change leads to water scarcity, this severely limits irrigation and constrains food production
- Rapidly identifying new plant varieties that are tolerant to drought is key to breeding the food crops of tomorrow

Candidate Technology

- Electrical Capacitance Tomography (ECT)
- Finite Element Modelling (FEM) using COMSOL Multiphysics

Methodology

- Currently, separate Hydrology and ECT models are used




Simulated soil water distribution + **Simulated electric field distribution**


Soil Water Content

- Soil water content simulations were compared to digital video of the wetting phase incident from a point injection
- Initial simulations demonstrate a wetting front that closely matches those observed via experimentation
- Simulations based on the saturated hydraulic conductivity of various soil samples determined experimentally
- Van Genuchten parameters were estimated


Results



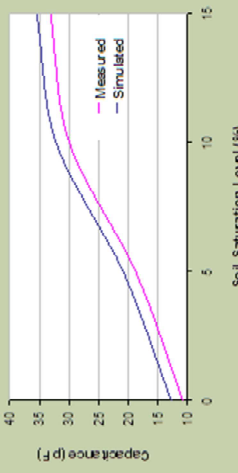
1 Minute 10 Seconds



2 Minutes 45 Seconds



4 Minutes 20 Seconds



Comparison between measured and simulated capacitance data for varied soil water contents

Conclusions

- Hydrology models are able to simulate the wetting front
- Electrical capacitance can be used to measure the soil water distribution in dry soils (up to 15% saturated)
- The model will further facilitate the implementation of a multiphysics based forward solver

Future Work

- Further parameterise soil samples to determine the Van Genuchten parameters
- Testing of a low cost measurement instrument under highly controlled conditions for imaging localised soil water distributions using a typical tomographic sensor array
- Integrate root growth and water uptake models with soil transport and electrostatics models

Electrical Properties for Varied Soil Saturation Levels

- Experimental errors due to inconsistencies in the level of compaction of soil and/or any bowing of the vessel walls
- Average error of simulated measurements vs. real measurements is 8.96%

Email: robert.hayes@postgrad.manchester.ac.uk

**Appendix C – Journal of Physics Conference Series Paper -
An investigation into the use of a mixture model for
simulating the electrical properties of soil with varying
effective saturation levels for sub-soil imaging using ECT**

An investigation into the use of a mixture model for simulating the electrical properties of soil with varying effective saturation levels for sub-soil imaging using ECT

R R Hayes¹, P A Newill¹, F J W Podd¹, T A York¹, B D Grieve¹, O Dorn²

¹SSUIC, School of Electrical and Electronic Engineering, University of Manchester, UK

²Inverse Problems Group, School of Mathematics, University of Manchester, UK

Email: Robert.Hayes@postgrad.manchester.ac.uk

Abstract. A new visualisation tool is being developed for seed breeders, providing on-line data for each individual plant in a screening programme. It will be used to indicate how efficiently each plant utilises the water and nutrients available in the surrounding soil. This will facilitate early detection of desirable genetic traits with the aim of increased efficiency in identification and delivery of tomorrow's drought tolerant food crops. Visualisation takes the form of Electrical Capacitance Tomography (ECT), a non-destructive and non-intrusive imaging technique. Measurements are to be obtained for an individual plant thus allowing water and nutrient absorption levels for an individual specimen to be inferred. This paper presents the inverse problem, discusses the inherent challenges and presents the early experimental results. Two mixture models are evaluated for the prediction of electrical capacitance measurement data for varying effective soil saturation levels using a finite element model implemented in COMSOL Multiphysics. These early studies have given the research team an understanding of the technical challenges that must now be addressed to take the current research into the world of agri-science and food supply.

1. Introduction

Crops are one of the world's major water consumers [1], as climate change leads to water scarcity there is an increase in competition for water. This severely limits irrigation and constrains food production. In the face of climate change the ability to rapidly identify new plant varieties that will be tolerant to drought, and other stresses, is going to be key to breeding the food crops of tomorrow. With large areas of Africa and South America expecting major water scarcity by 2025 [2], it is very important to develop crops that can survive in these conditions. Currently, above soil features (phenotypes) are monitored in industrial greenhouses and field trials during seed breeding programmes so as to provide an indication of which plants have the most likely preferential genetics to thrive in the future global environments [3]. These indicators of "plant vigour" are often based on loosely related features which may be straightforward to examine, such as an additional ear of corn on a maize plant, but which are labour intensive and often lacking in direct linkage to the required crop features.

A new visualisation tool is being developed for seed breeders, providing on-line data for each individual plant in a screening programme indicating how efficiently each plant utilises the water and nutrients available in the surrounding soil. It will be used as an in-field tool for early detection of desirable genetic traits with the aim of increased efficiency in identification and delivery of tomorrow's drought tolerant food crops.

Imaging the moisture distribution in the sub-soil environment carries a number of challenges. For in-field measurements any instrumentation must be portable, relatively low cost, internally powered and weather resistant. High resolution imaging modalities such as magnetic resonance imaging (MRI) and X-ray computed tomography (CT), while offering superior image quality, cannot be used in this capacity as the technology is costly (>£30k) and requires large high powered instrumentation (>500W). Therefore a compromise to reduce size and cost at the expense of image quality must be made. For this reason, electrical impedance imaging is an ideal candidate technology.

This modality however poses its own significant technical challenges in light of the intricacy of the medium. Electrical impedance imaging is a soft field reconstruction problem. That is to say that the regions of interaction are altered by the sample under investigation. It also suffers from being an ill-posed problem. Furthermore the medium (soil) exhibits both conductive (wet) dominating phases and dielectric (dry) dominating phases. The implication of this is the formation and breaking of conducting paths between measurement electrodes and a transition between the dominance of the real and imaginary impedance components. As a result of water loss, soil is prone to shrinking and cracking which further complicates the measurement process due to the quality of the connection at the contact points between the medium and the electrodes.

The forward solution for simulating water movement in soil measured via electrical capacitance tomography (ECT) is a complex problem and requires the consideration of several theoretical backgrounds. For this reason simulation is a valuable tool. Simulation of plant growth, root water uptake and soil water transport and the integration of these models has been an area of high activity over recent years. A number of realistic root growth models have been developed and implemented in MATLAB (including meshing functions) [4][5] and ANSI C, respectively [6]. The R-SWMS code implemented in FORTRAN 90 integrates root growth, root water uptake and soil water transport models [7]. In addition to this several commercial products such as HYDRUS 3D [8] and COMSOL Multiphysics [9] allow the simulation of soil water transport in three dimensions.

As a first step, separate ECT and hydrology models are used. However in the future these will be combined into a multiphysics model to enable joint reconstructions. Multiphysics simulation allows the relationships between different physics backgrounds to be coupled. Hence providing a means by which the required models can be combined in one software package, this is advantageous as it negates the need for interfacing two separate software packages and potentially reduces computation time. Simulation also facilitates the optimisation of sensor design by allowing a number of sensor geometries to be compared, while avoiding error introduced by measurement instrumentation as the signal-to-noise levels and power density functions can be set precisely. In addition, simulation facilitates the comparison and optimisation of image reconstruction algorithms as the 'unknown' permittivity distribution that is to be reconstructed can be precisely defined. Furthermore, the desire is to incorporate the simulation model into the reconstruction process so that plant water uptake can be directly estimated from the time varying moisture distribution.

COMSOL Multiphysics has been used to simulate capacitance data for a soil fluid flow experiment and will further facilitate the implementation of a multiphysics based forward solver and potentially the use of prior information in the inverse problem.

2. Background

Simulation of the electrical capacitance measurements in this application is a multiphysics problem combining, flow through a porous media to describe the movement of water through a soil column, and electrostatics for the calculation of the electrical fields resulting from the moisture distribution.

2.1. Flow in porous media

The Richards equation governs the saturated-unsaturated flow of water in non-swelling soils [117] and is given by

$$(C + S_e S) \frac{\partial H_p}{\partial t} + \nabla \cdot (-K \nabla (H_p + D)) = Q_s \quad (1)$$

where C is specific moisture capacity (m^{-1}), S_e is the effective saturation of the soil, S is a storage coefficient (m^{-1}), H_p is the pressure head (m), D is the vertical elevation (m), t is time (d), K is the hydraulic conductivity (m/d) and Q_s is a fluid source defined by volumetric flow rate per unit volume of soil (d^{-1}).

Applying the Richards equation for a point injection with a given pressure head to a rectangular soil geometry allows the calculation of the soil water distribution at a given time. Figure 1 is an example soil water distribution obtained from the solution of the Richards equation for a rectangular soil geometry simulated using the COMSOL Multiphysics Earth Science module. The soil retention characteristics and saturated hydraulic conductivity in this example were chosen arbitrarily.

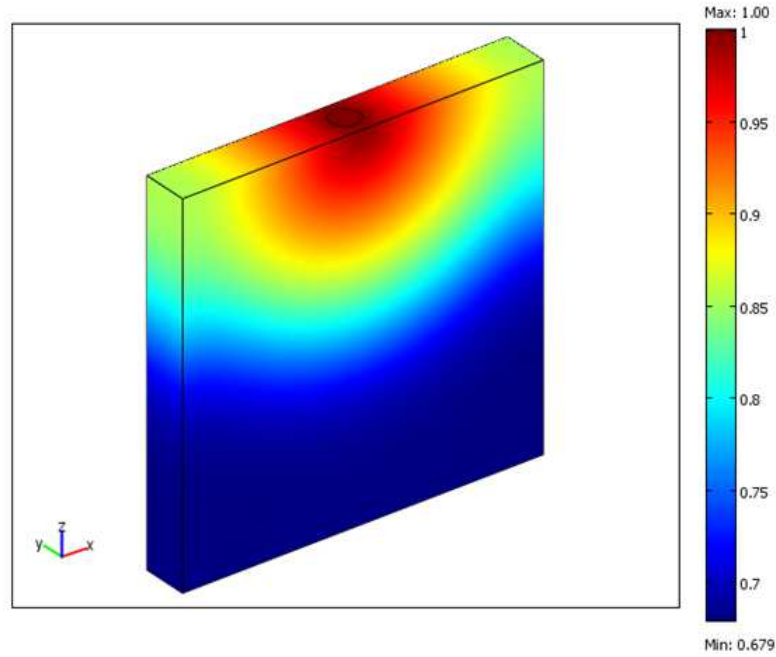


Figure 1. 3D Simulated soil water distribution at a time, t , for a point injection.

Root water uptake can be included in the Richards equation via a sink term. If a root network is considered as a series of nodes and interconnecting segments, the Doussan model can be used to calculate the water potential at each of the root nodes from a system of equations expressed in terms of the length of the interconnecting segments, the Xylem conductivity, the water potential of the surrounding soil, the radial conductivity and the surface area of the interconnecting segments [118].

2.2. Electrostatics

The forward problem in ECT is to calculate the potential distribution for a known dielectric constant and then to determine the corresponding capacitances measured at the surface. Assuming no free charge conditions, the electric scalar potential, V , between the electrodes mounted on the vessel satisfy Poisson's equation [96]

$$-\nabla \cdot (\epsilon_0 \epsilon_r \nabla V) = \rho \quad (2)$$

where ϵ_0 and ϵ_r are the permittivity of free space and the dielectric constant respectively, ρ is the space charge density. The electric field (E) and displacement field (D) can be obtained from the potential gradient

$$E = -\nabla V \quad (3)$$

$$D = \epsilon_0 \epsilon_r E \quad (4)$$

For the plastic surfaces of the vessel, the conditions of zero surface charge are applied at the boundary, thus

$$n \cdot D = 0 \quad (5)$$

A finite element based implementation of this mathematical model was validated experimentally (see section 3.1).

2.3. Multiphysics Coupling

The dielectric permittivity of a partially saturated soil matrix varies as a function of water content. The implication of being able to describe this relationship mathematically is the ability to infer the water content in a soil sample via electrical measurement.

Electromagnetic techniques for inferring soil moisture content, such as time domain reflectometry (TDR) and capacitance methods [40] rely on this strong dependence of electrical signals on dielectric permittivity [43]. The permittivity can be related to soil water content using a calibration curve [44].

This consists of establishing the relationship between the signal provided by the instrumentation and the soil moisture content by using a reference method. This relationship is comprised of two subsequent relationships. Firstly the relationship between the probes output signal and the soil dielectric permittivity, which may be determined experimentally. Secondly the relationship between soil dielectric permittivity and soil water content. This may be determined using theoretical models or empirically [49].

One further interesting property of being able to mathematically model the relationship between soil moisture content and dielectric content is the potential to estimate electrical measurements (i.e. capacitance measurements) for a given soil sample based on a simulated soil moisture distribution. This provides a basis for the implementation of a multi-physics simulation.

Fluid flow and electrostatics models can be coupled via the dielectric constant, if the dielectric constant of soil can be predicted based on effective soil saturation. The dielectric constant vs. soil saturation curve may be obtained experimentally or predicted using theoretical methods.

A number of methods have been proposed to predict the dielectric constant of water saturated rocks and soils at varied soil saturation levels. Two of the more popular theoretical methods are the Topp model [130] and the Complex Refractive Index Method (CRIM) [131]. These methods have been tested extensively [132][133] and are commonly used in the calibration of dielectric soil moisture probes [43].

The popular empirical model known as the Topp model was developed by Topp et al by compiling data for many soils under varying moisture conditions [134]. This model is given by the third-order polynomial equation

$$\varepsilon = 3.03 + 9.3\theta + 146\theta^2 - 76.7\theta^3 \quad (6)$$

where ε denotes the effective dielectric constant of the soil mixture and θ denotes the water content. Extensive testing has shown the Topp model to be reasonably accurate for many soils [48]. However its validity has not been demonstrated over a full range of possible water contents and porosities [47].

The complex refractive index method (CRIM) involves using simple mixing laws to calculate the dielectric constant of a material (ε_T) given the dielectric constant (ε_i) and the volume fraction (V_i) as given by

$$\sqrt{\varepsilon_T} = \sum_i V_i \sqrt{\varepsilon_i} \quad (7)$$

This can be expanded for the case of a soil sample at a given level of water saturation (θ), where θ is the volume fraction of the pore space that is filled with water, the remainder being filled with air [137]. The system is composed of soil (ε_s), water (ε_w) and air (ε_a). Porosity is given by ϕ and the dielectric constant for a given soil saturation level is expressed as

$$\sqrt{\varepsilon_T} = (1-\phi)\sqrt{\varepsilon_s} + \theta\phi\sqrt{\varepsilon_w} + (1-\theta)\phi\sqrt{\varepsilon_a} \quad (8)$$

Assuming that the soil and air components have negligible conductivity, the dielectric constants of both soil and air can be assumed to be entirely real [137][138].

An obvious limitation of both models is that they assume localised homogeneity and complete mixing. They also do not take into account electro-chemical interactions amongst the constituent components [137].

This paper will discuss the validity of the FEM model and compare simulated capacitance data, based on the dielectric permittivity predicted by the Topp and CRIM models, with measured capacitance data (see section 3.2).

3. Experimental Procedure and Results

3.1. Validation of the FEM through observing the effect of water fill level

In order to validate an electrostatic simulation implemented in COMSOL Multiphysics, the capacitance of a rectangular vessel as described in figure 16 was measured for varying water fill levels. The vessel walls were manufactured to include two parallel plate electrodes of dimension 130mm x 85mm as shown in figure 3. These electrodes were insulated from the medium using a solder mask layer of 75 μ m thickness. Measurements were carried out using a Hewlett Packard 4192A Impedance analyser.

The dielectric constant of the solder mask layer was set to 3.56 (as defined by the manufacturer) in the FEM. Simulations were then carried out for fill levels ranging from 0mm (100% air) to 120mm (100% water) in 10mm steps. The dielectric constant of air was taken as 1.00059 [140] and the dielectric constant of water was taken as 79 at 20 degrees Celsius [141][142].

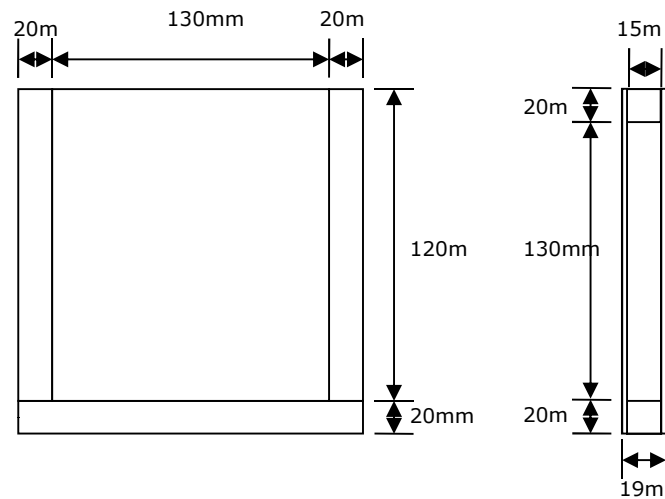


Figure 2. Schematic diagram of the rectangular vessel. Left: Front view, Right: Top view.

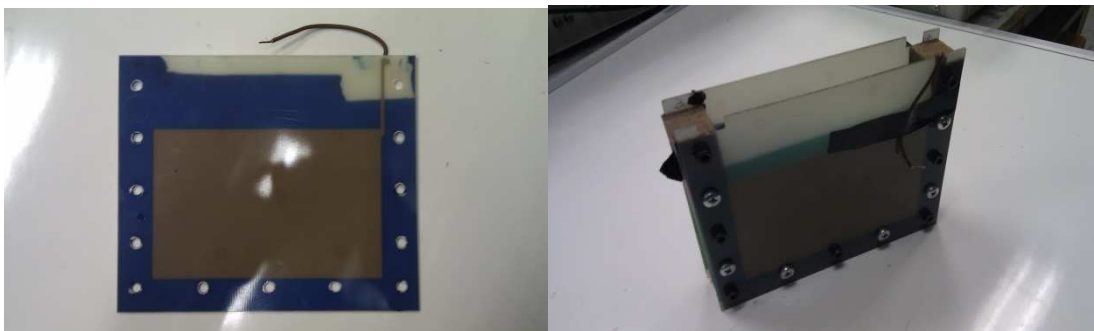


Figure 3. Left: Vessel wall showing electrode Right: Constructed measurement vessel

A comparison between measured and simulated data is shown in figure 4. The point at which both measurement sets cease to increase linearly is the point at which the water fill level exceeds the height of the electrode. Beyond this level, the change is in the fringing field only and variations are of $\sim 11\text{pF}$ corresponding to approximately 3% of the total measured capacitance. The maximum error between simulation and measurement is 43.64% corresponding to an error of 5.26 pF. This error occurs when the vessel is empty, i.e. filled with air. This point is the lowest measured capacitance, hence the most sensitive to measurement error. The average error is 8.88%. Possible sources of error include experimental error and the absence of temperature data in order to account for the temperature dependency of the dielectric constant of water. Analysis of the potential sources of error is presented in section 3.3.

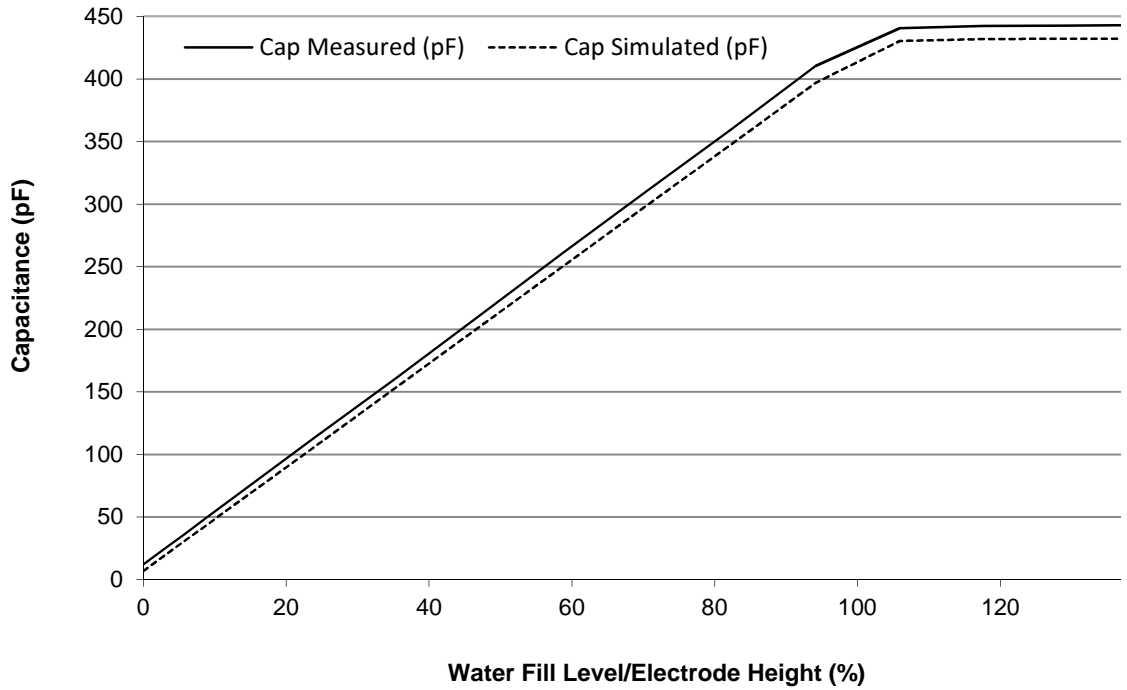


Figure 4. Plot of capacitance vs. fill level for measured and simulated capacitance data.

Figure 5 shows the simulated electric fields for a half filled vessel. Note the electric field is highest in the region of higher dielectric constant (i.e. the water) as represented by the largest arrows. The smaller arrows represent the weaker electric field in the air filled region.

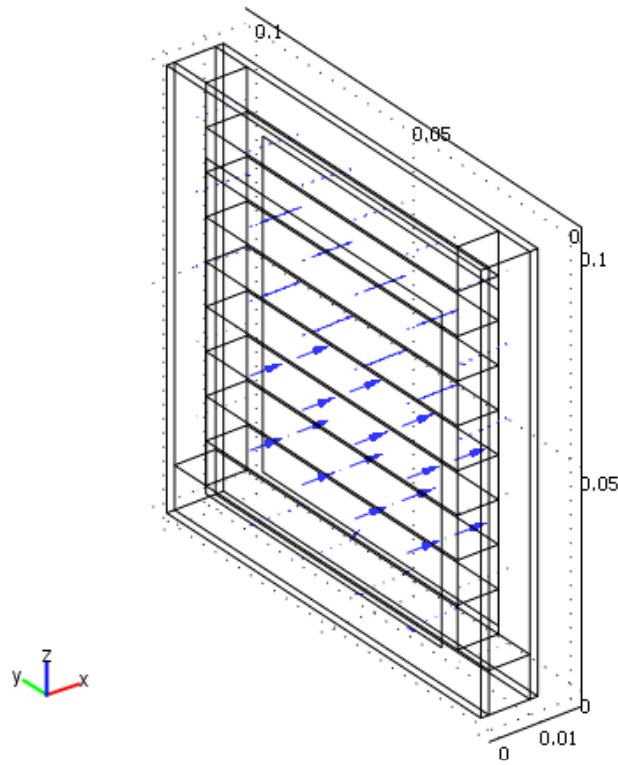


Figure 5. Simulated electric fields for a half filled rectangular vessel.

3.2. Varying soil saturation

To determine the validity of the Topp and CRIM models, the HP impedance analyser was also used to measure the capacitance of the vessel when filled with soil of varying levels of saturation. The dielectric constant of the soil matrix was predicted for the corresponding saturation levels using both the Topp and CRIM models. For the CRIM model porosity was taken as 0.54. This value was calculated from data provided by a soil analysis service offered by Forest Research Surrey using the following

$$\phi = 1 - \frac{\rho_{bulk}}{\rho_{particle}} \quad (9)$$

where ϕ is the porosity, ρ_{bulk} is the bulk density, defined as the average density of dry soil. $\rho_{particle}$ is the particle density, defined as the density of the particles that the soil consists of. It is equal to the dry density of the solid material comprising the soil matrix i.e. the mass of air is negligible [1]. The particle density of a soil may be estimated using the weighted average of the solid components [1] and is given by

$$\rho_{particle} = \rho_m X_m + \rho_{om} X_{om} \quad (10)$$

where $\rho_{particle}$ is total soil density, ρ_m and ρ_{om} are the mineral fraction density and organic matter fraction density respectively, X_m and X_{om} are the mineral volume fraction and the organic matter volume fraction respectively. The porosity value of 0.54 is consistent with values for silty soils [113].

The predicted dielectric constants from the Topp and CRIM models were substituted into the FEM and the respective capacitance measurements were calculated by simulation.

As the soil water content was increased, the capacitance measurements had two distinct regions of linearity, as can be seen in figure 6. Any non-linearity is likely to be caused by inconsistencies in the level of compaction of soil and/or any bowing of the vessel wall between subsequent measurements.

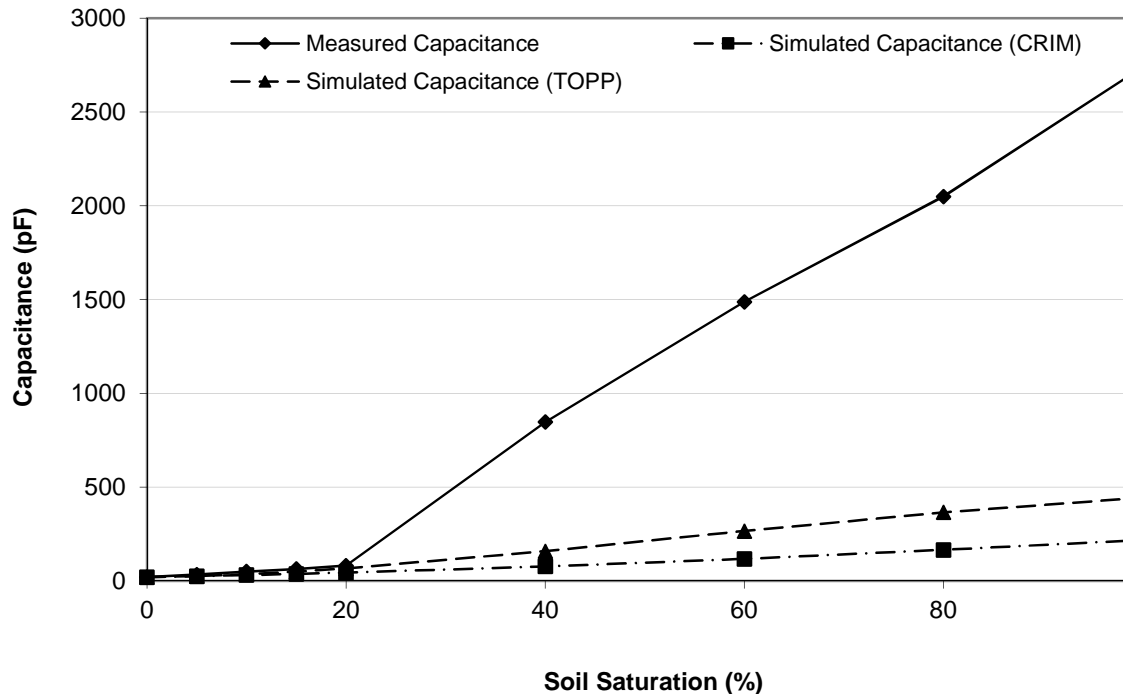


Figure 6. Measured and simulated capacitance measurements vs. soil saturation level.

Beyond a saturation level of ~20% there is a sudden increase in the slope. This discrepancy to the mathematical model is believed to be the result of resistive coupling on the reading from the HP impedance analyser for conductivities greater than 0.48 mS. Distilled water was used. However the mineral content of the soil increased the conductivity of the water from 0 mS to 0.75 mS. This hypothesis was investigated by repeating the procedure using a non-conductive liquid (Rapeseed oil) to saturate the soil. It is assumed that the ions present in the soil are not oil soluble and do not increase the conductivity of the oil. An equivalent experiment using “washed” sand and distilled water was also carried out.

The CRIM equation was used to predict the dielectric constant of the soil/sand matrix for varying saturation levels and substituted into the FEM to simulate the expected capacitance measurement data. This simulated data was compared with measured data. In this case, the dielectric constant of rapeseed oil was taken as 3.1 [114]. The Topp model was not considered in these experiments as it is formulated for a soil-water matrix and cannot be modified to describe other components.

As can be seen in figures 7 and 8, the change of slope is no longer present. This suggests that the hypothesis of instrumentation limitations for high conductivities appears valid. Any non-linearity in the measured data is likely due to variations in the level of compaction between subsequent measurements. Predictions based on the CRIM model had an average error of 3.77% and 5.25% for the soil-oil and sand-water experiments respectively as compared to measured data.

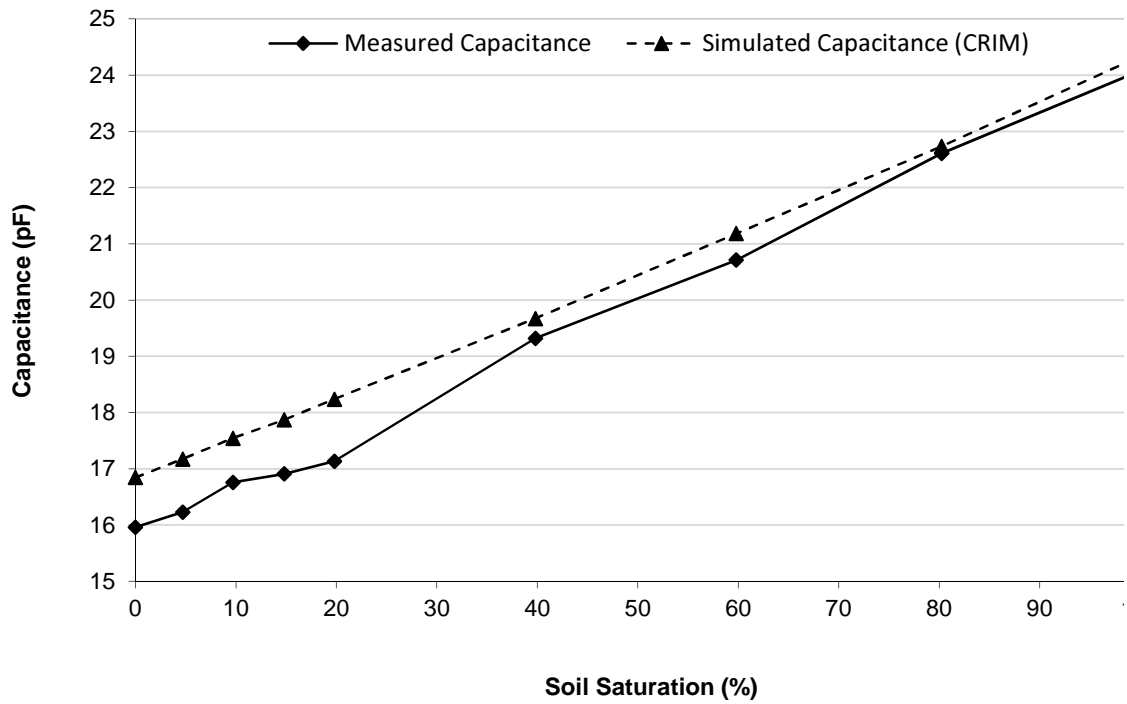


Figure 7. Measured and simulated capacitance measurements vs. level of soil saturation using rapeseed oil.

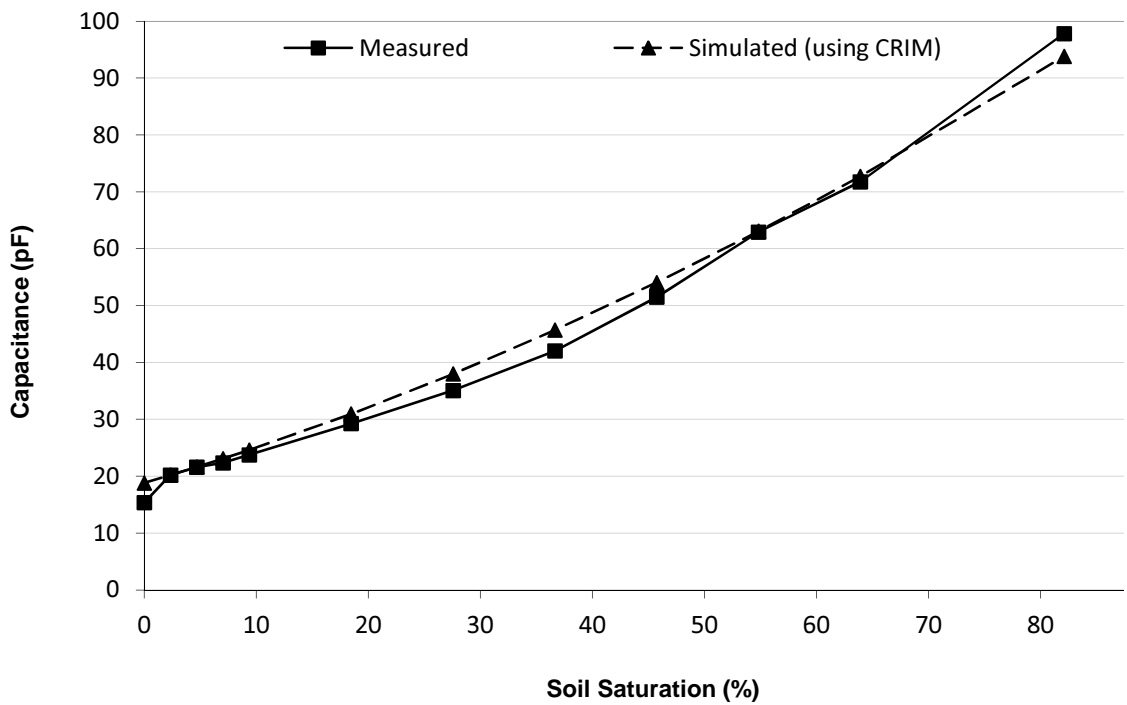


Figure 8. Measured and simulated capacitance measurements vs. level of sand saturation using distilled water

It is thought that at lower measurement frequencies the effects of soil type and soil conductivity are prevalent. The result is a requirement for higher excitation frequencies this is due to decreased conductive losses at higher frequencies hence reducing the effect of soil conductivity [116]. At present the measurement instrument is limited to 1MHz. The result of

using a higher frequency is a simplification of the calibration process. In many cases a single calibration curve may be used for numerous soil types [53]. The literature suggests that using suitable calibration curves capacitance measurements can provide reliable results over the full typical range of saturation levels (0-60%) [40][54]. Typically soil dielectric measurement instruments operate in the 10-200 MHz region [40].

3.3. Investigating the source of error

In order to determine the sensitivity of measurement data with respect to temperature, the variability of the dielectric constant of water vs. temperature was investigated. The variation of dielectric constant of water with respect to temperature was modelled using the polynomial equation [115]

$$\epsilon_w = 5321T^{-1} + 233.76 - 0.9297T + 0.1417 \times 10^{-2}T^2 - 0.8292 \times 10^{-6}T^3 \quad (11)$$

where ϵ_w is the dielectric constant of water and T is the temperature in Kelvin.

The modelled dielectric constant of water for the temperature range of 0 to 100 degrees Celsius is shown in figure 9. The standard parallel plate capacitor equation was then used to calculate the capacitance for the vessel fully filled with distilled water. The thickness and dielectric constant of the dielectric layer is known. The dielectric constant of water was taken as 79 at 20 degrees Celsius [115]. These values were taken as a reference. To determine the extent to which the measurements were sensitive to temperature changes of water, the dielectric constant of water was varied until the resulting expected capacitance changed by ~10% of the reference. This corresponds to a change of 12.6% in the value of the dielectric constant of water which is equivalent to a temperature rise of approximately 25-30 degrees Celsius. This results in a temperature of approx 50 degree Celsius. It is unlikely that such an error in temperature measurement occurred. Figure 10 shows the change in capacitance calculated for the temperature varied dielectric constant of water.

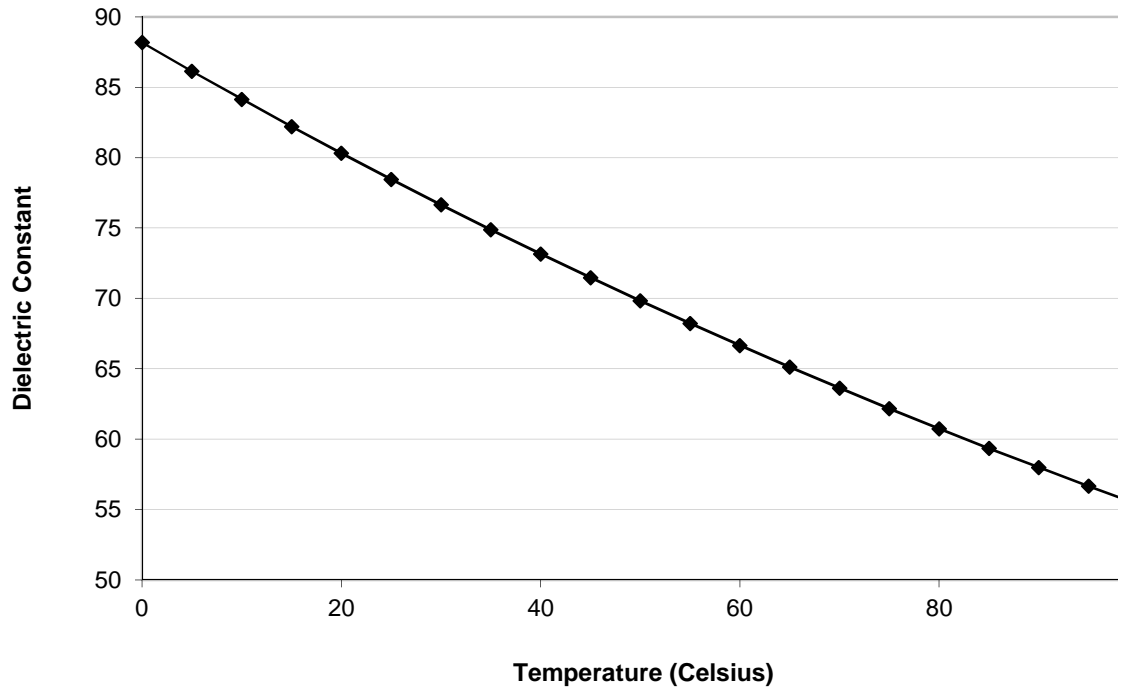


Figure 9. Variation of the dielectric constant of water with respect to temperature.

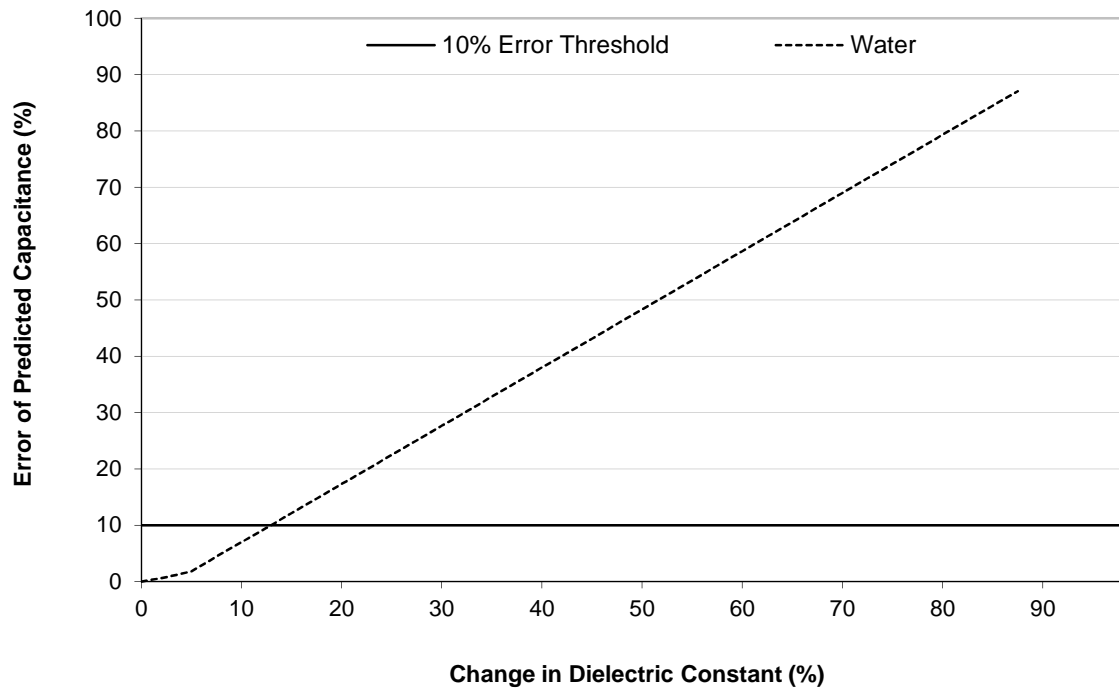


Figure 10. Error in predicted capacitance vs. temperature induced drift in dielectric constant of water for determining the extent to which the temperature dependence of the dielectric constant of water contributes to measurement error.

4. Conclusions

4.1. Initial findings

Experiments have shown that the simulation is able to predict changes in capacitance due to varying levels of soil saturation based on two methods for predicting the dielectric constant of varying soil water saturation levels.

The electrostatic model has been shown to exhibit an average error of 8.88% for varying water fill levels in comparison to measured data. Predictions generated using both the Topp and CRIM models were compared to measured data for varying soil saturation levels. It has been noted that beyond 20% soil saturation, there are difficulties in measuring the capacitance of the wetted soil. This has been attributed to the limitations of the measurement instrumentation for highly conductive media.

The CRIM model was evaluated for two further matrices in addition to water wet soil. This was not possible with the Topp model as this relation is only valid for a matrix of water wet soil. Predictions based on the CRIM model had an average error of between 3.77% and 5.25% for the soil-oil and sand-water experiments respectively compared to measured data. As a result, the CRIM model will be implemented in COMSOL multiphysics to couple the electrostatic simulation to the soil transport simulation to allow for multiphysics simulations.

Experiments have shown that the temperature dependency of the dielectric constant of water will not contribute substantial error over the normal operating temperature range of the instrument. However temperature correction may be easily integrated using a simple mathematical model [115].

Ultimately, for further evaluation of the simulation it is felt that a higher frequency range will improve capacitance measurement capabilities for water-wet soils. Typically soil dielectric measurement instruments operate in the 10-200 MHz region [40] however the current instrumentation is limited to 1 MHz. It is anticipated that a measurement range up to 75 MHz will be sufficient [53].

4.2. Future work

Some time must be spent to further understand the limitations of the measurement instrument. Ideally a calibration curve may be generated using complex impedance measurements, allowing the correction of measurement data and hence extending the measurement range of the instrument.

Further work will be carried out to greater parameterise the soil samples. In doing so any uncertainty regarding the current porosity value will be minimised, this will allow a better comparison between the Topp and CRIM models.

The current measurement vessel will be replaced with one allowing the spatial moisture distribution to be mapped, i.e. a vessel with a larger number of independent electrodes.

Fluid flow in a porous media and electrostatics models have been implemented in isolation, this paper focused only on the latter. These models will be coupled through the dielectric constant vs. soil saturation curve as predicted by a mixture model. This will allow the simulation of electric fields due to varying soil water distributions hence facilitating the implementation of a multiphysics based forward solver in COMSOL multiphysics. The forward solver will be optimised for typical tomographic vessel geometries and will allow the generation of calibration curves in order to correct for measurement error. Ultimately a fully integrated electrostatics model based on the fluid flow as predicted by the Richards equation will be developed.

In the long term, the soil retention curves will be obtained experimentally and the resulting parameterisation substituted into the Richards equation solver in COMSOL Multiphysics. Root growth models and root water uptake models will be integrated into the multiphysics models. The final, fully integrated model will be used in the reconstruction of ECT images and enable prior information in the inverse problem.

References

- [1] Bontemps C and Couture S 2002 Irrigation water demand for the decision maker *Environment and Development Economics* **7** 643–57
- [2] Lange M D 2001 Water law and human rights – roles and responsibilities *Water Science and Technology* **43** 4 143–50
- [3] Hunt R, Causton D R, Shipley B and Askew A P 2002 A modern tool for classical plant growth analysis *Annals of Botany* **90** 485–88
- [4] Leitner D and Schnepf 2009 Root growth simulation using L-systems *Proceedings of Algoritmy* 313–20
- [5] Schnepf A and Leitner D 2009 FEM simulation of below ground processes on a 3-dimensional root system geometry using Distmesh and COMSOL Multiphysics, *Proceedings of Algoritmy* 321–30
- [6] Lynch J P, Nielsen K L, Davis R D and Jablowski A G 1997 SimRoot: Modelling and visualization of root systems *Plant and Soil* **188** 139–51
- [7] Javaux M, Schröder T, Vanderborght J and Vereecken H 2008 Use of a three-dimensional detailed modelling approach for predicting root water uptake *Vadose Zone J.* **7** 1079–88
- [8] Šimůnek J, van Genuchten M T and Šejna M 2008 Development and applications of the HYDRUS and STANMOD software packages and related codes *Vadose Zone J.* **7** 587–600
- [9] COMSOL: Earth Science Module [cited 2010 Feb 23] Available from: <http://www.comsol.com/products/es/>
- [10] Richards L A 1931 Capillary conduction of liquids through porous mediums *Physics* **1** 318–33
- [11] Claude Doussan, Loïc Pagès and Gilles Vercambre 1998 Modelling of the Hydraulic Architecture of Root System: An Integrated Approach to Water Absorption – Model Description *Annals of Botany* **81** 213–23
- [12] Zhang L, Tian P, Jin X and Tong W 2010 Numerical simulation of forward problem for electrical capacitance tomography using element-free Galerkin method *Engineering Analysis with Boundary Elements* **34** 477–82
- [13] Eller H and Denoth A 1996 A capacitive soil moisture sensor *Journal of Hydrology* **185** 137–46
- [14] Seyfried M S, Grant L E, Du E and Humes K 2005 Dielectric Loss and Calibration of the Hydra Probe Soil Water Sensor *Vadose Zone* **4** 1070–79
- [15] Bogaen H R, Huisman J A, Oberdörster and Vereecken H 2007 Evaluation of a low-cost soil water content sensor for wireless network applications *Journal of Hydrology* **344** 32–42
- [16] Dobson M C, Ulaby F T, Hallikainen M T and Mohamed A E R 1985 Microwave dielectric behaviour of wet soil – part II: Dielectric mixing models *IEEE Transactions on Geoscience and Remote Sensing* **GE-23** 1 35–46
- [17] Topp G C, Davis J L and Annan A P 1980 Electromagnetic determination of soil water content: Measurements in coaxial transmission lines *Water Resources Research* **16** 3 574–82
- [18] Whalley W R 1993 Consideration on the use of time-domain reflectometry (TDR) for measuring soil water content *Journal of Soil Science* **44** 1–9
- [19] Seyfried M S and Murdock M D 2003 Measurement of soil water content with a 50-MHz soil dielectric sensor *Soil Sci. Soc. Am. J.* **68** 394–403
- [20] Francisca F M and Rinaldi V A 2003 Complex dielectric permittivity of soil-organic mixtures (20 MHz – 1.3 GHz) *Journal of Environmental Engineering* 347–57
- [21] Kowalsky M B and Rubin Y 2004 The use of ground-penetrating radar for characterizing sediments under transient flow conditions *Aquifer Characterization, SEPM Special Publication* **80** 107–27
- [22] Noborio K 2001 Measurement of soil water content and electrical conductivity by time domain reflectometry: A review *Computers and Electronics in Agriculture* **31** 213–37

- [23] Roth K, Schulin R, Flühler H and Attinger W 1990 Calibration of time domain reflectometry for water content measurement using a composite dielectric approach *Water Resources Research* **26** 4 2267-73
- [24] Knight R and Endres A 1990 A new concept in modelling the dielectric response of sandstones: Defining a wetted rock and bulk water system *Geophysics* **55** 5 586-94
- [25] Knight R and Abad A 1995 Rock/water interaction in dielectric properties: Experiments with hydrophobic sandstones *Geophysics* **60** 2 431-36
- [26] Hector L G and Schultz H L 1936 The dielectric constant of air at radiofrequencies *Physics* **7** 133-36
- [27] Nightingale N R V, Szwarnowski S, Sheppard J and Grant E H 1981 A coaxial line cell for measuring the permittivity of medium to high loss liquids in the frequency range 2 to 15 GHz *J. Phys. E: Sci. Instrum.* **14** 156-60
- [28] Liebe H J, Hufford G A and Manabe T 1991 A model for the complex permittivity of water at frequencies below 1 THz *International Journal of Infrared and Millimeter Waves* **12** 7 659-75
- [29] William A J and Horton R 2004 *Soil Physics 6th Edition* John Wiley and Sons, Inc. Hoboken New Jersey 29-30
- [30] Sasal M C, Andriulo A E and Taboada M A 2006 Soil porosity characteristics and water movement under zero tillage in silty soils in Argentinian Pampas *Soil & Tillage Research* **87** 9-18
- [31] Kusdiana D and Saka S 2004 Two-Step Preparation for catalyst-free biodiesel fuel production hydrolysis and methyl esterification *Applied Biochemistry and Biotechnology* **113-116** 781-91
- [32] Zhang N et al 2004 Simultaneous measurement of soil water content and salinity using a frequency-response method *Soil Sci. Soc. Am. J.* **68** 1515-25
- [33] Kizito CS et al 2008 Frequency, electrical conductivity and temperature analysis of a low-cost capacitance soil moisture sensor *Journal of Hydrology* **352** 367-78
- [34] Robinson M and Dean T J 1993 Measurement of near surface soil water content using a capacitance probe *Hydrological Processes* **7** 77-86
- [35] Catenaccio A, Daruich Y and Magallanes C 2003 Temperature dependence of the permittivity of water *Chemical Physics Letters* **367** 669-71

**Appendix D – 6th International Symposium on Process Tomography, Cape Town, South Africa, 26-28 March 2012
Paper - Capacitively-Coupled Impedance Measurements for ERT**

Capacitively-Coupled Impedance Measurements for ERT

R. Hayes, F. Podd, P. Newill, B.D. Grieve and T.A. York

School of Electrical & Electronic Engineering, University of Manchester, Manchester, UK

ABSTRACT

The paper explores the potential for using capacitively-coupled electrodes in electrical resistance tomography. Such electrodes are less vulnerable to corrosion and electrochemical effects that plague conventional electrical resistance tomographs utilising electrodes that are in intimate contact with the material. A model is proposed that takes account of the complex impedance of the insulating layer. The performance of the resulting passive network of components has been simulated up to 1 MHz excitation frequency. 2D finite element modelling has been used to explore the measurements that might be expected from electrodes distributed around the boundary of a vessel. Except for the adjacent measurements the modelled impedances are within 1% of those for conventional electrodes.

Keywords : electrical tomography; capacitively coupled electrodes, finite element modelling, COMSOL

1 INTRODUCTION

Electrical tomography emerged in the 1980's following the reported success of X-ray and magnetic resonance imaging in the medical field. Early work in Sheffield on electrical resistance tomography (ERT) (Barber and Brown, 1984) was followed by efforts in Manchester that extended to capacitance (ECT) and electromagnetic (EMT) modalities (Williams and Beck, 1995). The activity now attracts practitioners worldwide and progress is regularly reported at the World Congress on Industrial Process Tomography and has also been captured in a number of review articles (York, 2005; Yang, 2010; York et al, 2011).

The work reported here is primarily concerned with ERT in which, conventionally, a small number of electrodes are placed on the inner wall of a process vessel in intimate contact with the materials of interest. These materials are frequently corrosive, for instance acetic acid used in pressure filtration (York et al 2005) and nylon polymerisation (Dyakowski et al, 2000) and this can result in rapid degradation of the electrodes. In addition, with this arrangement, the measurements are subject to electrochemical effects, typically manifested as a contact impedance which is influenced by the materials present, the current density and the frequency of the signals (Geddes et al, 1971). Efforts to mitigate these effects for ERT has only attracted modest interest, for instance by McNaughtan et al (2000). Typically, measurements adopt a 4-electrode protocol. Two electrodes are used to deliver a known current, typically of the order of milli-amperes, into the region of interest. Any voltage drop across the in-series contact impedance associated with these electrodes is irrelevant as it is the current that is of interest. Two further electrodes are used to determine the potential differences around the boundary of the region which then allows associated resistances to be determined. The circuit for the voltage measurement is designed to have high input impedance such that it draws almost zero current which reduces the effect of the contact impedance. The measured voltage is therefore a good representation of the potential difference across the region of interest. In practice this arrangement is not perfect, not least because of DC offsets in the signals.

Driven by the desire to reduce electrochemical effects and corrosion of the electrodes the present work explores the use of capacitively-coupled electrodes that are covered with a protective insulating layer. The work is motivated by our interests in using electrical tomography to image the root zone of plants under the surface of the soil. Clearly, this application area presents a significant challenge due to the complex biological, chemical and physical nature of the medium which increases concerns regarding corrosion and electrochemical effects.

The remainder of the paper is organised as follows. Section 2 describes previous research into capacitively-coupled electrodes. Section 3 presents the model used here and this is followed by a discussion of the finite element modelling that has been undertaken to explore how well the model performs.

2 BACKGROUND

Capacitively-Coupled Contactless Conductivity Detection (C4D) originated in the 1980's in the field of electrophoresis (Gas, B., M. Demjanenko, and J. Vacík, 1980). Da Silva and do Lago (1998) concluded that the polarisation effects were insignificant due to no direct galvanic contact and developed an axial arrangement using two tubular electrodes around a capillary. It was found, however, that measurement frequency had a significant effect on the sensitivity of the equipment. Zemmann et al (1998) also implemented a two electrode system and noted that frequencies between 20 kHz to 2 MHz provide results sensitive enough for typical electrophoresis applications. Figure 1 shows the simplified electrical equivalent of a C4D measurement where the capacitance of the insulating walls and the resistance of the medium are shown as CW and RB respectively. Vi and Vo are the input and output voltages respectively.

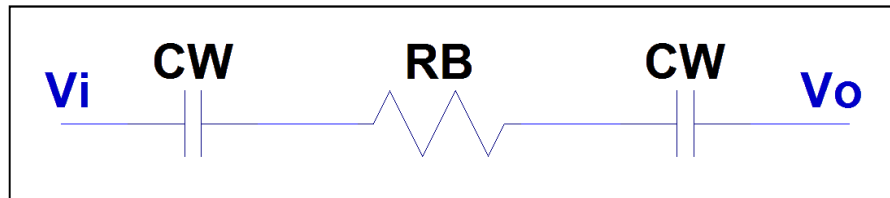


Figure 1: Simplified equivalent circuit for a C4D system

Huang et al (2009) discuss the use of a series inductor to counter capacitive effects as shown in Figure 2. They also consider the use of a shield between electrodes to reduce stray capacitance.

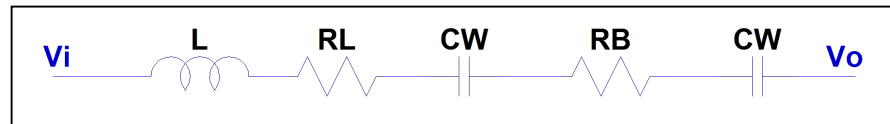


Figure 2: Equivalent C4D circuit with a series inductor (L) having resistance RL

Very little work has been reported regarding the use of C4D in electrical tomography. Wang et al (2010) utilised the C4D method to detect the presence of a plastic pipe within a water filled phantom. The apparatus was similar to that of an ECT system, with 12 large copper electrodes around the outer wall of an insulating vessel. They note that when the vessel is filled with a homogeneous conductive fluid the impedance between any two electrodes can be represented by the model shown in Figure 1, with the value of resistance RB changing dependent on the conductance of the medium and the distance between electrodes. A forward model was created to predict values of resistance, from which reconstructed images were created using the Linear Back Projection algorithm from both measurement and forward model data. The reconstructed image clearly showed the plastic pipe in the vessel but suffered from poor quality due to lack of measurement optimisation.

Kuras et al (2007) looked at the use of the C4D technique to measure underground moisture in areas where typical penetrating rods could not be inserted for contact based resistance measurements such as urban environments or hard ground. The equipment consisted of sensor arrays that were pulled along the ground to create a profile of the underground moisture content. Tomographic images were comparable with those using regular galvanic contact measurements.

3 ELECTRICAL MODEL

In contrast to the earlier work the electrical model for C4D measurements that is presented here considers both the resistance and capacitance of the wall and medium under test. The electrical equivalent circuit is shown in Figure 3, where CW and RW are the capacitance and resistance of the wall. CB and RB represent the capacitance and resistance of the bulk material within the vessel. The inclusion of parallel connected wall resistances RW and bulk capacitance CB should be noted in comparison to previous models. Considering the electrodes to be arranged as plates that are placed either side of the medium, as suggested in Figure 3, the analytical solution for the combined impedance “Z” is shown in Equation 1. In this analysis the two wall impedances are combined into a single impedance with twice the resistance ($R_w = 2RW$) and half the capacitance ($X_w = CW/2$).

$$Z = \left(\frac{1}{R_w} + \frac{1}{jX_w} \right)^{-1} + \left(\frac{1}{R_B} + \frac{1}{jX_B} \right)^{-1} = \left(\frac{R_w X_w^2}{R_w^2 + X_w^2} + \frac{R_B X_B^2}{R_B^2 + X_B^2} \right) + j \left(\frac{R_w^2 X_w}{R_w^2 + X_w^2} + \frac{R_B^2 X_B}{R_B^2 + X_B^2} \right) \quad (1)$$

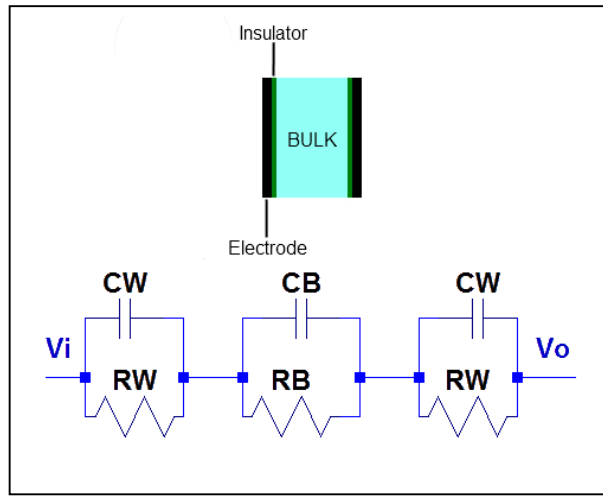


Figure 3: Equivalent Circuit for C4D

The analytical model has been simulated for electrodes having insulation resistance between 100kΩ and 1GΩ and a fixed wall capacitance of 100pF. Results are shown in Figure 4. The small circles indicate the wall transition frequency (WTF). Below this frequency current flow is primarily impeded by the wall. Above the WTF the bulk impedance dictates the current. Resistance of the bulk is inferred from the magnitude of the impedance in the plateau region above the transition frequency. For the present example this plateau lies between 40 kHz and 900 kHz. As can be seen the location of the plateau is, essentially, independent of wall resistance for the wide range of values considered. Consequently the model provides the ability to deduce the bulk resistance, as required in ERT, using insulated electrodes. In practice it is necessary to first interrogate the electrodes with multiple frequencies in order to deduce the location of the plateau.

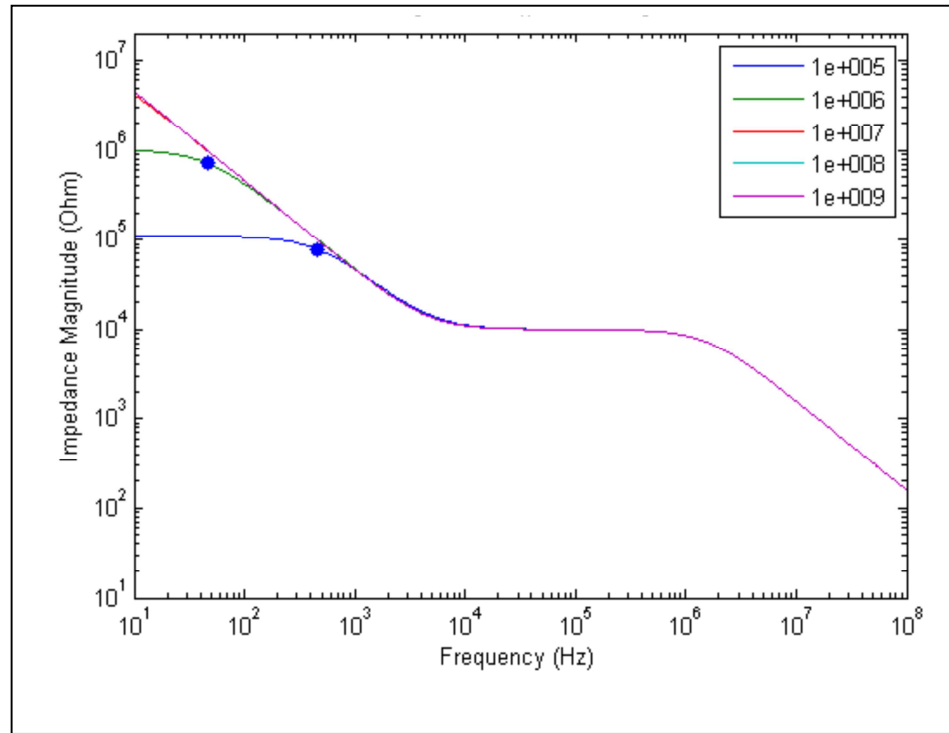


Figure 4: Simulated impedance spectra for a variety of wall resistance
 $C_B = 10\text{pF}$, $C_W = 100\text{pF}$, $R_B = 10\text{ k}\Omega$. Wall resistance = $10^5\Omega$ to $10^9\Omega$

4 FINITE ELEMENT MODELLING

COMSOL Multiphysics 3.5a has been used to explore the behaviour of C4D electrodes in a tomographic configuration. Results are compared to those using “bare” electrodes in which direct galvanic contact is made between electrode and medium. A challenge arises due to the contrasting dimensions in the model that arise, largely, due to the thin insulating “wall” covering on the electrodes which demands a very fine mesh granularity. Therefore, for the present initial explorations, a 2D modelling approach has been used. The solution to the 2D problem is in effect a pseudo-3D solution as COMSOL Multiphysics assumes a depth of 1 metre for the purpose of computation. The solution can be scaled appropriately according to the actual electrode height.

Initially a 2D rectangular idealised parallel plate arrangement, without fringing effects, was considered to provide a comparison with the analytical approach. Two fixed bulk dielectric constants were used representing air ($\epsilon_r=1$) and water ($\epsilon_r=79$) with varying conductivity values ranging from 1×10^{-9} to 1×10^9 . For each bulk conductivity/dielectric pairing, the resulting electric field distribution for a 1V excitation with a range of measurement frequencies between 10Hz and 1GHz was simulated. The complex impedance was extracted from the electric field simulation and plotted against the excitation frequency. As an example, Figure 5 shows a plot of the real component, imaginary component and magnitude of the complex impedance for a background relative permittivity of 79 and a bulk electrical conductivity of 1×10^{-3} S/m. The plateau where conductivity data can be extracted lies between 5 kHz and 40 kHz.

From the complex impedance spectra the ‘measured’ bulk conductivity can be extracted and compared to the original values that were used for the simulation. For the conductivity range between 1×10^{-8} S/m and 1×10^7 S/m these values displayed an average error of less than 1.5% and 4% for bulk dielectrics of 1 and 79 respectively. For bulk conductivities below 1×10^{-7} S/m and above 1×10^7 S/m the simulations must be extended to include both lower and higher excitation frequencies. For practical implementation this implies increased demands on the necessary instrumentation. Wall resistance has been extracted from the

simulated data and the resulting values are observed to be approximately constant with a value of $\sim 60 \text{ M}\Omega$ across the range of bulk conductivity. This suggests that, once a sensor has been characterised, further consideration of the wall resistance may not be necessary.

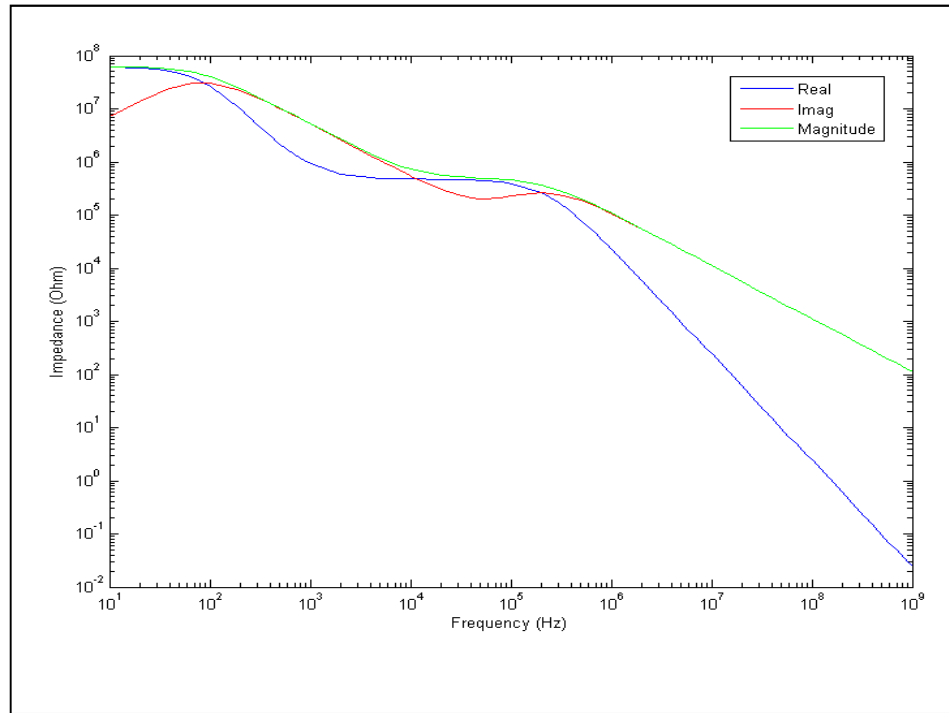
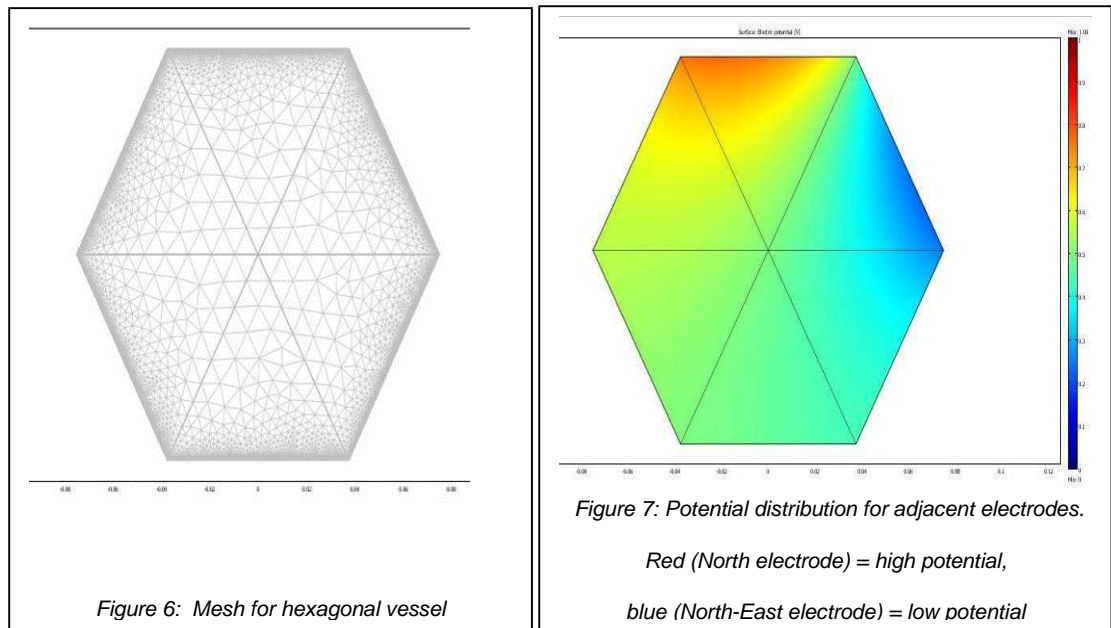


Figure 5: Real and Imaginary components and Magnitude of impedance ($\epsilon_r = 79$, $\sigma = 1 \times 10^{-3} \text{ S/m}$)

Conventional ERT arrangements might locate 16 electrodes around a circular boundary but for the present geometry, for reasons suggested above, this presents challenges for the modelling. Therefore initial efforts to model the capacitively-coupled electrodes in a tomographic configuration have considered a hexagonal arrangement. This is sufficient to satisfy the present aim of comparing the resulting impedance values to those using conventional “bare” electrodes. A hexagonal vessel of dimension 140mm and wall thickness, corresponding to the insulating layer, of 75 μm has been considered. Each of the faces of the hexagon is identified as an electrode having width 75mm. The model was simulated in 2D using an excitation voltage of 1V and a frequency of 30 kHz, selected to be located on the “plateau” region of the spectrum. Figures 6 and 7 show the mesh and a sample solution for an adjacent electrode excitation respectively. Note the extremely high mesh density in the vicinity of the vessel walls.



Four test cases have been considered comprising bulk regions of water and air each with insulating and bare electrodes. Figures 8, 9 and 10 show the real and imaginary components of the modelled impedances for the test cases.

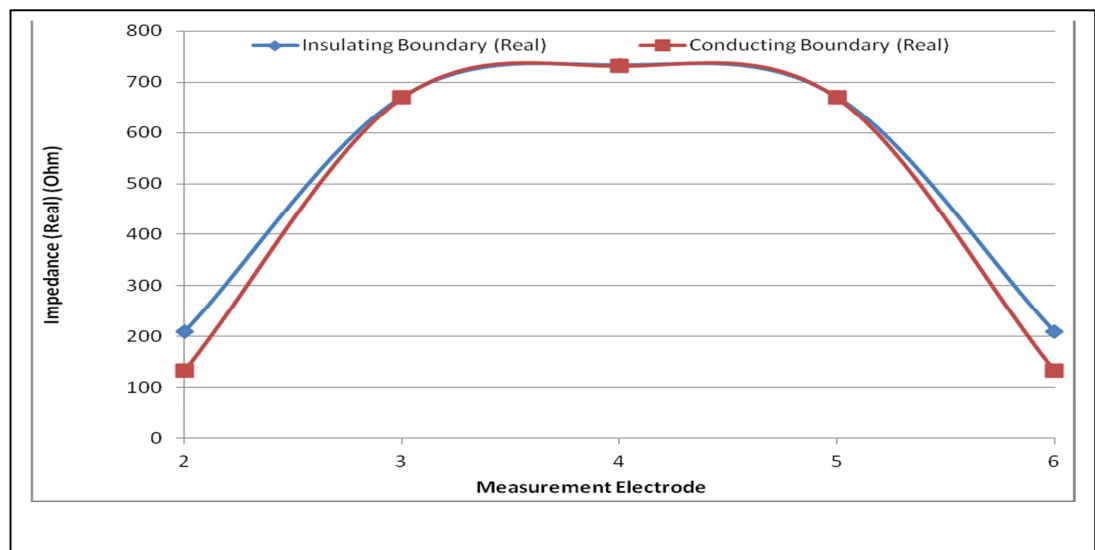


Figure 8: Modelled resistance for water

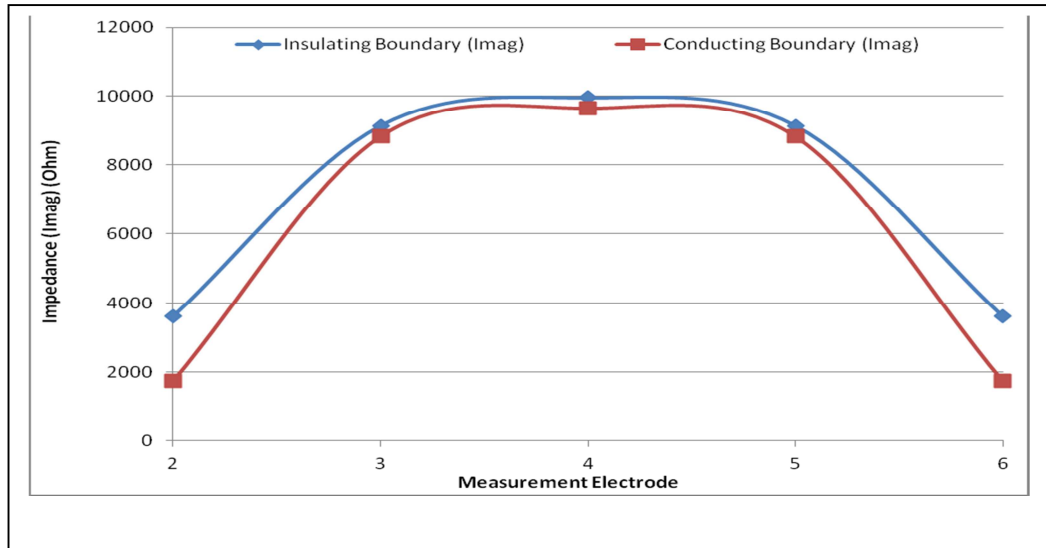


Figure 9: Modelled reactance for water

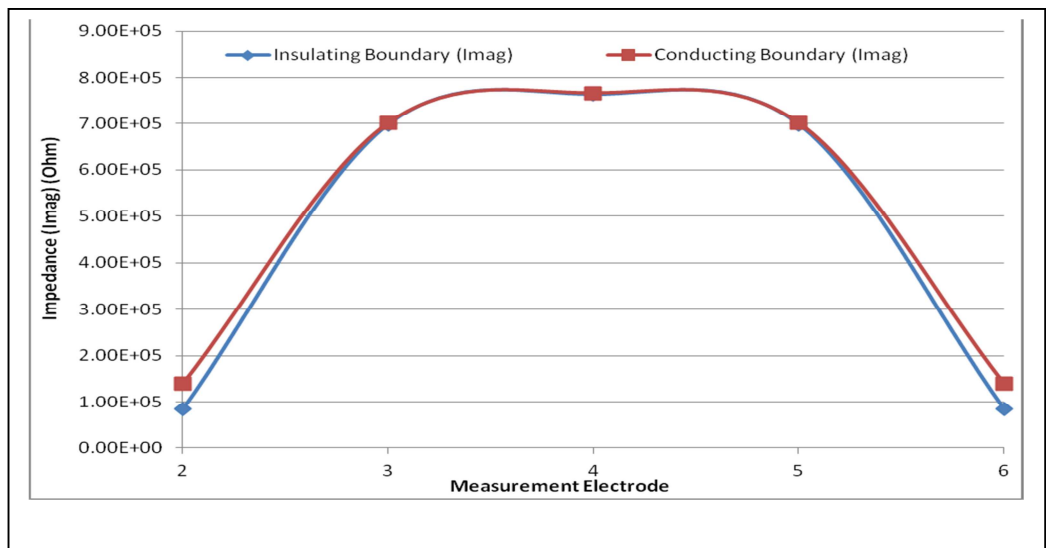


Figure 10 : Modelled reactance for air

As shown in Figure 8, apart from the adjacent electrodes, the modeling suggests that the capacitively coupled approach provides resistance estimates that are on average less than 1% different to those using conventional bare electrodes. The differences for the adjacent electrodes requires further exploration but may require modifications to the model. Related effects have been considered previously for ECT where the use of radial guards was proposed (Jaworski and Bolton, 2000). This approach will be considered in our future work. The results for the imaginary component, shown in Figure 9, display an average difference of 23%. It should be noted that, in reality, there are substantial challenges in measuring the imaginary component with conductive media.

As anticipated, for an insulating medium (air), there is no conducting path to provide a measurement of the real part of the impedance. However, as shown in Figure 10, the imaginary component of the impedance using the capacitively-coupled electrodes compares well under these conditions when compared with the bare electrode case. Again, excluding adjacent electrodes, average differences of less than 1% are suggested.

These results demonstrate that data collected using the proposed electrode arrangement differs very little from conventional electrode arrangements reported in the literature to date. In addition, the results demonstrate that the same electrode arrangement may be used for interrogating both conductive and insulating media, thus providing the basis for monitoring processes with both conducting and insulating phases, such as in sub-surface imaging of the root zone where there are both very wet (conducting) and very dry (insulating) phases.

5 SUMMARY

The paper reports exploration of the potential for using capacitively-coupled contactless electrodes for electrical resistance tomography. A model is suggested which, in contrast to previous reports, includes parallel connected wall resistance and bulk capacitance. Analytical consideration of the frequency response of an idealised parallel-plate capacitor suggest that a plateau region exists in the spectrum and that measurements in this region reflect the bulk resistance of the materials under consideration. Finite element modelling is compromised due to the contrasting geometries that arise, primarily due to the thin insulating layer on the electrodes. Results from 2D modelling of geometries which approximate tomographic arrangements suggest that for all except neighbouring electrodes the extracted resistances match to within 1% those using conventional bare electrodes. Future work will progress the modeling to the 3D case of more realistic geometries and results will be compared to measurements on a laboratory-based prototype.

6 REFERENCES

- BARBER B., BROWN B.H. (1984), Applied potential tomography, *J Phys. E*, 17, 9, 723–733.
- DYAKOWSKI T, YORK T.A, MIKOS M, VLAEV D, MANN R, FOLLOWS G, BOXMAN A., WILSON M. (2000), Imaging Nylon Polymerisation Processes by Applying Electrical Tomography, *Chem. Eng. J.*, 77, 05-109.
- FRACASSI DA SILVA J.A., DO LAGO C.L. (1998), An Oscillometric Detector for Capillary Electrophoresis. *Analytical Chemistry*, 70(20): p. 4339-4343.
- GAS B, DEMJANENKO M., VACÍK J. (1980), High-frequency contactless conductivity detection in isotachopheresis. *J. Chromatography A*, 192, 2, 253-257.
- GEDDES L.A., DA COSTA C.P. WISE G. (1971), The Impedance of Stainless-Steel Electrodes, *Medical & Biological Engineering*, 9, 5, 511-521 (DOI: 10.1007/BF02474708)
- HUANG Z.Y, JIANG W.W, ZHOU X.M, WANG B.L, JI H.F, LI H.Q (2009), A new method of capacitively coupled contactless conductivity detection based on series resonance, *Sensors and Actuators B*, 143, 1, 239-245.
- JAWORSKI A.J., BOLTON G.T. (2000), The design of an electrical capacitance tomography sensor for use with media of high dielectric permittivity, *Meas. Sci. Tech.*, 11, 6, 743-757.
- KURAS O, MELDRUM P.I, BEAMISH D, OGILVY R.D., LALA D (2007), Capacitive resistivity imaging with towed arrays, *J. Environmental and Engineering Geophysics*, 12, 3, 267-279 (DOI: 10.2113/JEEG12.3.267)
- MCNAUGHTAN A, MENEY K., GRIEVE B. (2000), Electrochemical issues in impedance tomography, *Chem. Eng. J.*, 77, 1-2, 27-30 (DOI: 10.1016/S1385-8947(99)00131-X)
- WANG B.L., HUANG Z.Y (2010), Towards Capacitively Coupled Electrical Resistance Tomography, *6th World Congress on Industrial Process Tomography*, Beijing, China

WILLIAMS R.A., BECK M.S. (1995), Process Tomography: Principles Techniques and Applications. London, U.K.: Butterworth.

YANG W.Q. (2010), Design of electrical capacitance tomography sensors, *Meas. Sci. Tech.*, 21, 4, 042001. (DOI: 10.1088/0957-0233/21/4/042001).

YORK T.A. (2005), Electrical Tomography for Industrial Applications, invited chapter in *Electrical Impedance Tomography : Methods, History and Applications*”, edited by D.S. Holder, *IOP series in Medical Physics and Biomedical Engineering*, 295-347 (ISBN 0 7503 0952 0)

YORK T.A, DAVIDSON J.L, MAZURKIEWICH L, MANN R., GRIEVE B.D. (2005), Towards process tomography for monitoring pressure filtration, *IEEE Sensors J.*, 5, 2, 139–152.

YORK T.A, MCCANN H., Ozanyan K.B. (2011), Agile Sensing Systems for Tomography, *IEEE Sensors J.*, 11, 12, 3086 - 3105 (DOI 10.1109/JSEN.2011.2164905)

ZEMANN, A.J, SCHNELL E, VOLGGER D., BONN G.K. (1998), Contactless Conductivity Detection for Capillary Electrophoresis, *Analytical Chemistry*, 70, 3, 563-567.

ACKNOWLEDGEMENTS

The authors are grateful to the Engineering & Physical Sciences Research Council of the UK for research studentships held by PN and RH. Also, to Syngenta for on-going support of research into root-zone monitoring.

Appendix E – Eurosoil 2012 Abstract

Sub-surface imaging using Electrical Impedance Tomography: A modelling approach for simulating the electrical properties of soil with varying saturation levels

R R Hayes^{1*}, P A Newill¹, F J W Podd¹, O Dorn², T A York¹, B D Grieve¹

¹ SSUIC, School of Electrical and Electronic Engineering, University of Manchester, UK

² Inverse Problems Group, School of Mathematics, University of Manchester, UK

* Syngenta Sensors University Innovation Centre, School of Electrical and Electronic Engineering, The University of Manchester, PO Box 88, Sackville Street, Manchester, M13 9PL, UK

Contact: robert.hayes@postgrad.manchester.ac.uk

Abstract

In light of climatic change, rapid identification of new plant varieties that will thrive in future climates is increasingly important. The root system is critical to plant water uptake but this cannot easily be assessed without destroying the crop or disturbing the plant/soil matrix through extractive sampling.

We are developing a new visualisation tool for seed breeders that will provide on-line data indicating how efficiently each plant in a screening programme utilises the water available in the surrounding soil. This will facilitate the early detection of desirable genetic traits.

Visualisation of spatial water distribution takes the form of Electrical Impedance Tomography (EIT), a non-destructive and non-intrusive imaging technique. Measurements will allow water utilisation levels for each specimen to be inferred.

An investigation into the relationship between soil moisture content and electrical properties has been carried out. A mixture model was implemented as a coupling mechanism between the Richards equation for describing fluid flow in an unsaturated soil and the electrostatics problem for predicting electric fields. This facilitates the estimation of electrical impedance measurement data for varying soil saturation levels. Experiments have shown that the finite element model (FEM) electrostatics simulation implemented in COMSOL Multiphysics exhibits an error of less than 9% and is able to predict capacitance measurements of soil at varying homogenous soil moisture levels within an average error of less than 6% based on the implementation of the mixture model.

We present the inverse problem, discuss the inherent challenges and present the early experimental results.

Appendix F – Eurosoil 2012 Poster

MANCHESTER
1824

The University
of Manchester

Sub-surface imaging using Electrical Impedance Tomography: A modelling approach for simulating the electrical properties of soil with varying saturation levels

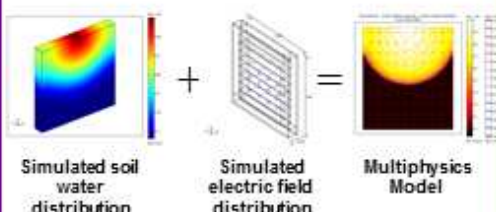
R.R.Hayes^{1*}, P.A.Newill¹, F.J.W.Podd¹, O.Dorn², T.A.York¹, B.D.Grieve¹

Aims

- To image moisture distributions in the sub-surface environment
- To monitor the efficiency of water utilisation by maize crops
- To provide a new visualisation tool for seed breeders
- To improve the fidelity of both images and data inferred from EIT data

Candidate Technology

- Electrical Impedance Tomography (EIT)
- Finite Element Modelling (FEM) using COMSOL Multiphysics



Methodology

- Coupled Soil Hydrology and EIT models are used in a Multiphysics simulation that allows the relationship between soil water content and electrical impedance to be coupled.
- COMSOL Multiphysics has been used to simulate electrical impedance data for a homogeneously packed soil with dynamic moisture contents.
- Multiphysics simulation facilitates the use of model based parameter optimisation methods to avoid some of the disadvantages of traditional inversion routines typically used in EIT image reconstruction.
- The Ensemble Kalman Filter (EnKF) is one such parameter estimation method and is an attractive option for such studies for several reasons:
 - It has a sequential structure that is convenient for processing remotely sensed measurements in real time.
 - It provides information on the accuracy of estimates.
 - It is able to account for a wide range of possible model errors

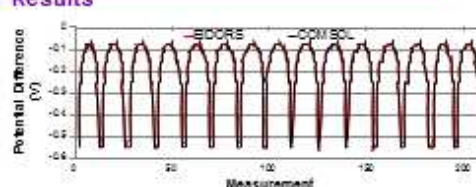
Conclusions

- The model facilitates the implementation of a Multiphysics based forward solver.
- The error between EIDORS and COMSOL reference predictions is due to the implementation of the contact impedance model.
- The forward solver can be used in EIT data interpretation using methods such as the EnKF, thus negating the need for a traditional inversion techniques or the use of adjoint states.

Motivations

- Climate change leads to water scarcity, this severely limits irrigation and constrains food production
- Rapid identification of new plant varieties that are tolerant to drought is key to breeding the food crops of tomorrow

Results



Simulated boundary voltage comparison between EIDORS and COMSOL Multiphysics at time = 0 i.e. Reference.

Time (Min)	Effective Saturation	Conductivity	Image Reconstruction
5.6			
11.2			
16.8			

From left to right: Predicted fluid flow, corresponding conductivity distribution and reconstructed conductivity distribution (red indicates high conductivities, blue indicates low conductivities)

Syngenta Sensors University Innovation Centre
School of Electrical and Electronic Engineering
The University of Manchester

¹EEUC, School of Electrical and Electronic Engineering, University of Manchester, UK

²Inverse Problems Group, School of Mathematics, University of Manchester, UK

*EEUC, School of Electrical and Electronic Engineering, The University of Manchester, PO Box 55, Sackville Street, Manchester, M13 9PL, UK
Contact: robert.hayes@postgrad.manchester.ac.uk

Appendix G – MATLAB function to define model for the generation of tomographic data COMSOL Multiphysics

```
function [vmeas] = AsymmetricalObjects(z, zmax, bg_conductivity,
object1_conductivity,object2_conductivity, forward_parameters,
boundary_condition, forward_results)

% COMSOL Multiphysics Model M-file
% Generated by COMSOL 3.5a (COMSOL 3.5.0.608, $Date: 2009/05/11
07:38:49 $)
% Modified by Robert Hayes to provide tomographic measurement
functionality
% Some geometry objects are stored in a separate file.
% The name of this file is given by the variable 'flbinaryfile'.

vmeas=[];
electrode_faces = [82 85;
                  100 106;
                  126 120;
                  144 138;
                  155 151;
                  143 134;
                  125 116;
                  105 96;
                  84 81;
                  61 67;
                  43 39;
                  25 21;
                  7 8;
                  22 26;
                  40 44;
                  68 62];

flclear xfem

% COMSOL version
clear vrsn
vrsn.name = 'COMSOL 3.5';
vrsn.ext = 'a';
vrsn.major = 0;
vrsn.build = 608;
vrsn.rcs = '$Name: v35ap $';
vrsn.date = '$Date: 2009/05/11 07:38:49 $';
xfem.version = vrsn;

flbinaryfile='AsymmetricalObjects.mphm';
flclear fem

% Geometry 1
clear draw
g52=flbinary('g52','draw',flbinaryfile);
g51=flbinary('g51','draw',flbinaryfile);
g6=flbinary('g6','draw',flbinaryfile);
g5=flbinary('g5','draw',flbinaryfile);
draw.s.objs = {g52,g51,g6,g5};
draw.s.name = {'EXT2','EXT1','EXT4','EXT3'};
draw.s.tags = {'g52','g51','g6','g5'};
fem.draw = draw;
fem.geom = geomcsg(fem);
```

```

fem.mesh = flbinary('m1','mesh',flbinaryfile);
xfem.fem{1}=fem;
flclear fem

% Geometry 2
clear draw
g49=flbinary('g49','draw',flbinaryfile);
g50=flbinary('g50','draw',flbinaryfile);
g3=flbinary('g3','draw',flbinaryfile);
draw.s.objs = {g49,g50,g3};
draw.s.name = {'CO17','C1','C2'};
draw.s.tags = {'g49','g50','g3'};
fem.draw = draw;
xfem.fem{2}=fem;

% (Default values are not included)

fem=xfem.fem{1};

% Application mode 1
clear appl
appl.mode.class = 'EmConductiveMediaDC';
appl.module = 'ACDC';
appl.border = 'on';
appl.assignsuffix = '_emdc';
clear bnd
bnd.I0 =
{forward_parameters.I_inj,0,0,forward_parameters.I_inj,forward_param
eters.I_inj,forward_parameters.I_inj,forward_parameters.I_inj,0,forw
ard_parameters.I_inj,forward_parameters.I_inj, ...

forward_parameters.I_inj,forward_parameters.I_inj,forward_parameters
.I_inj,forward_parameters.I_inj,forward_parameters.I_inj,forward_par
ameters.I_inj,forward_parameters.I_inj,forward_parameters.I_inj,forw
ard_parameters.I_inj};
bnd.type =
{boundary_condition(forward_parameters.sw(z,13)), 'cont', 'nJ0', bounda
ry_condition(forward_parameters.sw(z,12)), boundary_condition(forward
_parameters.sw(z,14)), boundary_condition(forward_parameters.sw(z,11)
), boundary_condition(forward_parameters.sw(z,15)), 'cont', boundary_co
ndition(forward_parameters.sw(z,10)), boundary_condition(forward_para
meters.sw(z,16)) ...

boundary_condition(forward_parameters.sw(z,9)), boundary_condition(fo
rward_parameters.sw(z,1)), boundary_condition(forward_parameters.sw(z
,8)), boundary_condition(forward_parameters.sw(z,2)), boundary_conditi
on(forward_parameters.sw(z,7)), boundary_condition(forward_parameters
.sw(z,3)), boundary_condition(forward_parameters.sw(z,6)), boundary_co
ndition(forward_parameters.sw(z,4)), boundary_condition(forward_param
eters.sw(z,5))};
bnd.name = {'Electrode
13', 'Contact_Surface', 'Medium_Surface', 'Electrode 12', ...
'Electrode 14', 'Electrode 11', 'Electrode
15', 'object_bg_interface', 'Electrode 10', 'Electrode 16', ...
'Electrode 9', 'Electrode 1', 'Electrode 8', 'Electrode 2', 'Electrode
7', 'Electrode 3', ...
'Electrode 6', 'Electrode 4', 'Electrode 5'};
bnd.ind =
[1,1,1,1,1,1,2,2,3,3,3,3,4,4,4,4,5,5,5,5,2,2,4,5,2,2,4,5,3,3, ...

```

```

6,6,6,6,7,7,7,7,2,2,6,7,2,2,8,8,3,3,6,7,3,3,9,9,9,9,10,10,10,10,2,2,
8, ...

8,9,10,2,2,9,10,3,3,11,11,11,11,12,12,12,12,2,2,11,2,2,12,11,3,12,3,
8, ...

8,3,3,13,2,13,13,14,2,14,14,13,14,2,2,13,14,8,8,13,3,14,3,15,2,15,15
, ...

16,2,16,16,15,16,2,2,15,16,15,3,16,3,17,2,17,17,18,2,18,18,17,18,2,2
, ...
17,18,17,3,18,3,2,19,19,19,2,19,19,19];
appl.bnd = bnd;
clear equ
equ.sigma =
{5.99e7,bg_conductivity,object1_conductivity,object2_conductivity};
equ.ind = [1,2,1,1,1,1,3,1,1,1,1,4,1,1,1,1,1,1];
appl.equ = equ;
fem.appl{1} = appl;
fem.frame = {'ref'};
fem.border = 1;
clear units;
units.basesystem = 'SI';
fem.units = units;
xfem.fem{1} = fem;

fem=xfem.fem{2};
fem.sdim = {'x','y'};
fem.border = 1;
clear units;
units.basesystem = 'SI';
fem.units = units;
xfem.fem{2} = fem;

% ODE Settings
clear ode
clear units;
units.basesystem = 'SI';
ode.units = units;
xfem.ode=ode;

% Multiphysics
xfem=multiphysics(xfem);

% Extend mesh
xfem.xmesh=mesnextend(xfem, ...
                      'geoms',[1]);

% Solve problem
xfem.sol=femstatic(xfem, ...
                  'solcomp',{'V','Vconstr0_g1_emdc'}, ...
                  'outcomp',{'V','Vconstr0_g1_emdc'}, ...
                  'blocksize','auto', ...
                  'linsolver','UMFPACK', ...
                  'prefun','amg');

% Save current fem structure for restart purposes
fem0=xfem;

```

```

% % Plot solution
% postplot(xfem, ...
%         'tridata',{ 'V','cont','internal','unit','V'}, ...
%         'trimap','Rainbow', ...
%         'title','Boundary: Electric potential [V]', ...
%         'grid','on', ...
%         'campos',[0,0,1.0143888048980696], ...
%         'camtarget',[0,0,0.007499999832361937], ...
%         'camup',[0,1,0], ...
%         'camva',9.07138228878535);

% Geometry 2
fem=xfem.fem{2};

% Geometry objects
clear s
s.objs={g49,g50,g3};
s.name={'C017','C1','C2'};
s.tags={'g49','g50','g3'};

fem.draw=struct('s',s);
xfem.fem{2}=fem;

mstart=(z*(zmax-3))-(zmax-4);
    for n=1:1:(zmax-3)

        % Integrate
        vmeas(1,n)=postint(xfem,'V', ...
                           'unit','V*m^2', ...
                           'recover','off', ...

'dl',[electrode_faces(forward_results.indH((mstart+n-
1),1),1),electrode_faces(forward_results.indH((mstart+n-1),1),2)],
...
                           'edim',2);

        % Integrate
        vmeas(2,n)=postint(xfem,'V', ...
                           'unit','V*m^2', ...
                           'recover','off', ...

'dl',[electrode_faces(forward_results.indH((mstart+n-
1),2),1),electrode_faces(forward_results.indH((mstart+n-1),2),2)],
...
                           'edim',2);
    end

vmeas = transpose(vmeas);
vmeas = reshape(vmeas,1,26);

```

Appendix H – MATLAB function for the generation of tomographic data with and without inclusions using COMSOL Multiphysics – Output is formatted such as it is compatible with EIDORS

```
forward_parameters.sw=COMSOL_switching_pattern(model_parameters,
forward_parameters);
boundary_condition = {'n' 'v' 'V0' 'nD0' 'nJ0' 'n' 'n' 'fp'};

zmax=length(forward_parameters.Ib);
voltages=zeros(zmax,((zmax-3)*2));
potentials1=[];
potentials2=[];
bg_conductivity=forward_parameters.mat_ref(1,1);
object1_conductivity=0.3;%0.01;
object2_conductivity=bg_conductivity;%0.3;

h=waitbar(0,'Please wait...');

for z=1:1:zmax
    %I(z,:)=ReferenceERT_Fun2(z, conductivity, switching_pattern,
    boundary_condition, measurement_pattern);
    %I(z,:)= ObjectERT_Fun(z, bg_conductivity, obj_conductivity,
    switching_pattern, boundary_condition, measurement_pattern);
    voltages(z,:) = AsymetricalObjects(z, zmax, bg_conductivity,
    bg_conductivity, bg_conductivity, forward_parameters,
    boundary_condition, forward_results);
    count=z;
    waitbar(count/(2*zmax));
end

voltages=transpose(voltages);

for m=1:1:zmax

    for n=1:1:(zmax-3)
        potentials1(m,n)=voltages(n+(zmax-3),m)-voltages(n,m);
    end
end

potentials1=transpose(potentials1);
potentials1=reshape(potentials1,208,1);
potentials1=potentials1*(1/(0.015*0.015))*-1;
plot(potentials1, 'r');
hold on

voltages=zeros(zmax,((zmax-3)*2));
```

```

for z=1:1:zmax
    %I(z,:)=ReferenceERT_Fun2(z, conductivity, switching_pattern,
    boundary_condition, measurement_pattern);
    %I(z,:)= ObjectERT_Fun(z, bg_conductivity, obj_conductivity,
    switching_pattern, boundary_condition, measurement_pattern);
    voltages(z,:) = AsymetricalObjects(z, zmax, bg_conductivity,
    object1_conductivity, object2_conductivity, forward_parameters,
    boundary_condition, forward_results);
    count=z+zmax;
    waitbar(count/(2*zmax));
end

close(h)
voltages=transpose(voltages);

for m=1:1:zmax

    for n=1:1:(zmax-3)
        potentials2(m,n)=voltages(n+(zmax-3),m)-voltages(n,m);
    end

end

potentials2=transpose(potentials2);
potentials2=reshape(potentials2,208,1);
potentials2=potentials2*(1/(0.015*0.015))*-1;
plot(potentials2, 'b');

v_diff=potentials2-potentials1;

measurement_data.v_ref=(potentials1);
measurement_data.v_meas=(potentials2);
measurement_data.v_diff=v_diff;

clearvars -except model_parameters forward_parameters
forward_results measurement_data inverse_results

```

Appendix I – Python code for data acquisition from 3 laboratory scales

```
import serial
import time

def waituntil(start, duration):
    if (time.time()<start+duration):
        time.sleep(0.1)

# define variables
interval = 2                                #interval between readings in seconds
Balance_1 = '\\.\COM5'                      #name of serial port that balance 1
appears as
Balance_2 = '\\.\COM3'                      #name of serial port that balance 2
appears as
Balance_3 = '\\.\COM1'                      #name of serial port that balance 3
appears as
path = "WeightScales.csv"                  #name of file to dump to

print 'Attempting to log weight data using three lab balances every
', str(interval),' seconds'
time.sleep(1)

try:
    with open(path,'a')as file:

        # define and open serial ports
        print 'Attempting to open serial ports'
        time.sleep (1)

        ser1 = serial.Serial(Balance_1, 9600, timeout=0.5)
    #set up Serial communication
        ser1.flush()
        if ser1.isOpen()!= True:
            ser1.open()
            print 'Successfully opened serial port for
Balance 1'

            print 'Successfully opened serial port for Balance 1'

            time.sleep(1)
```

```

        ser2 = serial.Serial(Balance_2, 9600, timeout=0.5)
#set up Serial communication
        ser2.flush()
        if ser2.isOpen() != True:
            ser2.open()
            print 'Successfully opened serial port for
Balance 2'

        print 'Successfully opened serial port for Balance 2'

        time.sleep(1)

        ser3 = serial.Serial(Balance_3, 9600, timeout=0.5)
#set up Serial communication
        ser3.flush()
        if ser3.isOpen() != True:
            ser3.open()
            print 'Successfully opened serial port for
Balance 3'

        print 'Successfully opened serial port for Balance 3'

#Acquire Measurements
        try:
            while(ser1.isOpen() & ser2.isOpen() & ser3.isOpen()):
                timestamp = time.time()

#Get current time stamp
                s = str(timestamp)

#Convert to string
                s += ' , '
                tries = 1

#Reset number of attempts to acquire data
                while tries <= 10:
                    ser1.write('w')

#Request current value

                    try:
                        data = ser1.readline()

#Read current value

                        if '-' in data:
                            p = data.index('-
')

```



```

s += str(-
float(data[p+1:-5]))#Convert to string
else:
s +=
str(float(data[2:-5]))#Convert to string

tries = 100
#If data is recieved set tried to 100 to exit loop
except Exception, e:
#In the case of no data recieved
tries +=1
#Increment the number of tries

if tries ==100:
    if 'g' not in data:
        s+='X'

    else:
        s+='B'

s+= ' , '

tries = 1
while tries <=10:
    ser2.write('w')

#Request current value
try:
    data = ser2.readline()

#Read current value
    if '-' in data:
        p = data.index('-
')

s += str(-
float(data[p+1:-5]))#Convert to string
else:
s +=
str(float(data[2:-5]))#Convert to string

tries = 100
#If data is recieved set tried to 100 to exit loop

```

```

except Exception, e:

#In the case of no data recieved

        tries +=1

#Increment the number of tries

        if tries ==100:
            if 'g' not in data:
                s+='X'

        else:
            s+='B'

        s+= ' , '

        tries = 1
        while tries <=10:
            ser3.write('w')

#Request current value

        try:
            data = ser3.readline()
            if '-' in data:
                p = data.index('-')

            s += str(-
float(data[p+1:-5]))#Convert to string

        else:
            s +=
str(float(data[2:-5]))#Convert to string

        tries = 100

#If data is recieved set tried to 100 to exit loop
except Exception, e:

#In the case of no data recieved

        tries +=1

#Increment the number of tries

        if tries ==100:
            if 'g' not in data:
                s+='X'

```

```

        else:
            s+='B'

            s += '\n'
#increment the line number

            file.write(s)
#write data to file
            print s[0:-1]

            waituntil(timestamp,interval)      #wait
for defined interval minus time taken to acquire data before
requesting the next value
        except:
            print 'Closing serial ports'
            ser1.close()
            ser2.close()
            ser3.close()
            time.sleep (1)
            print '...'
            time.sleep(1)
            print 'Serial ports closed'

    except:
        print 'Error Opening file'

raw_input("Press enter to close the program")      #holds
window open untill user closes it so they can see any outputs

```

Appendix J – MATLAB generated function for importing laboratory scale data for centre of gravity calculations

```
function importfile(fileToRead1)
%IMPORTFILE(FILETOREAD1)
% Imports data from the specified file
% FILETOREAD1: file to read

% Auto-generated by MATLAB on 08-Jan-2014 09:45:12

% Import the file
rawData1 = importdata(fileToRead1);

% For some simple files (such as a CSV or JPEG files), IMPORTDATA
might
% return a simple array. If so, generate a structure so that the
output
% matches that from the Import Wizard.
[~,name] = fileparts(fileToRead1);
newData1.(genvarname(name)) = rawData1;

% Create new variables in the base workspace from those fields.
vars = fieldnames(newData1);
for i = 1:length(vars)
    assignin('base', vars{i}, newData1.(vars{i}));
end
```

Appendix K – MATLAB function for calculating the centre of gravity of a vessel suspended on a triangular support between 3 laboratory scales

```
% Define length of sides of triangle rig (should be equal as design
is
% equilateral triangle, however manufacturing process introduces
some
% error)

Triangle_Size_AB = 266;
Triangle_Size_BC = 263.5;
Triangle_Size_AC = 263.5;

% Take length of sides as average of all 3 sides
D=(Triangle_Size_AB+Triangle_Size_BC+Triangle_Size_AC)/3;

% Calculate length of line A to centre pt between B & C
L= (sqrt(3)*D)/2;

Vessel_Diam = 165; %Diameter of vessel (mm)

CG = []; %Initialise Centre of Gravity variable

% Read in measurement data from scales
M = importdata('TestingCG.csv');

n=1; % Set n to 1

while n<=size(M,1)
A=M(n,2); % Extract scale A value for current time step
B=M(n,3); % Extract scale B value for current time step
C=M(n,4); % Extract scale C value for current time step

W=A+B+C; % Calculate total weight

x=((B+C)*L)/W % Calculate x co-ordinate of centre of gravity at
current time step
y=((C-B)*D)/(2*W)% Calculate y co-ordinate of centre of gravity at
current time step

CG=[CG; M(n,1) x y]; % Add current time step data to the end of the
matrix CG
n=n+1; % Move to next time step
end

hold on

for n=1:size(CG,1)
scatter(CG(n,2),CG(n,3),'+') % Plot the centre of gravity for each
time step
end

axis([0 300 -150 150]) % Scale axis to match dimensions of rig
axis square
line([0 L],[0 D/2]); % Draw triangle rig Line A-C
line([0 L],[0 -D/2]); % Draw triangle rig Line A-B
```

```

line([L L],[-D/2 D/2]); % Draw triangle rig Line B-C
rectangle('Curvature', [1 1],'Position', [(D/sqrt(3))-
(Vessel_Diam/2) -Vessel_Diam/2 Vessel_Diam Vessel_Diam]) % Draw
vessel location

% Now to find which points lay within the vessel and which lay
outside of
% it, this can be helpful to find erroneous data.

radius= Vessel_Diam/2; % cut-off distance / cut-off radius (radius
of vessel)
origin= [D/sqrt(3) 0]; % Origin of search radius (centre pt. of
vessel) - D/sqrt(3) = centre of triangle

% Plot origin of search
scatter(origin(1),origin(2),'X')
line([origin(1) origin(1)],[origin(2) radius]); %
line([origin(1) origin(1)],[origin(2) -radius]); %
line([origin(1) (origin(1)+radius)],[origin(2) origin(2)]); %
line([origin(1) (origin(1)-radius)],[origin(2) origin(2)]); %

% Calculate distance within which points should lay
dist = sqrt((origin(1) - CG(:,2)).^2 + (origin(2) -
CG(:,3)).^2); % distance calc.

% Find points inside vessel
in = find(dist<radius);
points.in = [CG(in,2) CG(in,3)];

% Find points outside vessel
out = find(dist>radius);
points.out = [CG(out,2) CG(out,3)];

% Plot points within the vessel
for n=1:size(points.in,1)
scatter(points.in(n,1),points.in(n,2),'O') % Plot the centre of
gravity for each time step
end

hold off

clear L D M n A B C W x y dist origin in out radius Vessel_Diam
Triangle_Size_AB Triangle_Size_BC Triangle_Size_AC

```

Appendix L –MATLAB Function for separating 2D planar and 3D tomographic measurement data acquired using the LCT2 instrument and one large measurement sequence

```
clear;
disp('starting');
disp(char(10));
directory = 'C:\Users\mbcx3sh2\Desktop\rob\tomographicdata\';
delete([directory,'\split\*.txt']);
files = dir([directory, '*.txt']);
[x,y] = size(files);
row = 1;
while(row <= x)
    fid = fopen([directory,files(row).name]);

    headerln0 =fgets(fid);
    headerln1 = fgets(fid)
    headerln2 = fgets(fid)
    headerln3 = fgets(fid)
    headerln4 = fgets(fid)
    headerln5 = fgets(fid)
    headerln6 = fgets(fid)
    headerln7 = fgets(fid)
    headerln8 = fgets(fid)
    headerln9 = fgets(fid)
    headerln10 = fgets(fid)
    fclose(fid);

    inputData =
    dlmread([directory,files(row).name],',',[10,0,1353,3]);
    diary([directory,'split\1_',files(row).name]);
    i=1;

    disp([headerln0,headerln2,headerln4,char(10),headerln7,headerln9(1:en
nd-2)]);
        while(i<=416)
            disp([num2str(inputData(i,1),
'%0.6f'),' ',num2str(inputData(i,2),'%0.6f'),' ',num2str(inputData(i
,3),'%0.8f'),' ',num2str(inputData(i,4),'%0.4f')]);
            i = i+1;
        end
        disp('#END');
        diary off;

        diary([directory,'split\2_',files(row).name]);

    disp([headerln0,headerln2,headerln4,char(10),headerln7,headerln9(1:en
nd-2)]);
        while(i<=1344)
            disp([num2str(inputData(i,1),
'%0.6f'),' ',num2str(inputData(i,2),'%0.6f'),' ',num2str(inputData(i
,3),'%0.8f'),' ',num2str(inputData(i,4),'%0.4f')]);
            i = i+1;
        end
        disp('#END');
        diary off;
        row = row+1;
end
```